(10)

NORSAR

ROYAL NORWEGIAN COUNCIL FOR SCIENTIFIC AND INDUSTRIAL RESEARCH

Scientific Report No. 2-84/85

SEMIANNUAL TECHNICAL SUMMARY

1 October 1984 – 31 March 1985

L. B. Loughran (Ed.)

Kjeller, July 1985

UNCLASSIFIED
SECURITY CLASSIFICATION OF THIS PAGE

REPORT DOCUMENTATION PAGE

1a. REPORT SECURITY CLASSIFICATION UNCLASSIFIED	1b. RESTRICTIVE MARKINGS NOT APPLICABLE
2a. SECURITY CLASSIFICATION AUTHORITY NOT APPLICABLE	3. DISTRIBUTION/AVAILABILITY OF REPORT APPROVED FOR PUBLIC RELEASE DISTRIBUTION UNLIMITED
2b. DECLASSIFICATION/DOWNGRADING SCHEDULE NOT APPLICABLE	
4. PERFORMING ORGANIZATION REPORT NUMBER(S) SCIENTIFIC REPORT 2-84/85	5. MONITORING ORGANIZATION REPORT NUMBER(S) SCIENTIFIC REPORT 2-84/85
6a. NAME OF PERFORMING ORGANIZATION NTNF/NORSAR 6b. OFFICE SYMBOL (If applicable)	7a. NAME OF MONITORING ORGANIZATION HQ AFTAC/TGX
6c. ADDRESS (City, State and ZIP Code) POST BOX 51 N-2007 KJELLER, NORWAY	7b. ADDRESS (City, State and ZIP Code) PATRICK AFB, FL 32925-6471
8a. NAME OF FUNDING/SPONSORING ORGANIZATION DEFENSE ADVANCED RESEARCH PROJECTS AGENCY 8b. OFFICE SYMBOL (If applicable)	9. PROCUREMENT INSTRUMENT IDENTIFICATION NUMBER CONTRACT NO. F08606-84-C-0002-P00002
8c. ADDRESS (City, State and ZIP Code) ARLINGTON, VA 22209	10. SOURCE OF FUNDING NOS. PROGRAM ELEMENT NO: R&D PROJECT NO: NORSAR PHASE 3 TASK NO: SOW TASK 5.0 WORK UNIT NO: SEQUENCE NUMBER 003A2
11. TITLE (Include Security Classification) SEMIANNUAL TECHNICAL SUMMARY 1 OCT 84-31 MAR 85 (UNCLASSIFIED)	
12. PERSONAL AUTHOR(S) L.B. LOUGHRAN (ED.)	
13a. TYPE OF REPORT SCIENTIFIC SUMMARY 13b. TIME COVERED FROM 1 OCT 84 TO 31 MAR 85	14. DATE OF REPORT (Yr., Mo., Day) July 1985 15. PAGE COUNT 118
16. SUPPLEMENTARY NOTATION NOT APPLICABLE	

17. COSATI CODES			18. SUBJECT TERMS (Continue on reverse if necessary and identify by block number)
FIELD	GROUP	SUB. GR.	NORSAR, NORWEGIAN SEISMIC ARRAY

19. ABSTRACT (Continue on reverse if necessary and identify by block number)

During this reporting period
The Norwegian Seismic Array (NORSAR) Detection Processing System has been operated through the period 1 October 1984 - 31 March 1985, with an average uptime of 98.2 per cent. Most of the down time has been caused by disk failure at the central recording computer. A total of 1792 seismic events have been reported by NORSAR in the period. The online IBM 4331 processing computer has been replaced by a more powerful IBM 4341 unit, which will make it possible to test and implement improved real time detection algorithms. The performance of the continuous alarm system and the automatic telex bulletin transfer to AFTAC have been satisfactory in the period.

(over)

20. DISTRIBUTION/AVAILABILITY OF ABSTRACT UNCLASSIFIED/UNLIMITED ☒ SAME AS RPT. ☐ DTIC USERS ☐	21. ABSTRACT SECURITY CLASSIFICATION UNCLASSIFIED
22a. NAME OF RESPONSIBLE INDIVIDUAL CAPT JAMES A. ROBB	22b. TELEPHONE NUMBER (Include Area Code) ((305) 494-7665 22c. OFFICE SYMBOL AFTAC/TGX

DD FORM 1473, 83 APR EDITION OF 1 JAN 73 IS OBSOLETE

UNCLASSIFIED
SECURITY CLASSIFICATION OF THIS PAGE

A

UNCLASSIFIED

19. (cont.)

Preliminary evaluation of the real time detection system for the NORESS array has shown an excellent P-wave detection performance at high signal frequencies. Such frequencies are commonly observed for all seismic events at regional distances, and for many teleseismic events, especially in Eurasia. The detection of secondary regional phases (Sn and Lg), which is important for the location procedure in the NORESS system, needs further refinement. A newly developed off-line interactive analysis package ~~has been~~ applied to study in detail a NORESS data base of 18 regional events from Western Russia, and this study has shown that estimates of azimuth and phase velocity using F-k analysis are quite strongly dependent on the analysis frequency selected. A newly developed broad-band spectral estimation technique gives promise of more stable estimates. Studies of travel time residuals using GSDN network data for both deep and shallow events have indicated that the reference earth model ~~(PREM)~~ needs to be modified, both with regard to the upper and lower mantle. A study of teleseismic P coda using NORSAR and NORESS data has given evidence to confirm the hypothesis that the coda is composed of on-azimuth P and off-azimuth Lg, the former being due to scattering of Lg to P near the source and the latter being due to scattering to P to Lg near the receiver. A maximum likelihood method to extract azimuth and angle of incidence using 3-component data has been applied to NORESS recordings with promising results in regard to event location estimation. A study has been initiated on methods to use available travel time information from a global network to simultaneously determine earth structural and focal parameters. A status report on a development project for a remote seismic terminal system is presented. Gravity observations in the NORSAR siting area have been studied and interpreted in the context of fault mechanisms of small earthquakes in the northern part of the Oslo Graben.

AFTAC Project Authorization	:	T/4141/B/PMP
ARPA Order No.	:	4138
Program Code No.	:	0F10
Name of Contractor	:	Royal Norwegian Council for Scientific and Industrial Research
Effective Date of Contract	:	1 October 1984
Contract Expiration Date	:	30 September 1985
Project Manager	:	Frode Ringdal (02) 71 69 15
Title of Work	:	The Norwegian Seismic Array (NORSAR) Phase 3
Amount of Contract	:	$ 674 379
Contract Period Covered by the Report	:	1 Oct 1984 - 31 Mar 1985

This research was supported by the Advanced Research Projects Agency of the Department of Defense and was monitored by AFTAC, Patrick AFB, FL 32925, under contract no. F08606-84-C-0002-P00002.

NORSAR Contribution No. 354

TABLE OF CONTENTS

I. SUMMARY

This report describes the operation, maintenance and research activities at the Norwegian Seismic Array (NORSAR) for the period 1 October 1984 - 31 March 1985.

The uptime of the NORSAR online detection processor system has averaged 98.2 per cent as compared to 95.1 for the previous period. Disk failure and maintenance in connection with disk failure caused most of the downtime. A total of 1792 events were reported in this period, giving a daily average of 9.9 events.

During this period the 4331 IBM computer has been replaced by a more powerful 4341. The increased capacity will enable us to improve the processing algorithms, test processing together with online operation and will make program development easier. The new automatic bulletin transfer has been running for approximately 8 months, and experience so far has been good.

The majority of maintenance visits to the subarrays have been in connection with corrective maintenance, including repair of cables.

The research activity is summarized in section VII. Section VII.1 discusses real time event detection using the small-aperture NORESS array, while VII.2 presents a preliminary evaluation of the event detection and location capabilities of NORESS. Section VII.3 takes up seismic modelling of an anisotropic boundary layer, and Section VII.4 discusses an application of long-period waveform inversion to shallow sources under the Tibetan Plateau. In section VII.5 an interactive analysis program for use with NORESS data is presented. Analysis of teleseismic P coda using NORSAR and NORESS is discussed in section VII.6. Results from 3-component seismogram analysis are presented in section VII.7, while epicenter location scenarios are presented in section VII.8. In section VII.9 the current status of the RST/RSTE research project is presented. A study of the crustal structure in the NORSAR array siting area derived from gravity observations is described in section VII.10.

II. OPERATION OF ALL SYSTEMS

II.1 Detection Processor (DP) Operation

There have been 125 breaks in the otherwise continuous operation of the NORSAR online system within the current 6-month reporting interval. Disk failure and maintenance in connection with disk failure caused most of the downtime. The uptime percentage for the period is 98.2 as compared to 95.1 for the previous period.

Fig. II.1.1 and the accompanying Table II.1.1 both show the daily DP downtime for the days between 1 October 1984 and 31 March 1985. The monthly recording times and percentages are given in Table II.1.2.

The breaks can be grouped as follows:

a)	MODCOMP failure	:	4
b)	Disk failure	:	31
c)	Maintenance stops	:	16
d)	Power jumps and breaks	:	3
e)	Stops related to system operation	:	4
f)	TOD correction	:	49
g)	Communications lines	:	18

The total downtime for the period was 77 hours and 30 minutes. The mean-time-between-failure (MTBF) was 1.4, the same as for the previous period.

J. Torstveit

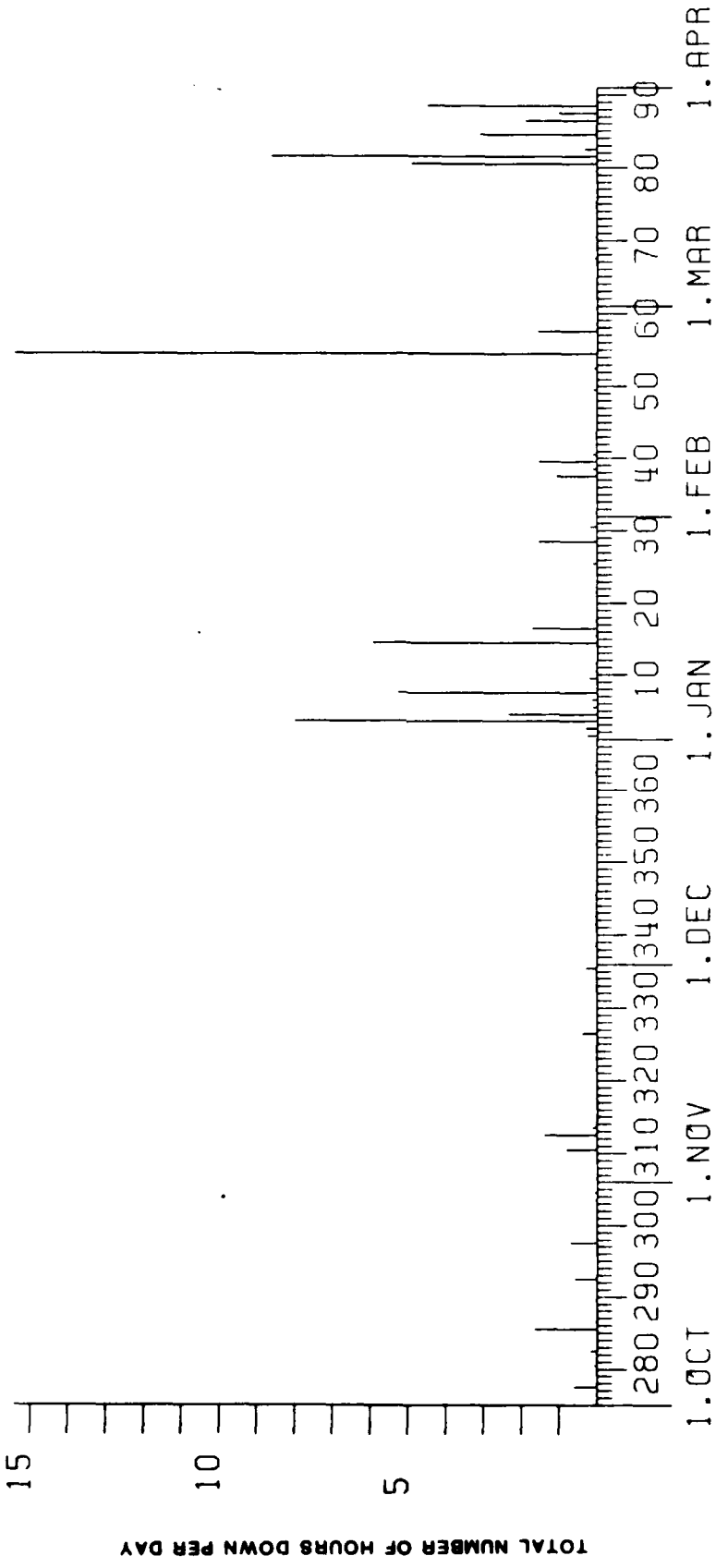

Fig. II.1.1 Detection Processor downtime in the period 1 October 1984 - 31 March 1985.

LIST OF BREAKS IN DP PROCESSING THE LAST HALF-YEAR

DAY	START		STOP		COMMENTS.....	DAY	START		STOP		COMMENTS.....
276	7	2	7	3	TOD CORRECTION	335	13	35	13	50	LINE FAILURE
277	12	16	12	53	MODCOMP FAILURE	338	7	0	7	2	TOD CORRECTION
279	7	1	7	2	TOD CORRECTION	340	7	1	7	2	TOD CORRECTION
280	11	26	11	30	LINE FAILURE	341	7	0	7	2	TOD CORRECTION
282	7	1	7	2	TOD CORRECTION	342	7	2	7	4	TOD CORRECTION
282	7	14	7	16	LINE FAILURE	345	7	1	7	3	TOD CORRECTION
282	7	35	7	37	LINE FAILURE	347	7	1	7	2	TOD CORRECTION
282	9	19	9	23	LINE FAILURE	352	7	2	7	3	TOD CORRECTION
285	9	16	10	54	LINE FAILURE	355	7	1	7	2	TOD CORRECTION
286	7	0	7	2	TOD CORRECTION	356	8	23	8	24	TOD CORRECTION
289	7	1	7	2	TOD CORRECTION	362	7	1	7	3	TOD CORRECTION
292	7	1	7	2	TOD CORRECTION	363	7	1	7	2	TOD CORRECTION
292	10	26	11	0	LINE FAILURE	1	11	0	11	16	RESTART DP
296	7	1	7	2	TOD CORRECTION	2	7	2	7	3	TOD CORRECTION
297	12	8	12	49	POWER FAILURE	2	23	43	24	0	DISK ERROR
299	7	2	7	3	TOD CORRECTION	3	0	0	7	28	DISK ERROR
303	7	2	7	3	TOD CORRECTION	3	8	9	8	40	DISK ERROR
304	7	1	7	2	TOD CORRECTION	4	5	42	6	51	DISK ERROR
304	7	19	7	20	LINE FAILURE	4	8	22	8	40	DISK ERROR
304	7	30	7	31	LINE FAILURE	4	10	43	11	30	DISK ERROR
306	7	1	7	2	TOD CORRECTION	4	11	37	11	38	DISK ERROR
310	7	16	8	4	SERVICE MODCOMP	4	14	55	15	0	DISK SERVICE
312	7	1	8	4	MODCOMP FAILURE	5	14	31	14	38	DISK ERROR
312	14	32	14	51	POWER FAILURE	6	17	42	17	50	DISK ERROR
313	8	13	8	20	SERVICE MODCOMP	7	7	1	7	2	TOD CORRECTION
314	7	1	7	2	TOD CORRECTION	7	9	1	9	11	DISK SERVICE
317	7	1	7	2	TOD CORRECTION	7	9	24	9	33	DISK SERVICE
321	7	1	7	2	TOD CORRECTION	7	10	4	14	58	DISK SERVICE
326	7	1	7	2	TOD CORRECTION	7	15	5	15	6	DISK ERROR
326	10	54	11	4	LINE FAILURE	9	6	39	6	51	DISK ERROR
326	11	18	11	24	LINE FAILURE	10	7	1	7	3	TOD CORRECTION
326	12	2	12	9	LINE FAILURE	11	8	6	8	7	RESYNC COM.LINE
328	7	1	7	2	TOD CORRECTION	14	7	6	13	0	MODCOMP ERROR
332	7	1	7	2	TOD CORRECTION	14	14	52	14	53	MODCOMP ERROR
335	7	1	7	2	TOD CORRECTION	15	11	44	11	46	DISK ERROR
335	13	30	13	31	LINE FAILURE	16	7	1	7	2	TOD CORRECTION

Table II.1.1 Daily DP downtime in the period 1 October 1984 - 31 March 1985.

LIST OF BREAKS IN DP PROCESSING THE LAST HALF-YEAR

DAY	START		STOP		COMMENTS.....	DAY	START		STOP		COMMENTS.....
16	8	14	8	17	DISK ERROR	80	12	14	12	59	DISK FAILURE
16	8	26	8	29	DISK ERROR	80	13	52	14	58	DISK FAILURE
16	8	37	8	40	DISK ERROR	80	17	15	19	30	DISK FAILURE
16	10	29	12	1	POWER BREAK	80	21	24	22	12	DISK FAILURE
17	7	1	7	3	TOD CORRECTION	81	0	29	7	13	DISK FAILURE
21	7	1	7	2	TOD CORRECTION	81	9	23	10	14	DISK FAILURE
25	7	1	7	3	TOD CORRECTION	81	12	22	12	23	TOD CORRECTION
25	14	32	14	36	DISK SERVICE	81	13	20	14	21	DISK FAILURE
28	7	1	7	3	TOD CORRECTION	82	9	23	9	32	DISK FAILURE
28	7	14	8	44	DISK ERROR	82	15	55	16	5	DISK FAILURE
30	7	0	7	9	COM.LINE ERROR	84	7	1	7	2	TOD CORRECTION
32	8	23	8	24	TOD CORRECTION	84	8	37	8	40	DISK SERVICE
37	7	4	7	6	TOD CORRECTION	84	12	17	15	0	DISK SERVICE
37	8	54	8	58	INST. NEW 4341	84	15	6	15	23	DISK SERVICE
37	10	17	10	59	INST. NEW 4341	86	12	44	14	37	DISK SERVICE
37	13	2	13	17	INST. NEW 4341	87	21	20	22	20	DISK FAILURE
38	8	24	8	30	DISK FAILURE	88	4	8	7	20	DISK FAILURE
39	8	53	10	24	DISK SERVICE	88	10	8	10	28	DISK SERVICE
40	11	18	11	24	CPU FAILURE	88	11	22	11	56	DISK SERVICE
43	7	2	7	4	TOD CORRECTION	88	13	25	13	49	DISK SERVICE
49	8	39	8	42	TOD CORRECTION						
49	10	19	10	21	LINE FAILURE						
52	7	2	7	4	TOD CORRECTION						
52	7	7	7	8	LINE FAILURE						
54	3	0	18	0	DISK FAILURE						
54	18	8	18	11	DISK FAILURE						
54	18	56	19	4	DISK FAILURE						
54	19	10	19	25	DISK FAILURE						
57	7	31	7	32	TOD CORRECTION						
57	13	7	14	40	DISK SERVICE						
58	12	44	12	45	LINE FAILURE						
63	7	21	7	22	TOD CORRECTION						
67	7	1	7	,	TOD CORRECTION						
70	5	31	5	33	LINE FAILURE						
74	9	44	9	46	TOD CORRECTION						
79	7	3	7	4	TOD CORRECTION						

Table II.1.1 (cont.)

Month	DP Uptime (hrs)	DP Uptime (%)	No. of DP breaks	No. of days with breaks	DP MTBF* (days)
Oct 84	740.05	99.5	20	14	1.5
Nov	717.12	99.6	15	11	1.9
Dec	743.44	99.9	11	11	2.6
Jan 85	717.54	96.5	34	18	0.9
Feb	652.01	97.0	20	11	1.3
Mar	719.34	96.7	25	12	1.2
	4290.30	98.2	125	77	1.4

Mean-time-between-failures = (total uptime/no. of up intervals)

Table II.1.2 Online system performance, 1 October 1984 - 31 March 1985.

II.2 Array Communications

The performance of the communications systems throughout the period is reflected in Table II.2.1. As the table indicates, the majority of the systems have been affected, mainly by broken cables or defective components causing unwanted effects such as delays and attenuation. Other incidents have been caused by NTA, mainly in connection with replacement/reconfiguration of equipment situated in the telestations at Lillestrøm, Hamar and Lillehammer. Tests and changes at the NDPC have also affected the communications system's uptime. Systems marked with asterisks are commented in the following paragraphs.

Summary

Oct. 84 Most systems were affected, 02B, 02C and 04C significantly. Also 01A, 01B and 03C had outages. Degradation of the 02B and 04C line performance started in August/September 84, and in both cases damaged pupin coils caused mismatch problems. Tests indicated improved conditions for both systems in C-loop tests (digital loop) 15 and 23 oct., respectively. Therefore the systems were temporarily reconnected awaiting NTA/Hamar's next initiative. 02C was disconnected from the MODCOMP 30 October due to excessive error rate caused by work going on at the NTA Lillehammer. Otherwise, scheduled work at NTA/Lillestrøm affected all communications systems weeks 41 and 42. 06C ordinary comm. line section between Hamar and the NTA central near Rokosjøen was by a mistake disconnected in the beginning of August 1984, when not needed for transfer of analog data from the NORESS experimental array. When starting recording from 06C (NORSAR) again, the short line between the CTV and Rokosjøen central was connected to the PCM equipment, which in the meantime had been installed there. Afterwards

Sub-array	Oct 84 (5) (1.10-4.11)	Nov 84 (4) (5.11-2.12)	Dec 84 (4) (3-31.12)	Jan 85 (5) (1.1-3.2)	Feb 85 (4) (4.2-3.2)	Mar 85 (4) (4-31.3)	Average ½ yr
01A	*0.71	0.002	0.02	*13.75	0.004	*31.70	7.69
01B	*1.07	*66.74	*58.93	*3.75	0.005	0.02	21.75
02B	*40.74	*19.21	0.001	0.003	0.004	0.02	9.99
02C	*5.72	*2.23	*1.17	0.002	0.004	*7.77	2.65
03C	*1.07	0.001	0.002	*5.10	0.009	0.01	1.03
04C	*47.52	0.50	0.05	*1.26	0.004	0.01	8.22
06C	*100.0	*100.0	*100.0	*21.70	*8.13	*9.13	56.49
AVER	42.40	26.89	22.88	9.11	1.17	6.81	15.40
Less	02B,02C 04C,06C	01B,02B 06C	01B,06C	01A,03C 06C	06C	01A,02C 06C	01B,06C
	0.95	0.68	0.25	1.26	0.005	0.02	5.92

* see item II.2 regarding figures with asterisks

Table II.2.1 Communications performance. The numbers represent error rates (per cent) based on total transmitted data frames. (1 Oct 1984 - 31 Mar 1985)

NTA has not been able to establish an acceptable communications channel. 03C error figures were caused by disconnection of the MODCOMP from the communications system for test purposes.

Nov. 84 Also this period NTA/Lillehammer caused 02C problems. Spikes were observed 5 November and communications tests proved bad performance in C-loop (digital loop on CTV modem). 6 November point-to-point test (Kjeller-Hornsjø) was carried out. Modems at both locations found in order; the line towards the CTV was suspected. In connection with work at Lillehammer telestation, including change of channel equipment, the original equalizers had not been reinstalled. The subarray was back in operation 7 November.

02B. Spikes observed 7 November. NTA/Hamar admitted last section of cable remained to be check. Fault location started but not finished (8 November). However, test proved noticeable improvement, but still a few errors in C-loop. The subarray was demasked and back in operation. NTA/Hamar resumed work 12 November and a "blown" pupin coil was found on the cable section near the CTV. Still a few errors were observed in the C-loop.

01B. 13 November spikes were observed on all channels due to a damaged cable, also input level to Kjeller low (- 35 dB).

02B. Communications cable broken 15 November. Cable repaired and subarray back in operation the same day. However, spikes in data were again observed on all channels (SP). NTA/Hamar found 3 more "blown" pupin coils on the last cable section. Finally, 22 November test proved error-free system.

02C. The system was down for about 2.5 hours 30 November. The same day all systems were down for a while. Afterwards 04C did not resume operation. Modem-to-modem test stated error-

free communications system. The conclusion was that a SLEM (subarray electronic module) "hang-up" had occurred. After a restart of the communications machine (MODCOMP), the system was operational again.

Dec. 84 01B resumed operation 20 December after having been down since 14 November. All communications systems were affected 28 December due to CF-channel change at Lillestrøm and Hamar telestations. 06C was still out of operation.

Jan. 85 01A. In the period 4-8 Jan we were not able to establish contact with the subarray. NMC staff visited the subarray 8 January and found in-level reduced by nearly 50%. A faulty equalizer was found and replaced (NTA/Hamar).

01B. 15 January the level toward the subarray was increased (on CF-channel level) as spikes in data were observed.

06C. As an attempt to solve the 06C communications problem, new NOKIA 2400 baud modems were installed 9 January (NDPC and CTV). After the installation a test was run modem-to-modem, apparently with acceptable results. When reconnecting the NDPC and CTV data equipment, error figures far outside specifications were observed.

Feb. 85 06C. In order to eliminate as many error sources as possible, the 06C SLEM was replaced 27 February. As no change in the error pattern was observed, the original unit was reinstalled.

Otherwise high performance of all systems in February.

Mar. 85 02C. Scheduled system work at Lillehammer telestation caused unwanted outages several times this period. Between 11 and 15 March the 02C communications system remained down. 19 and 28 March stops of approx. 2 hours duration were observed. A shorter outage occurred 22 March.

01A communication which stopped 19 March was back in operation 28 March. A bad cable caused this outage.

02B. Line work in the Hamar area caused an outage 21 March. 02B (telemetry) stations resumed operation 22 March after having been down since 18 February due to a bad communications cable. The reason for why the cable repair was postponed had connection with access problems caused by deep snow in the area.

06C. NTA/Lillestrøm and Hamar strapped the two new NOKIA 2400 modems to external clock, which is correct. We therefore believed that problem now was solved. The performance of the communications system is even worse than before the strapping. We have therefore in a letter to NTA recently asked them to reestablish the original communications path between Hamar and Rokoberget central.

O.A. Hansen

III. ARRAY PERFORMANCE

III.1 Event Processor Operation

In Table III.1 some monthly statistics of the Event Processor operation are given:

	Teleseismic	Core Phases	Sum	Daily
Oct 84	216	54	270	8.7
Nov 84	196	66	262	8.7
Dec 84	356	53	409	13.2
Jan 85	214	44	258	8.3
Feb 85	215	52	267	9.5
Mar 85	271	55	326	10.5
	1468	324	1792	9.9

Table III.1

Event Processor Statistics, Oct 1984 - Mar 1985

B. Paulsen

IV. IMPROVEMENTS AND MODIFICATIONS

IV.1 NORSAR Online System using 4331/4341 and MODCOMP Classic

We refer to the detection processor operation statistics for detailed information about uptime, communication and processing performance.

Up to January 1985 the NORSAR online and detection system consisted of oe IBM 4331 processing computer with a high-speed link to a front end communication processor which received data from all SLEMs. During this report period the 4331 has been replaced by a more powerful computer, the IBM 4341. The increased capacity gives us the opportunity to improve the processing algorithms, test processing together with online operation and makes program development easier. Together with the new processing system, we have the following main new features for the NORSAR online system:

- new disc controller
- data from 06C reestablished (06C previously used for NORESS developments)
- improved alarm system
- experience with new bulletin transfer
- ARPANET connection.

New computer

The 4331 has been replaced with our previous research computer (4341). The upgrade gives us the opportunity to more easily change the NORSAR online system with a minimum of processing stops. The 4341 is about 4 times the 4331 computer in CPU speed. The CPU speed is close to 1 Mips. The memory size on the IBM 4341 computer is 4 Mb while the 4331 only had 1 Mb. The increase memory size makes it easier to run additional programs together with the online processing.

New disc controller

In the 4331 system the disc controller was built into the computer. The built-in disc controller had some limitations such as addressing range, speed and high load on CPU. Together with the new computer (IBM 4341) we installed a new separate disc controller (3694) from Memorex.

Data from 06C

The 06C subarray is again connected to the NORSAR online system. Unfortunately, the line quality is not good enough to use the subarray as a part of the online processing. Work is being done to improve the line so the data can be used for processing purposes.

Experience with bulletin transfer

The new bulletin transfer has been running for about 8 months, and our experience is very good. Even with transfer 3 times a day our work is reduced to a minimum because the whole process is automatic. The transfer in weekend and holidays, which was difficult with the old system, is now running very well.

Future plans for bulletin transfer are to use ARPANET. The communication between the USA and NORSAR will be more flexible. Before ARPANET is used for bulletin transfer, some problems have to be cleared up. Problem areas are:

- regular use of an experimental network (the SATNET connection between Europe and the USA)
- availability of the Norwegian connection to SATNET.

Today we have an ARPANET connection through an IBM/PC. The IBM/PC is connected to Proteon's PRONET (10 Mbit network) which again is interfaced to SATNET.

We have done some experimental transfers to CSS. A new ARPANET interface directly connected to the 4341 is preferred for a regular transfer. The connection will eventually be made through a Device Attachment Control Unit (DACU) from IBM. The DACU is again connected to PRONET. With the DACU installed NORSAR can again be a full host on the ARPANET.

K. Paulsen

V. MAINTENANCE ACTIVITIES

V.1 Activities in the Field and at the Maintenance Center

The majority of the visits to the subarrays in the period have been in connection with corrective work, including repair of cables. Much time has been spent in the NORESS array covering investigations of noise and crosstalk problems, fitting up the station, clearing up and inspection of the NORESS area, improving the local oscillator stability and reducing noise and crosstalk.

Otherwise, repair of cards and other electronic equipment has been carried out at the NMC. At the NDPC different SP-channel parameters in the NORSAR array have been evaluated, after data collection and analysis. Remote adjustments of the mass position and free period on LP-instruments have been done.

A summary of the activities in the period are given in Table V.1.

Subarray/ area	Task	Date
04C	Visit to the subarray in connection with errors in the data from the subarray	3 Oct 84
01A	Location and repair of SP02 cable	17, 24, 25 Oct
04C	Remote Centering Device (RCD) replaced on EW LP-seismometer. Protection card SP04 replaced	18 Oct
02B	Visit to the subarray in connection with deteriorated data. After an attempt to replace the modem, the comm. cable was found to be the source of the errors. Repair was an NTA responsibility	18 Oct

Subarray/ area	Task	Date
06C	After the NORESS activities in the area, 15 cables had to be spliced in the period	Oct
NORSAR array	Under remote control from NDPC 17 mass position and 2 free period adjustments were done on totally 19 LP-seismometers (of which 2 had their FP adj.)	Oct
01A	SP cable (02) repaired after breakage	6,7 Nov
01B	Located damaged SP cable (04). Replaced Remote Centering Device (RCD) for FP and Mass Position (MP) NS seism., R-A5 SP02, 05 adjusted	
06C	Check-out of cables and electronic equipment in connection with restart of subarray operation	12, 15 Nov
NORESS area	Final inspection/clearing of the area after the field and construction work. Besides engagement in connection with erecting a fence and road bar	16, 19-21 23, 26-28 Nov
NORSAR array	Monitoring and control of the NORSAR array (from NDPC) resulted in 9 adjustments of MP and 2 FP adjustments on totally 11 LP-seismometers	Nov
01A	In connection with private trenching work in the area NMS staff had to point out NORSAR cables	5 Dec
NORESS	Quite a few days spent on different tasks, such as fitting up the central station, clearing the station area, etc.	Dec
NMC	Repaired faulty circuit cards on various electronic equipment	Dec
NORSAR array	Under remote control from NDPC 22 adjustments of Mass Position (on 21 LP-seismometers), and 4 adjustments of Free Period (on 1 LP-seismometer) were carried out	Dec

Subarray/ area	Task	Date
02B Telemetry	Battery replacement on receiver station	2 Jan 85
01A	Replaced RA-5 ampl. on SP01 and 00	4 Jan
01A	Attenuated channel (04) moved from 00 to the 60 m borehole	
01A	NMC staff to the subarray in connection with line problems	8 Jan
03C	On NS-seismometer replaced data coil, MP and FP motors. Battery charger repaired, distilled water added to batteries. Dry-out of the LPV started due to excessive moisture	17 Jan
02B Telemetry	Attempts to access the subarray failed due to snow problems	29 Jan
03C	Inspection of the LPV still indicated moisture	30 Jan
06C	New NOKIA modems 2400 baud installed in the CTV and at the NDPC. Also PCM line reconfigured with respect to equalizers. Good test results modem-to-modem, but with data equipment (Modcomp/SLEM) hooked up, error at an average of 0.2 % a day was observed. Investigation to be continued.	30 Jan
NORESS	Due to noise problems, RC-filters were installed	Jan
NORSAR Array	Remote adjustment (8) of Mass Pos. (on 6 LP seismometers). In addition regular checks of Mass Pos. (MP) and Free Period (FP)	Jan
01B, 02B, 02C, 03C	Data collection and analysis in connection with discovering possible missing numbers in ADC conversion	Jan
03C	Dry-out of LPV continued, conclusion after subarray visit	18 Feb
NORESS	NMC staff mainly engaged in solving noise and cross-talk problems	Feb
NORSAR array	Remote adjustment (5) of Mass Position (5 LP seismometers and 1 Free Period adjustment	Feb

Subarray/ area	Task	Date
01B, 04C	Channel parameters as RA-5 gain, seismometer sensitivity and channel resolution calculated (by means of the CHANEV SP program)	
01A, 04C	Data collection and analysis in connection with discovering possible missing numbers in the ADC conversion	
02B (Telemetry)	NTA Hamar finished the work on the telephone line and stations back in operation	12 Mar
01A	Subarray visited in connection with SP(04) data 180° out-of-phase	19 Mar
01A	NMC staff to the subarray to point out an SP cable in connection with trenching work	20 Mar
NORESS	Accuracy of the Local Oscillator improved by replacing the LO crystal	March
NORESS	Station D4 visited and Fiberoptic Transmitter replaced	March
NORSAR array	Remote adjustment (10) of Mass Pos. (on 8 LP seismometers) and Free Period (3) on same number of LP seismometers.	March

Table V.1 Activities in the field and at the NORSAR Maintenance Center, October 1984 - March 1985.

V.2 Improvements and Modifications

Attenuated channel (04) moved from borehole 00 to the 60 m hole.

V.3 Array Status

As of 31 March 1985 the following channels deviated from tolerances:

01B 05

04C 03

06C (not in operation due to comm. system)

01A 01 8 Hz filter

02 -"-

04 Attenuated 30 dB

O.A. Hansen

VI. DOCUMENTATION DEVELOPED

Bache, T. and H. Bungum (1985): High frequency P wave attenuation from Central Asia to Norway, Submitted for publication BSSA

Bungum, H., S. Mykkeltveit and T. Kværna (1985): Seismic noise in Fennoscandia, with emphasis on high frequencies, submitted for publication.

Husebye, E.S., G.L. Johnson and Y. Kristoffersen (1985): Geophysics of the Polar Regions, Elsevier Sci. Publ.

Kennett, B.L.N. and S. Mykkeltveit (1984): Guided wave propagation in laterally varying media - II. Lg waves in north-western Europe. Geophys. J.R. astr. Soc. 79, 257-267.

Loughran, L.B. (ed.): Semiannual Technical Summary, 1 April - 30 September 1984, NORSAR Scientific Report, November 1984.

Mykkeltveit, S. and H. Bungum (1984): Processing of regional seismic events using data from small-aperture arrays. Bull. Seism. Soc. Am. 74, 2313-2333.

L.B. Loughran

VII. SUMMARY OF TECHNICAL REPORTS/PAPERS PREPARED

VII.1 Real time event detection using the small-aperture NORESS Array

Since January 1985 data from the new small-aperture array NORESS in Norway have been processed in real time at the NORSAR data center at Kjeller. The data used in the detection processing comprise 25 SPZ channels, deployed over an area 3 km in aperture and sampled at a 40 Hz rate. The detection algorithm has been described by Mykkeltveit and Bungum (1984), and briefly consists of

- Digital narrow-band filtering (six filters)
- Beamforming (conventional and incoherent)
- STA/LTA detector applied to each beam
- Frequency-wavenumber analysis of detected signals
- Association of regional phases to aid in locating events.

In the following, initial results from this processing are described, together with recommendation for future research.

Teleseismic events

The P-wave signal-to-noise ratio at NORESS typically peaks in the 2-4 Hz band for teleseismic events in Eurasia, whereas lower dominant frequency is often observed for signals from the western hemisphere and for epicentral distances exceeding 70 degrees. Signal coherency is naturally very good for teleseismic P across NORESS, even at very high frequencies. Depending on signal frequency, the best beam SNR is obtained using various subsets of the array; e.g., at 2 Hz the best subset consists of the center instrument A0 together with the C and D rings (see Fig. VII.1.1). Using this subset, the beamforming gain meets

or exceeds $\sqrt{N}$, due to the noise suppression characteristics described in Section VII.2.

An example of teleseismic processing results from NORESS is given in Fig. VII.1.2. The improvement in SNR on the beam relative to the single sensors is quite remarkable.

The on-line procedure uses steered teleseismic beams rather than a single infinite-velocity beam for each filter. The resulting SNR gain is, as an example, 4-5 dB for an apparent velocity of 16 km/s, at 3 Hz frequency. For lower frequencies or higher velocities, the gain is less. Thus, applying only infinte-velocity beamforming for teleseismic detection is a viable alternative, in view of the possibility of operating at a lower detection threshold with the same false alarm rate.

The NORESS array detects many teleseismic signals not observed at the large aperture NORSAR array, which, like NORESS, is located in southeastern Norway; especially from selected regions in Eurasia. On the other hand, the signal focusing effects underneath NORSAR cause some instruments to have up to an order of magnitude stronger signals than NORESS sensors, for regions such as Hindu Kush and the Kuriles. For these regions, NORESS does not match the NORSAR detection capability.

Because of the small aperture of NORESS, only a very coarse automatic estimate of the location of teleseismic events is currently being made. Azimuth errors depend on phase velocity and frequency, and are often around 5-10 degrees for small events. Slowness estimates from the automatic process are typically about 1 sec/deg different from those of NORSAR. Nevertheless, it is clear that location estimates from a small array like NORESS will be very valuable to provide a starting point for association procedures using a seismic network.

Regional corrections and more detailed off-line analysis are required to assess the eventual capabilities of the array in this regard.

Local and regional events

At local and regional distances, the best SNR for the P wave varies from 3-5 Hz (at around 1000 km) to more than 8 Hz (local distances). Consequently, either steered beams or incoherent beamforming is necessary to exploit the array capability. P-signal coherency at NORESS is usually good enough to utilize the full array for F-K processing of local and regional P-phases, at least up to about 6-8 Hz.

The Lg phase is usually of slightly lower frequency than P. Conventional beamforming is not very efficient for Lg, since the preceding coda (from Sn) comes in with about the same phase velocity and azimuth. Consequently, little "noise" suppression takes place. A promising approach is that of performing narrow-band filtering at several frequencies for the purpose of Lg detection. It turns out that the SNR is greatly improved in those frequency bands where P and Sn coda energy are low relative to the Lg energy. Combining narrow-band filtering with incoherent beamforming has been found particularly effective.

An example of a complete record from a regional event processed at NORESS is given in Fig. VII.1.3. The detection times for P and Lg are marked on the panel of Fig. VII.1.3a, whereas Fig. VII.1.3b shows F-K solutions for P and Lg together with short plots of each phase in an expanded time scale. The estimated azimuths for P and Lg differ by 2 degrees in this case; and a deviation of 0-5 degrees is common. However, a difference of 10 degrees and more is also fairly often observed in the automatic solution.

The location accuracy of NORESS for regional events is currently being studied. No statistically reliable results are available so far due to the limited data base of known locations. The procedure of locating events by associating P and Lg is applicable only up to about 1200 km distance. At greater distances, the Lg usually is too weak to be detected automatically, but can sometimes be identified by visually inspecting the waveform plots.

In conclusion, the initial results obtained from NORESS are very encouraging, and have met and in some cases exceeded the expectations. Data quality has been excellent, and the operational stability has been very satisfactory, taken into account the complexity of the system. Particularly noteworthy is the excellent P detection in the 2-4 Hz band, which is due to greater than $\sqrt{N}$ noise suppression combined with strong P-wave energy. The automatic detection of secondary phases needs refinement, and in particular the narrow-band filter bank processing should be further investigated.

F. Ringdal

References

Mykkeltveit, S. and H. Bungum (1984). Processing of regional seismic events using data from small-aperture arrays, Bull. Seis. Soc. Am., 74, 2313-2333.

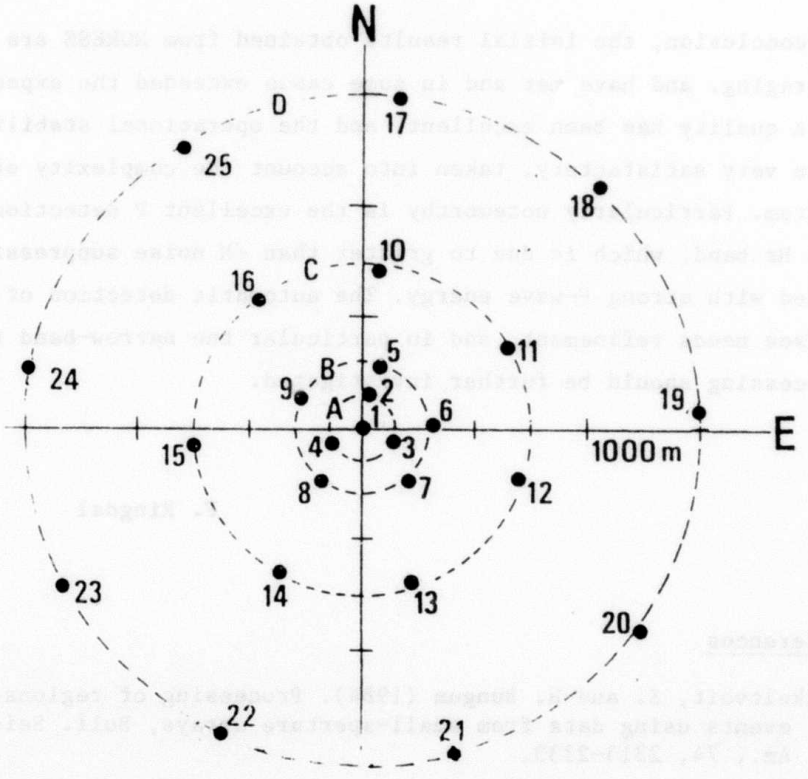

Fig. VII.1.1 Geometry of the NORESS array. The array comprises 25 SPZ seismometers over an area 3 km in diameter. The four rings - A, B, C, D - are marked on the figure.

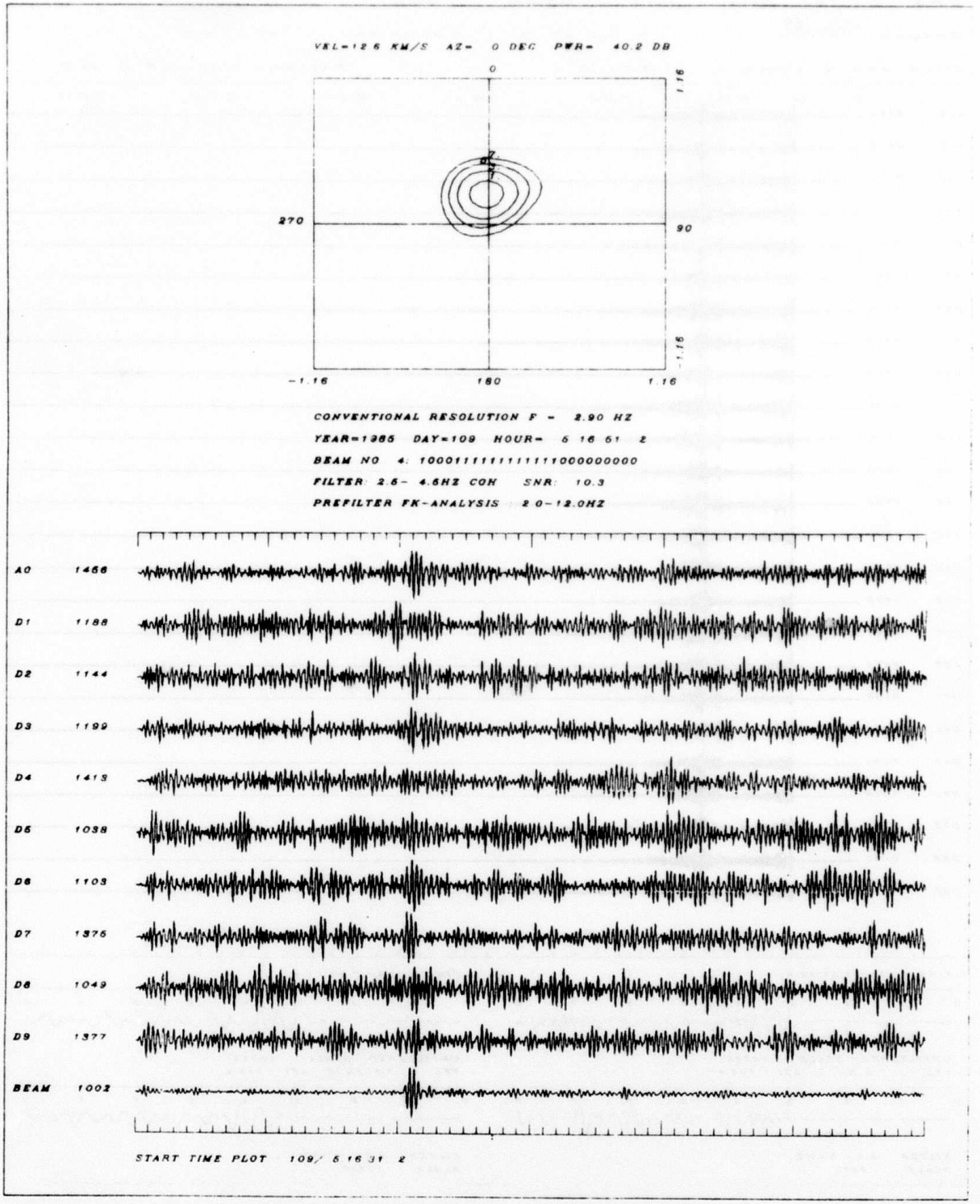

Fig. VII.1.2 Example of automatic processing of a teleseismic event using NORESS. The on-line F-K solution is shown at the top, together with detection parameters. Ten individual sensor traces (filtered 2.5-4.5 Hz) are plotted, together with the array beam (bottom).

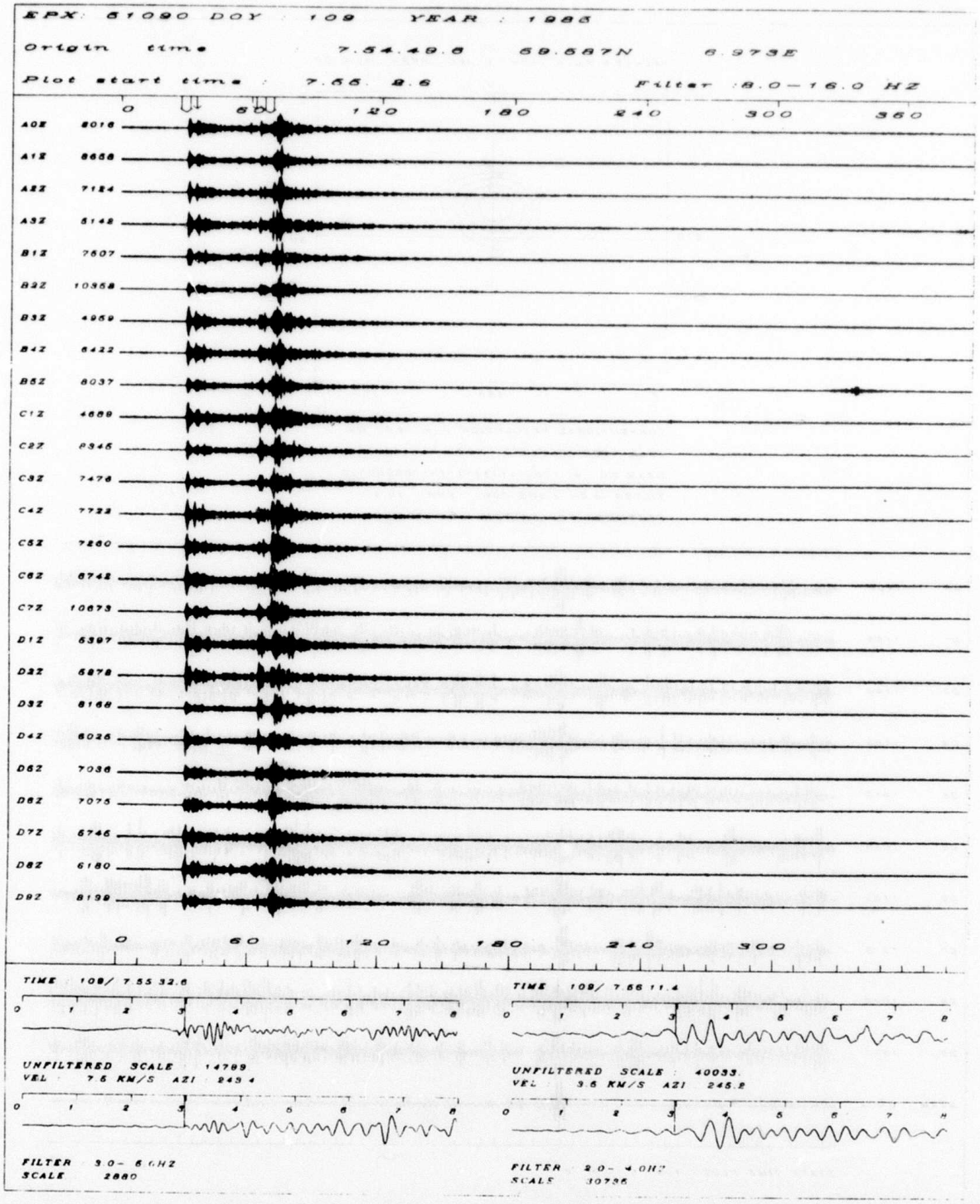

Fig. VII.1.3a Individual NORESS traces for regional event 19 April 1985. The panel covers 6 minutes of bandpass filtered records (8-16 Hz). P and Lg beams are also shown (bottom part).

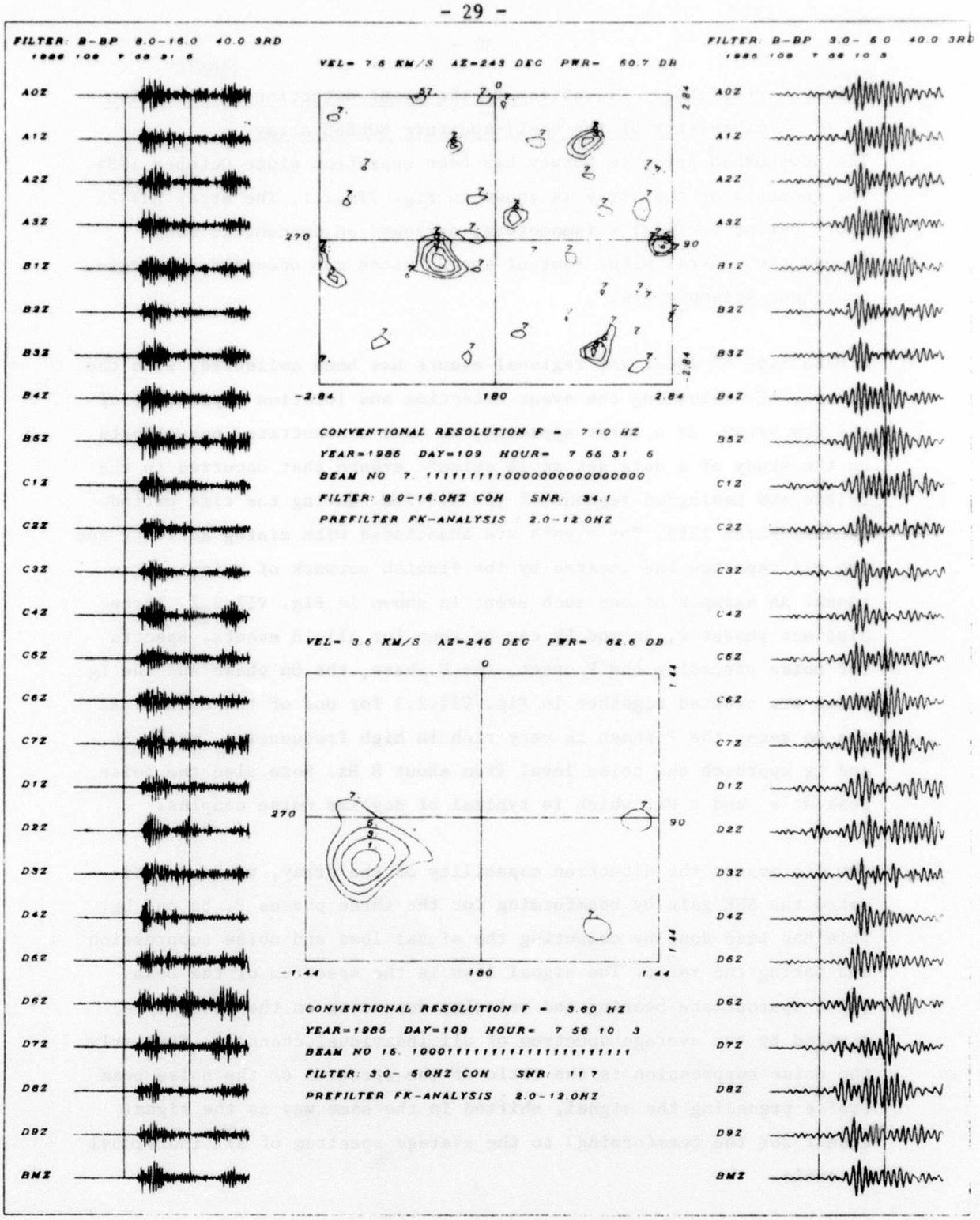

Fig. VII.1.3b NORESS automatic analysis results for the event of Fig. VII.1.3a. The P-phase (left) and Lg phase (right) are shown for all SPZ instruments. F-K solutions are shown for P (top) and Lg (bottom).

VII.2 Preliminary evaluation of the event detection and location capability of the small-aperture NORESS array

The new NORESS array in Norway has been operation since October 1984. The geometry of the array is shown in Fig. VII.2.1. The array has 25 short period vertical seismometers, arranged on concentric rings around the central site. Four of the 25 sites are occupied by three-component seismometers.

A data base of local and regional events has been collected, with the purpose of evaluating the event detection and location capability of the new array. As a first approach, we have concentrated our efforts on the study of a data set of 18 seismic events that occurred in the Baltic and Leningrad regions of the U.S.S.R. during the time period January-March 1985. The events are associated with mining activity and are all reported and located by the Finnish network of seismic stations. An example of one such event is shown in Fig. VII.2.2. Three distinct phases P, Sn and Lg can be seen for all 18 events. Spectra for noise preceding the P onset, the P phase, the Sn phase and the Lg phase are plotted together in Fig. VII.2.3 for one of the events. As can be seen, the P phase is very rich in high frequencies, while Sn and Lg approach the noise level from about 8 Hz. Note also the noise peak at around 6 Hz, which is typical of daytime noise samples.

Now, to assess the detection capability of the array, we have estimated the SNR gain by beamforming for the three phases P, Sn and Lg. This has been done by computing the signal loss and noise suppression and taking the ratio. The signal loss is the spectrum of the beam (with appropriate bearing and velocity depending on the phase type) divided by the average spectrum of all individual channels. Similarly, the noise suppression is the ratio of the spectrum of the noise beam (noise preceding the signal, shifted in the same way as the signal itself for the beamforming) to the average spectrum of all individual channels.

The noise spectra have been estimated using the indirect covariance method. We first estimate the correlation function by splitting a long data record into many windows, calculating a sample correlation function for each window, then averaging the sample correlation functions. Typically, we use 20 windows, each of which is 5 seconds long. Because the earth noise has such a large dynamic range, we prewhiten it prior to estimating the correlation function with a low-order prediction-error filter. The spectrum is then estimated by windowing the correlation function with a 3 second Hamming window, then computing the Fourier Transform. The spectral estimate obtained this way is compensated then for the effects of prewhitening.

The signal spectrum is calculated by windowing the signal with a 10% cosine taper window, 5 seconds long, then calculating the Fourier Transform and finally squaring the transform.

When we do direct comparison of the noise spectrum, which is a power density spectrum, with the signal, which is an energy density spectrum, we divide the signal spectrum by the length of the signal analysis window to convert energy density to power density. The two spectral quantities are then directly comparable. This has been done in Fig. VII.2.3.

The signal loss, noise suppression and SNR gain by beamforming have been computed for four different array configurations:

- All elements included ("ALLV" in the figures)
- All elements minus A-ring ("INTERMEDIATE")
- Center instrument, C-ring and D-ring ("TELEV")
- All elements minus D-ring ("HIFREQ").

In Fig. VII.2.4, noise suppression curves, representing averaging over the 18 events, are shown for all four array geometries. The horizontal lines represent $\sqrt{N}$ suppression of noise, where N is the number of sensors in the geometry under consideration. This is the expected level

for noise that is uncorrelated over the entire array. As can be seen, the "TELEV"-geometry is remarkably good in suppressing the noise in the 1.5-3.5 Hz band, while the other geometries approach the $\sqrt{N}$ level for various frequencies, but do not show better noise suppression than $\sqrt{N}$. These results partly reflect on the SNR gains shown in Fig. VII.2.5. the signal losses (not shown) tend to be larger for the larger geometries (including outer rings) because of the decaying signal correlation with increasing station separation. The overall effect is to level the gain curves, and we can see from Fig. VII.2.5 that only at fairly low and fairly high frequencies do the gain curves for the different geometries deviate substantially.

For the Sn and Lg phases, the "noise suppression" estimates reflect suppression by beamforming of the P and Sn coda, respectively, i.e., we address the problem of detecting a secondary phase in the coda of a preceding phase. Results shown in Fig. VII.2.6 are for the Lg phase and correspond to the best SNR result obtained among the four geometries. SNR-gain is now well below $\sqrt{N}$, essentially because of failure to suppress the Sn coda, which propagates with similar phase velocity and azimuth as the Lg onset. Still, there is a 6 dB gain from beamforming at 1.2 Hz.

Fig. VII.2.7 shows the P onset for a Novaya Zemlja explosion (distance approx. 20^{o}) recorded on NORESS, and the SNR gain by beamforming computed as before for the "TELEV" configuration. In the frequency range 1.0-2.7 Hz the gain is better than $\sqrt{N}$, because of a very modest signal loss in combination with optimum noise rejection, as for the "TELEV"-configuration in Fig. VII.2.3. The same result is visualized in the time domain in Fig. VII.2.8.

Our approach to the location performance evaluation has been to compute narrow-band FK-spectra for the P, Sn and Lg signals for the events in the data base. FK-spectra have been computed for the array subsets given above and for frequencies corresponding to distinct spectral maxima for each phase. Typical results are given in

Table VII.2.1 for one event. As can be seen, the analysis frequency is the critical parameter, and more so than the array subgeometry used in the evaluation of the FK-spectra. According to these results, then, the arrival azimuth varies fairly strongly with frequency and due care must be taken in selecting the analysis frequency. To gain more insight into these frequency-dependent lateral refraction effects, we have computed the broad-band maximum likelihood FK-spectra for a number of phases. One example is shown in Fig. VII.2.9, where the azimuth's dependency on frequency is given implicitly in the contour plot. The azimuth value of 89.5 serves to illustrate that the broad-band FK tends to give more stable estimates than those derived from narrow-band FK-spectra.

The research effort continues with analysis of events from other regions, in order to obtain the capabilities of the new NORESS array for local and regional events from all source regions of interest. As experience is gained, the results from this study will be utilized directly in the online processing of NORESS data.

S. Mykkeltveit
D.B. Harris, Lawrence
Livermore National Laboratory
T. Kværna

	P at 3.40 Hz		P at 6.35 Hz		Sn at 2.20 Hz		Lg at 1.33 Hz		Lg at 1.80 Hz	
Array	Vel	Az	Vel	Az	Vel	Az	Vel	Az	Vel	Az
HIFREQ	11.71	80.8	9.73	92.3	5.05	86.1	4.55	95.5	4.31	109.0
ALLV	11.58	86.1	10.14	95.8	5.02	84.0	4.29	95.4	4.07	106.9
INTERM	11.52	86.2	10.15	95.9	5.02	84.0	4.29	95.5	4.08	105.7
TELEV	11.51	86.3	10.07	98.1	5.03	84.0	4.28	95.0	4.10	102.3

Table VII.2.1 Narrow-band FK-results for one event in the Baltic-Leningrad region data base. According to the location reported by the network of Finnish seismic stations, the true azimuth for NORESS is 91.6°.

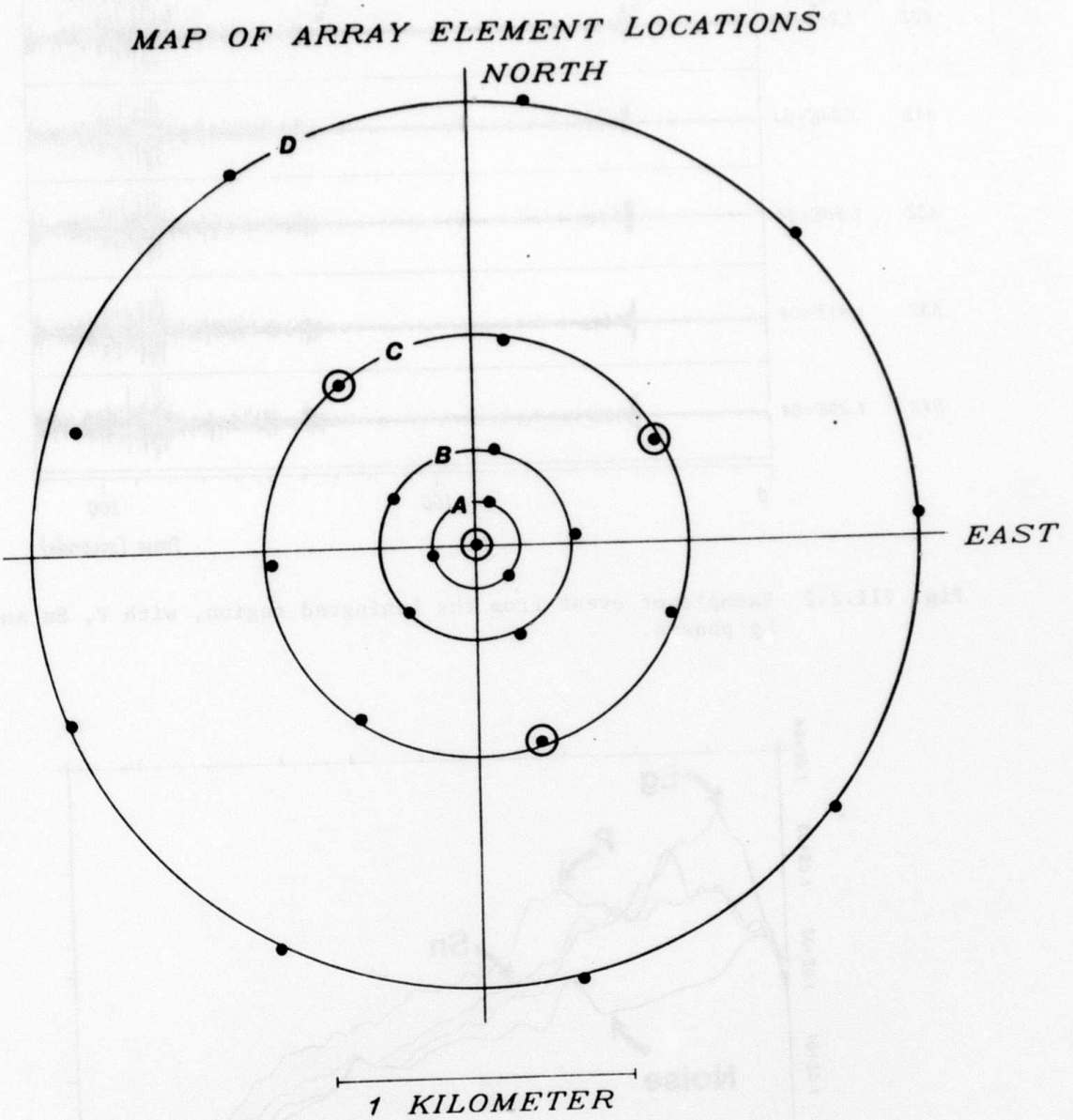

Fig. VII.2.1 Geometry of the new NORESS array. The four three-component stations are marked with special symbols.

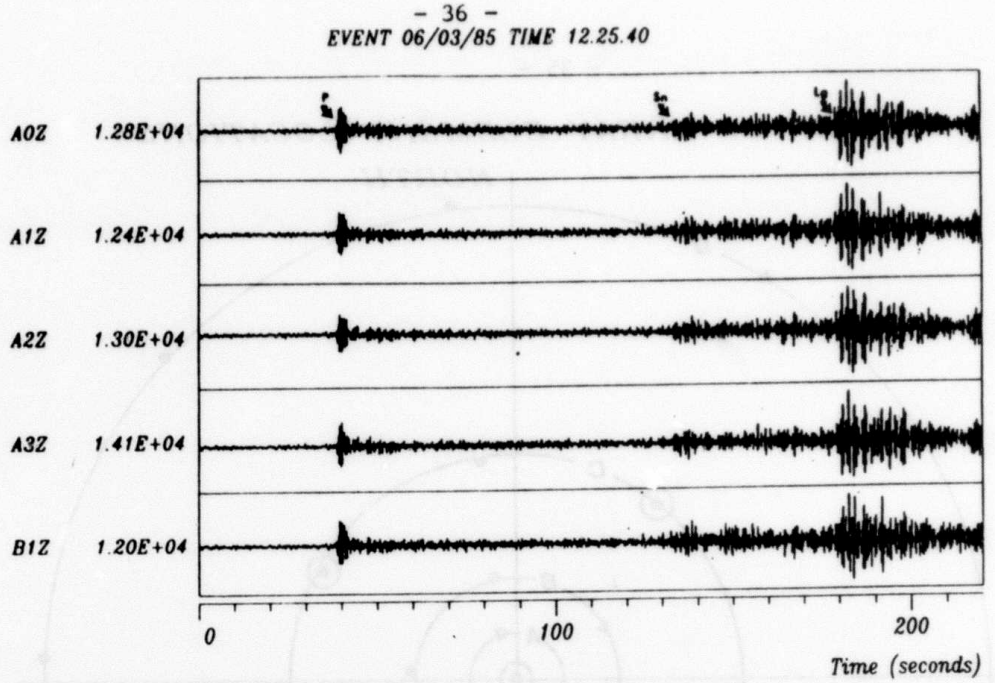

Fig. VII.2.2 Example of event from the Leningrad region, with P, Sn and Lg phases.

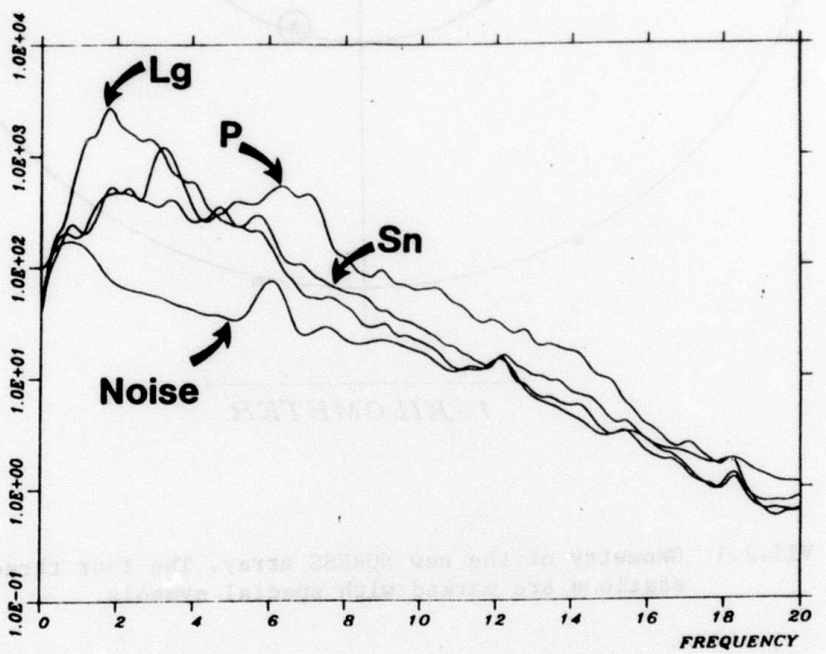

Fig. VII.2.3 Spectra for the P, Sn and Lg in Fig. VII.2.2 and for noise preceding the P arrival.

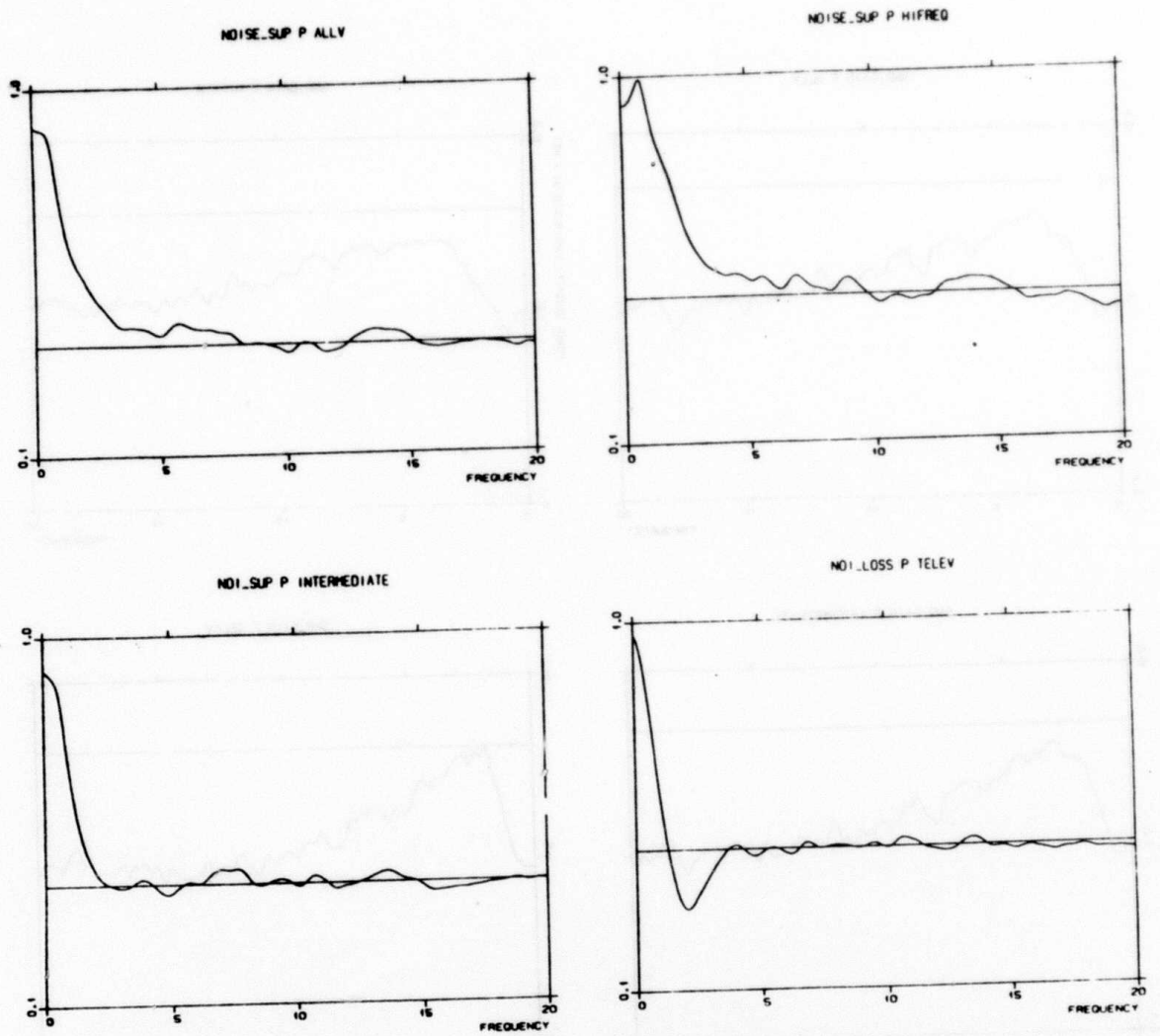

Fig. VII.2.4 Noise suppression for the four array subgeometries. The horizontal line represents $\sqrt{N}$ noise rejection, where N is the number of sensors in each subgeometry. The vertical scale is logarithmic.

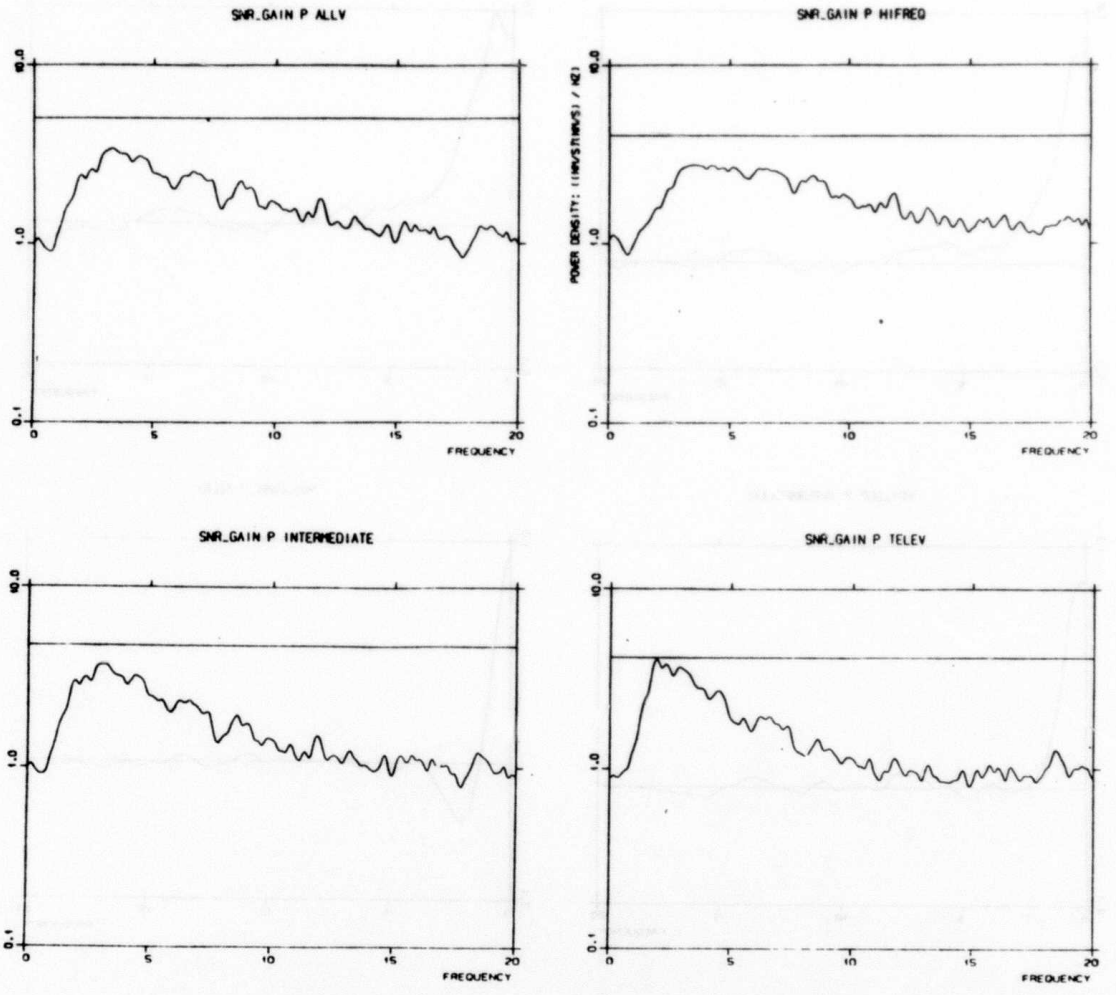

Fig. VII.2.5 SNR gain by beamforming of regional P phase for the four array subgeometries. The horizontal line represents $\sqrt{N}$ gain, where N is the number of sensors in each subgeometry. The vertical scale is logarithmic.

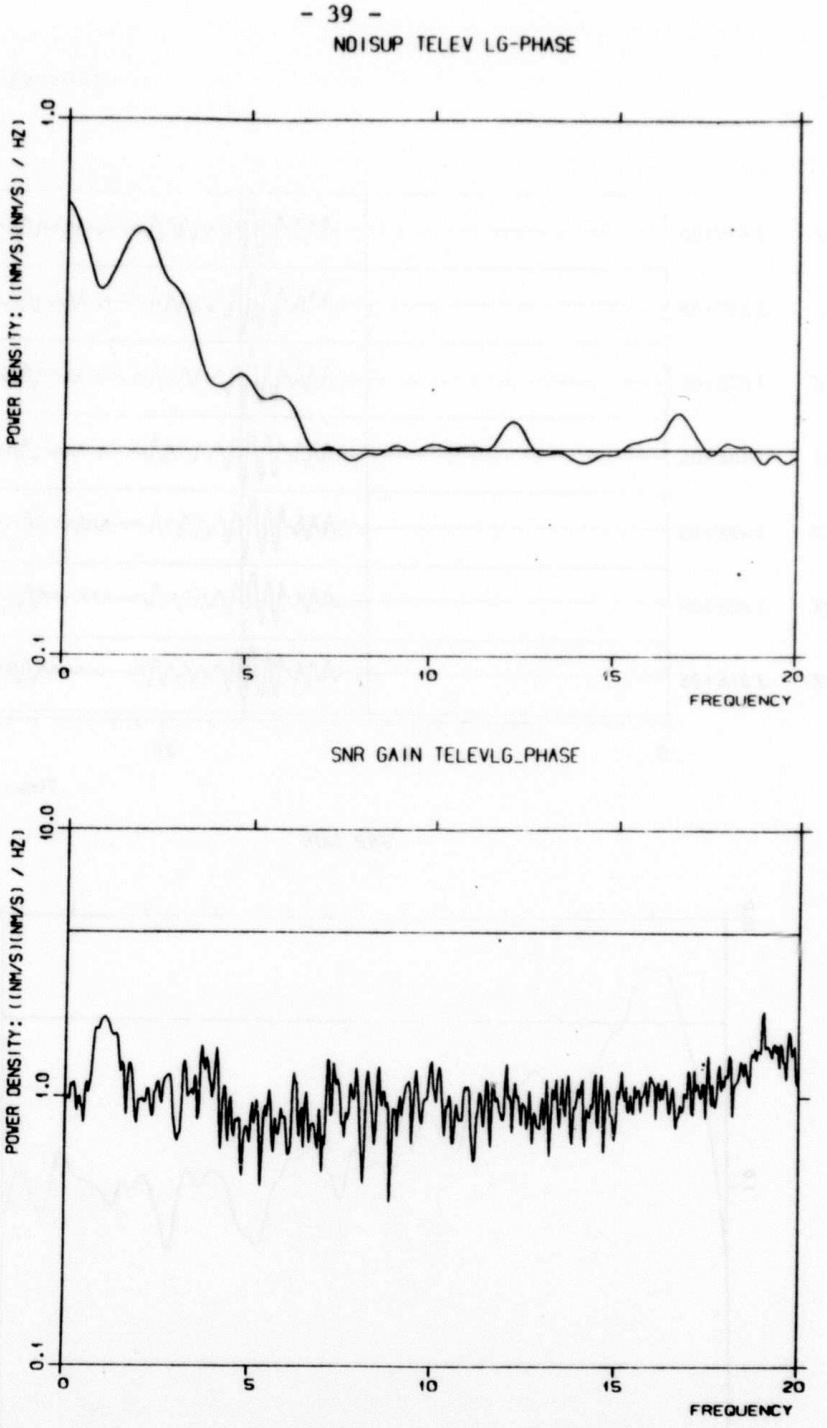

Fig. VII.2.6 Noise suppression and SNR gain for the Lg phase for subgeometry "TELEV". Horizontal lines represent √N-noise rejection (upper plot) and √N-beamforming gain (lower plot), with N = 17 for this subgeometry. Vertical scales are logarithmic.

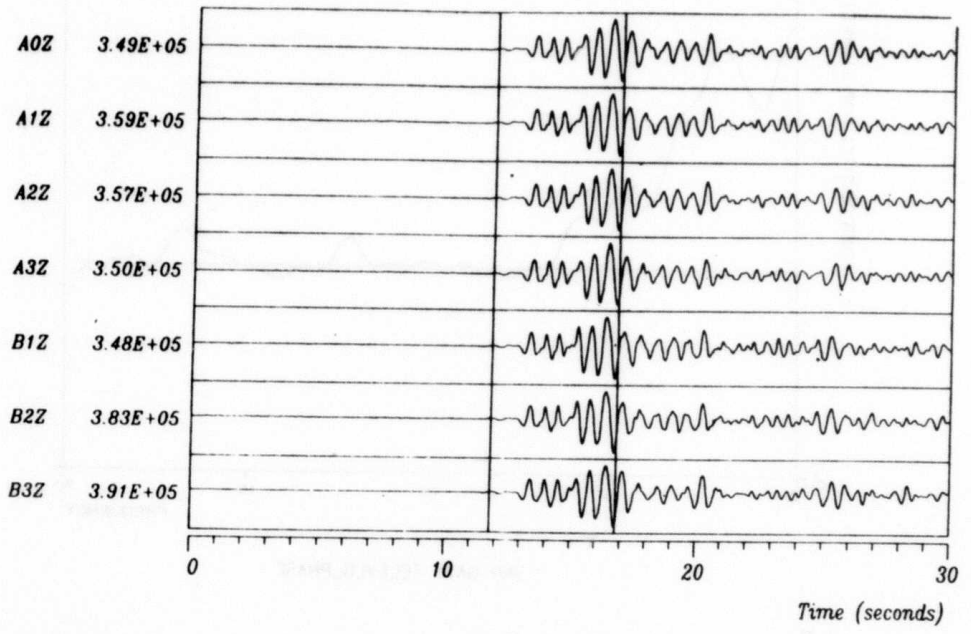

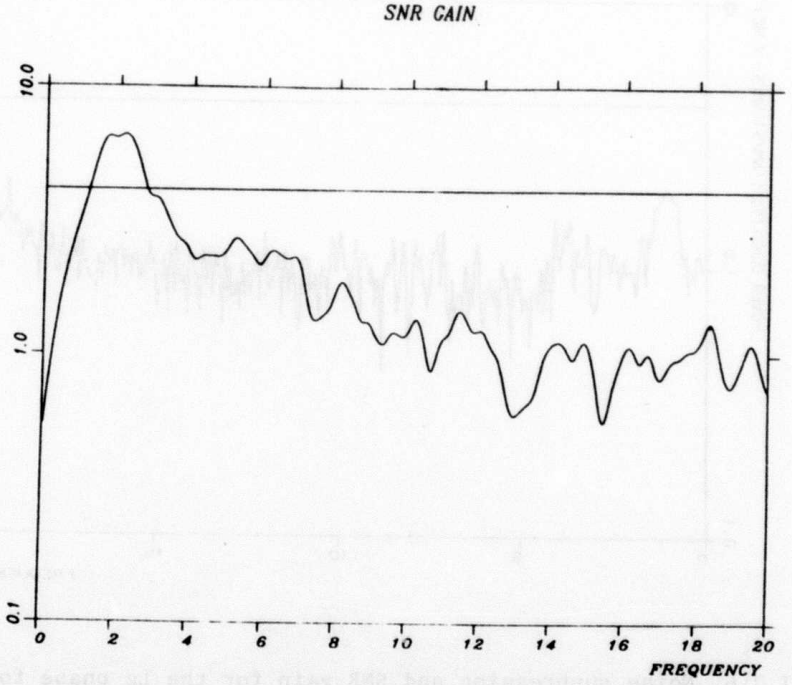

Fig. VII.2.7 Beamforming gain for array "TELEV" for P-arrival from Novaja Zemlja event. P-wave data analysis window on top. The horizontal line in the gain plot indicates $\sqrt{N}$ gain, with N = 17 for this subgeometry.

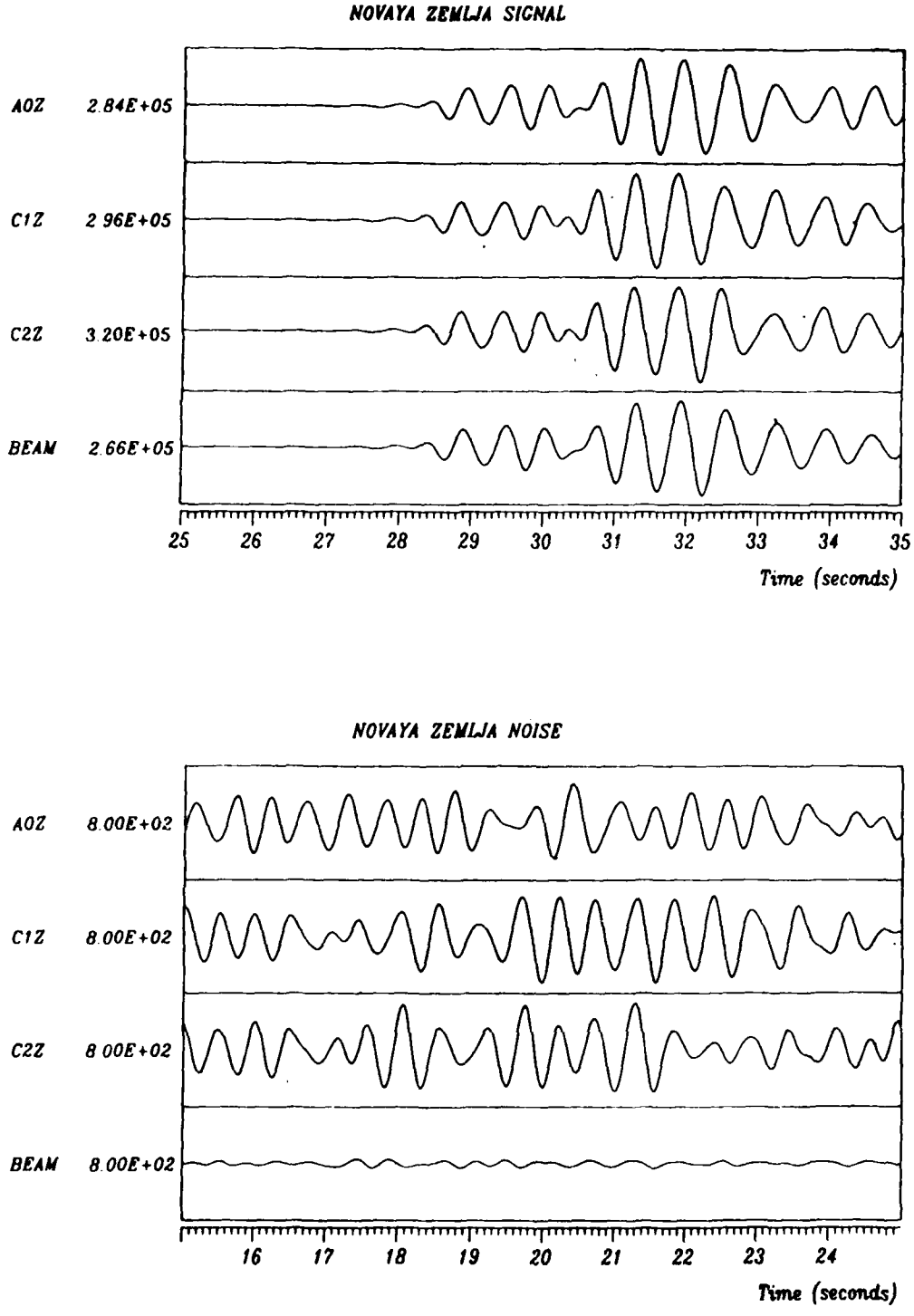

Fig. VII.2.8 Time domain illustration of the SNR-gain results in Fig. VII.2.7. Top: Normalized plot of three single channels (out of the 17 participating in the beam) and the beam, showing a very modest signal loss. Bottom: Noise rejection obtained on preceding noise (true amplitude plot). The filter bandpass is 1.3-2.5 Hz, corresponding to the peak in the gain curve in Fig. VII.2.7.

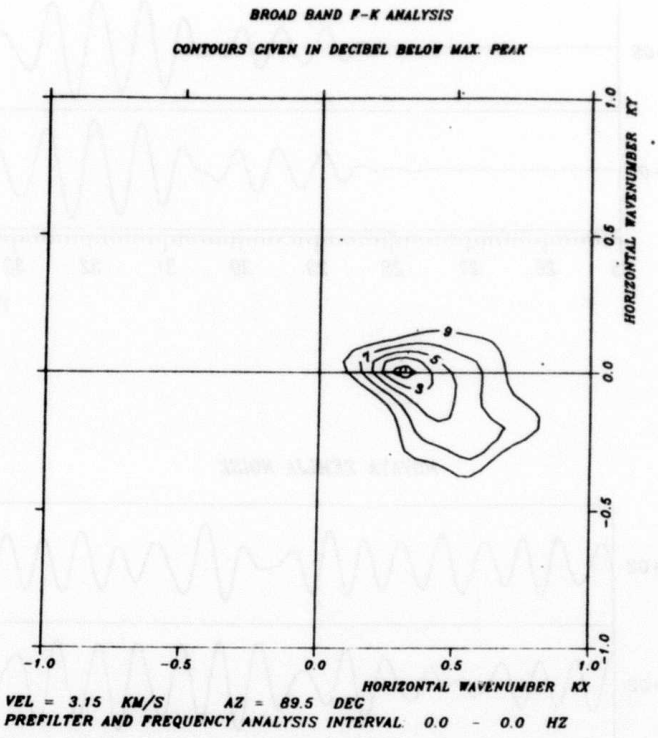

Fig. VII.2.9 Broad-band FK-analysis for the Lg phase of the event used in Table VII.2.1. In order to obtain the velocity corresponding to the peak, the value of 3.15 km/s must be multiplied by the dominant frequency of the Lg signal (1.33 Hz) to yield a phase velocity of 4.19 km/s.

VII.3 Seismic modelling of an anisotropic boundary layer

Various parts of the upper mantle have been proposed to be anisotropic. More recently it has been suggested that anisotropy may also be present at other depths, especially in boundary layers experiencing differential flow. D" is such a layer. More specifically, we may need to consider a model of D" with two distinct structures, resembling the continent-ocean division of the lithosphere. The possibility of observing the appearance of a layered structure would be restricted to the permanent (continental-type) zones, whereas intrinsic anisotropy predicted by boundary layer theory would prevail in the transient (ocean-floor type) zones. The possibility of lateral heterogeneity has an added significance in this context because it has been suggested that, when interpreted in terms of one-dimensional models, such structures may appear anisotropic (Crampin et al, 1984). For the purpose of seismic modelling, we assume uniaxial anisotropy (with symmetry axis vertical), often termed transverse isotropy in the seismological literature, not that we believe this to apply locally, but because we assume that azimuthal anisotropy is averaged out by the several wave paths used in observational work. The required modifications to reflectivity type of methods have been discussed, a.o. in a recent contribution (Doornbos et al, 1985). Piecewise smooth models were considered here. The formal expressions for (generalized) reflection coefficients are unchanged, but the required modifications concern the fundamental matrices, and the vertical slownesses and their integrals over radius, the so-called "Tau functions".

One inference is that for radius r not far from the turning point r_o, τ is determined mainly by the profile of horizontal wave velocity. This is in accordance with the results of a numerical experiment giving the effect of anisotropic D" on the diffracted wave fields of P and SH. In Fig. VII.3.1 are shown the changes (relative to the isotropic approximation) in logarithmic attenuation with distance and $dT/d\Delta$, as functions of frequency, which is the form in which most observational data have been presented. From these results we conclude that diffracted P and SH are mainly controlled by the horizontal velocities

α_L and β_L, respectively, and these are related to the elastic constants A and N of a uniaxial structure. On the other hand, five elastic constants (A,C,N,L and F) are needed to fully characterize this structure, and four constants (A,C,N and F) are needed to obtain the bulk modulus K. What is usually inferred for the purpose of temperature calculations is an apparent bulk modulus K' based on the assumption of an isotropic structure: $\lambda+2\mu = A$, $\mu = N$. We find

$$K/K' \simeq \frac{3}{(3-4N/A)} \cdot \frac{1-N/A-(F/A)^2}{2-N/A-2F/A} - \frac{1-C/A}{3(3-4N/A)} \qquad (1)$$

where

$$F/A = \eta\left(1-2\,\frac{N}{A}\cdot\frac{L}{N}\right)$$

Results based on eq. (1) are given in Table VII.3.1. These results can be used to conclude that a small amount of anisotropy requires a correction to the seismically inferred temperature increment based on K'. For D" it is estimated that the correction can be up to about 400°K.

D.J. Doornbos

References

Crampin, S., E.M. Chesnokov and R.G. Hipkin (1984): Seismic anisotropy - the state of the art, II. Geophys. J. R. astr. Soc. 76, 1-16.

Doornbos, D.J., S. Spiliopoulos and F.D. Stacey (1985): Seismological properties of D" and the structure of a thermal boundary layer, submitted for publication.

L/N / η	0.9	0.92	0.94	0.96	0.98	1.00
0.9	1.005	0.997	0.990	0.983	0.976	0.968
0.92	1.012	1.004	0.997	0.990	0.982	0.975
0.94	1.018	1.011	1.004	0.996	0.989	0.981
0.96	1.025	1.018	1.010	1.003	0.995	0.987
0.98	1.032	1.025	1.017	1.009	1.002	0.994
1.00	1.035	1.031	1.024	1.016	1.008	1.000

Table VII.3.1 **Ratio of uniaxial and isotropic bulk modulus K/K'**
Assumed relation between isotropic and uniaxial elastic constants:

$$\lambda + 2\mu = A, \quad \mu = N$$

Results based on eq. (1) with N/A = 0.28 and C/A = 1.
If C/A ≠ 1, subtract (1-C/A)/5.64 from all results.
The broken line encloses the ranges of elastic constants that appear to us to be the most plausible.

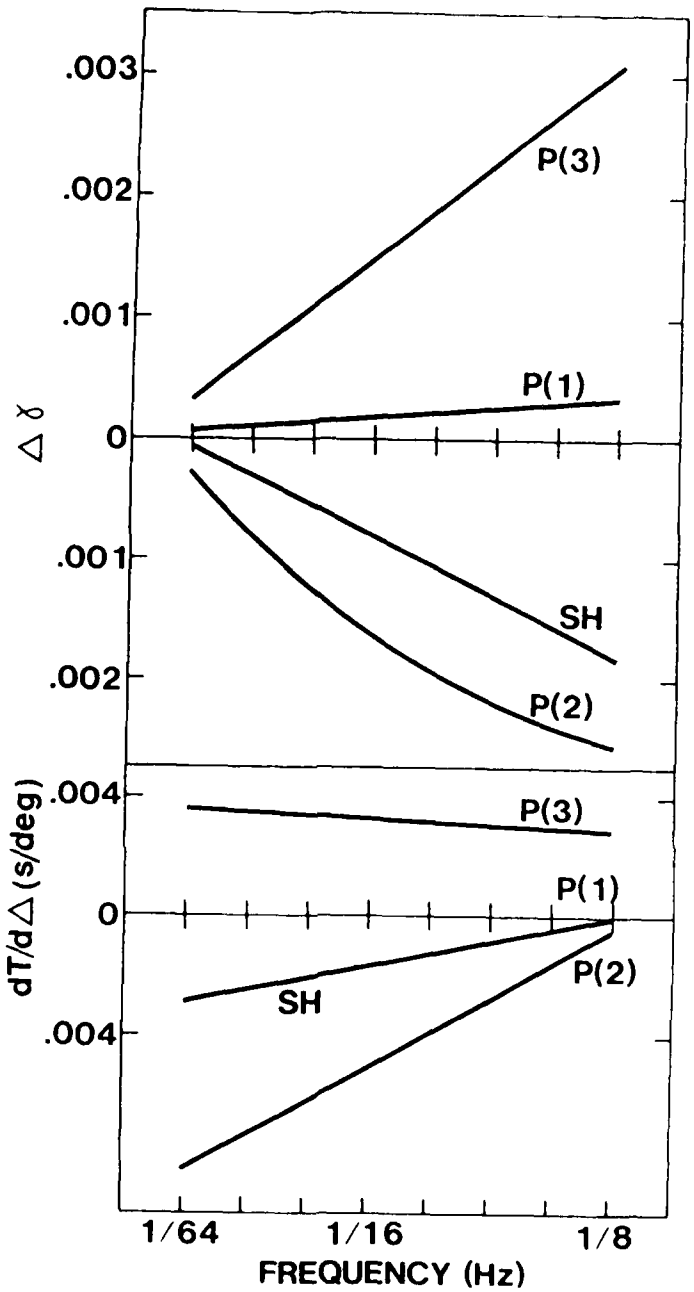

Fig. VII.3.1 Effect of a transversely isotropic layer on logarithmic attenuation (γ) and $dT/d\Delta$ of diffracted P and SH around the core. The distance range considered is 100-135°. The velocities α and β in the isotropic part of the model, and the horizontal velocities α_h for P and β_h for SH in the layer, correspond to model A of Doornbos et al (1985). The anisotropy is zero at the top of the layer, and the maximum at the bottom. The maximum anisotropy for SH is $\beta_h/\beta_v = 1.02$. The three P-wave anisotropies considered are (1) $\alpha_h/\alpha_v = 1.01$, $\eta = 1$, $\beta_h/\beta_v = 1$; (2) $\alpha_h/\alpha_v = 1$, $\eta = 0.95$, $\beta_h/\beta_v = 1$; (3) $\alpha_h/\alpha_v = 1$, $\eta = 1$, $\beta_h/\beta_v = 1.02$. The values plotted are differences from results with isotropic model A.

VII.4 An application of long-period waveform inversion to shallow sources under the Tibetan Plateau

In previous semiannual summaries we have reported on the development of long-period waveform inversion methods. We have now applied these methods to analyze shallow focus sources under the Tibetan Plateau. The purpose of this work was threefold:

1) To compare the performance of different methods for determining source parameters and location, and for determining travel time and amplitude residuals
2) To test current hypotheses concerning recent tectonics of Tibet, as implied by the principal stress pattern and the source depths
3) To determine station residuals and compare these residuals to those for deep events.

The methods we have applied include a centroid-moment tensor method comparable to the one described by Dziewonski and Woodhouse (1983), and a correlation method as described by Doornbos (1985). Both methods require the calculation of Green's functions in a realistic earth model; we have used a WKBJ method for mixed paths, and we have modified PREM by incorporating in the source region a crustal model for Tibet, and under the receivers an appropriate continental model. The principal differences between the methods concern the nature of the inversion procedure (linearized versus non-linear inversion) and the optimization criterion (least-squares error versus maximum correlation). On the basis of analysis of GDSN data with P and SH waveforms from seven events in Tibet, we conclude that the non-linear correlation method leads to more stable results. There are several reasons for this: (1) the correlation method is less sensitive to the initial value for source location. This is an important point since the standard focal depth value (33 km) used by NEIS for most of these events is significantly more than the values obtained in this work

(<10 km). (2) The correlation method explicitly accounts for travel time anomalies and is robust with respect to amplitude anomalies at the different stations. An example of a result by the correlation method is given in Fig. VII.4.1. The fault plane solution in this figure illustrates that faulting is consistent with east-west extensional tectonics. This was in fact found for all events as summarized in Fig. VII.4.2, and it supports one of the competing theories which have been proposed for this region. The fact that all focal depth values obtained by the correlation method are less than 10 km is moreover consistent with a relatively hot crust (c.f. Chen and Molnar, 1983). In the previously reported analysis of deep events it was found that the travel time residuals of S are surprisingly large; there was both a base line effect and a trend with epicentral distance. It is of interest to compare this result to the travel time residuals for the shallow focus events analyzed here. These residuals are plotted in Fig. VII.4.3; a correction for finite source duration has been applied here. To interpret the P residuals, note that the origin times given by NEIS involve the J-B velocity model and focal depths which are usually taken to be 33 km. Travel time effects due to systematic error in focal depth and due to the difference between the J-B model and the modified PREM model used here amount to about -3.5 s. This explains the P residuals in Fig. VII.4.3, as expected.

The S residuals would have to be correspondingly corrected by adding + 3.5 s. The corrected S residuals at the larger epicentral distances are then slightly negative, but on average the residuals are small. This contrasts with the large positive S residuals for deep events. It suggests the need for modifications of the PREM model involving both the upper and lower mantle.

Ø. Pettersen

D.J. Doornbos

References

Chen, W.P. and P. Molnar (1983): Focal depths of intracontinental and intraplate earthquakes and their implications for the thermal and mechanical properties of the lithosphere, J. Geophys. Res., 88, 4182-4214.

Doornbos, D.J. (1985): Source solutions and station residuals from long-period waveform inversion of deep events, J. Geophys. Res., in press.

Dziewonski, A.M., and J.H. Woodhouse (1983): An experiment in systematic study of global seismicity: Centroid-moment tensor solutions for 201 moderate and large earthquakes of 1981, J. Geophys. Res., 88, 3247-3271.

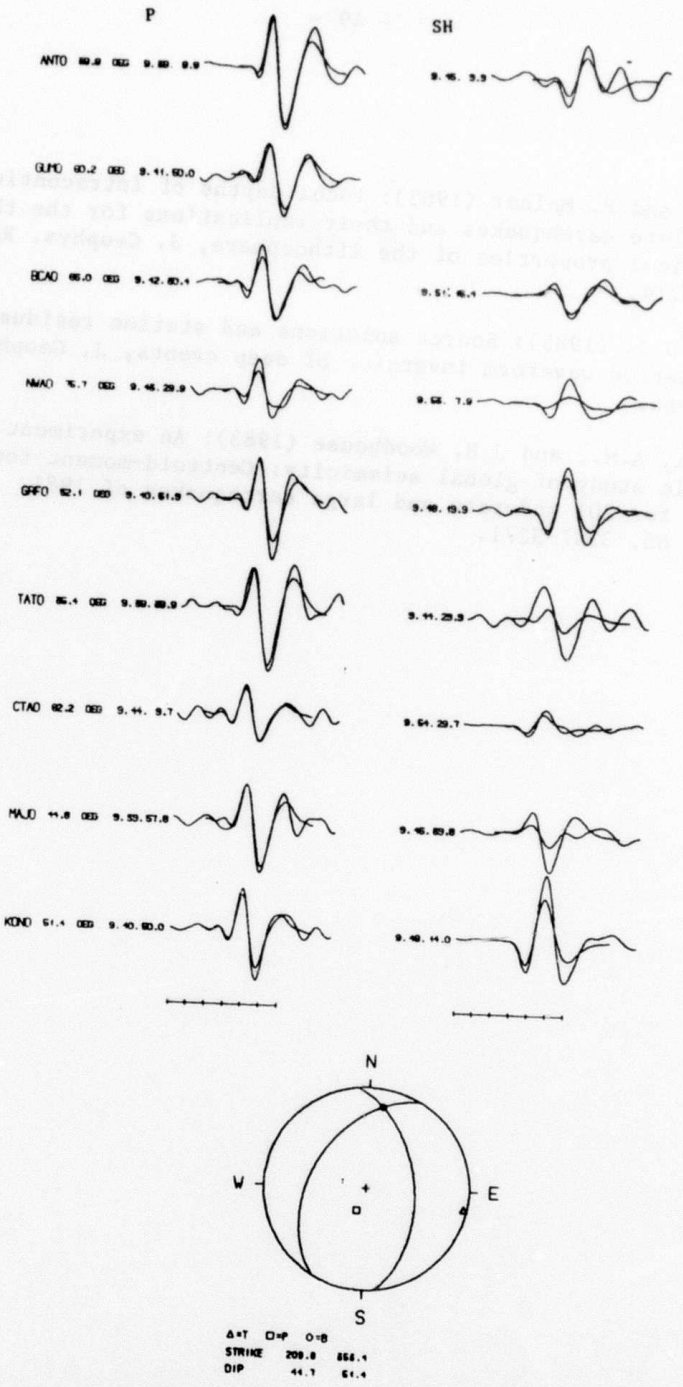

Fig. VII.4.1 Source analysis for one of the events in this study. Observed and synthetic waveforms at GDSN stations, together with the double-couple approximation to the moment tensor solution, in equal area projection of the lower focal hemisphere. The centroid depth is 5 km. The time axis is in 10 s intervals.

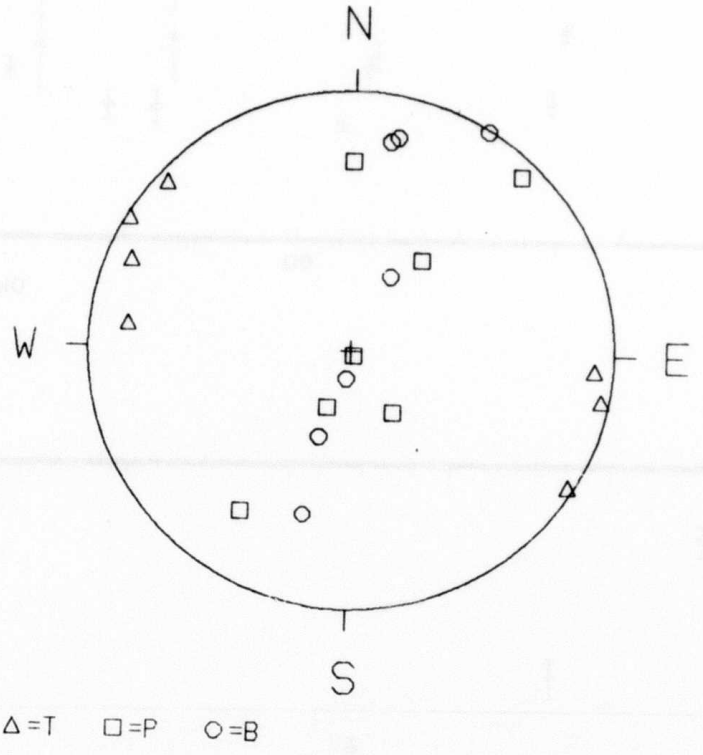

Fig. VII.4.2 **Principal axis of 7 shallow sources under the Tibetan Plateau, in equal area projection of the lower focal hemisphere.**

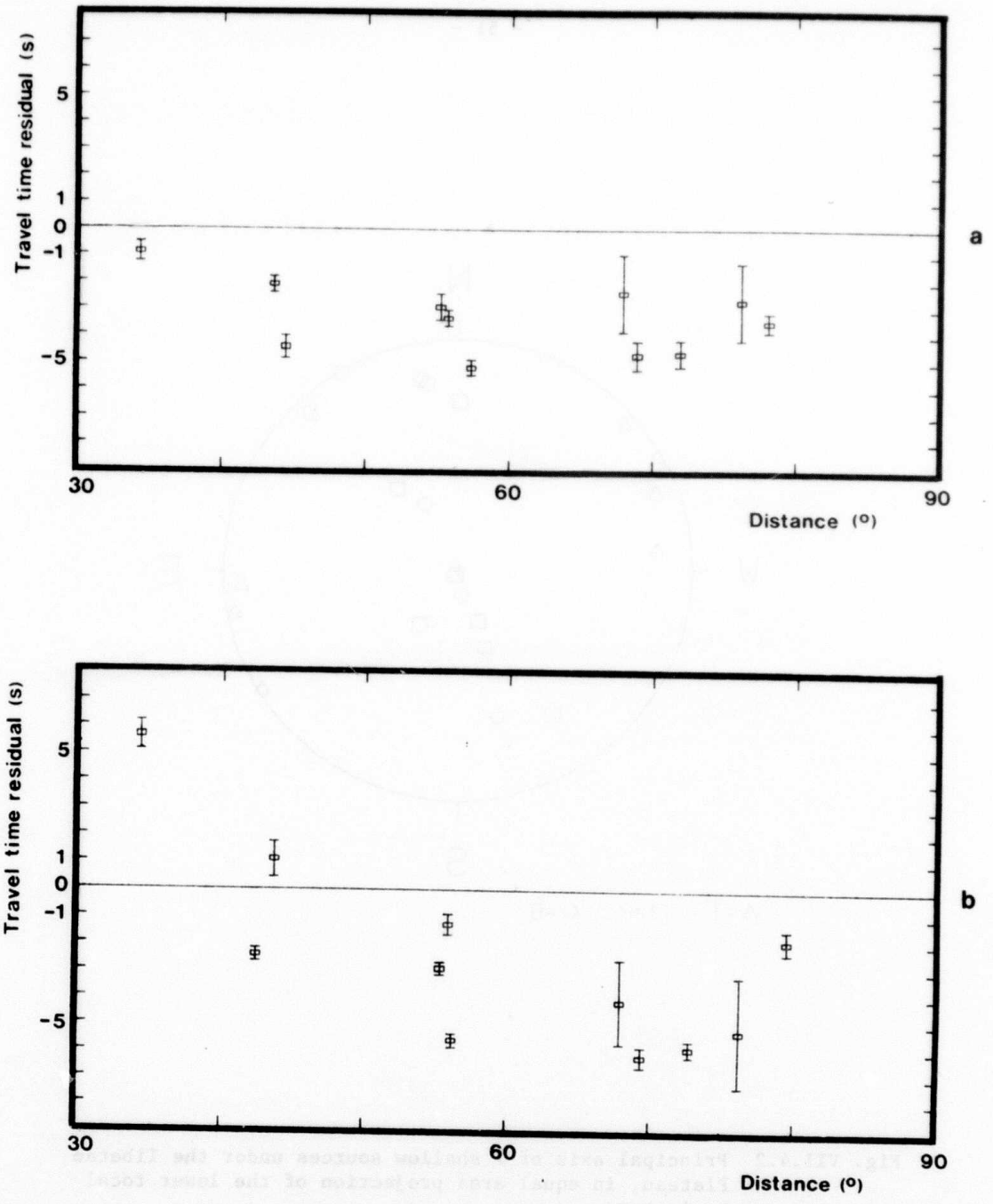

Fig. VII.4.3 Travel time residuals versus distance for P (a) and SH (b). The residuals are defined as observed minus predicted. Each station is positioned at the average distance from the events which were recorded.

VII.5 Interactive analysis program for use with NORESS data

We have completed a flexible analysis program for processing the NORESS data in an interactive manner. This code will be used in coming months to assess the performance of the new regional array and to examine a variety of aspects of wave propagation in the region.

The program provides basic file manipulation and plotting functions. Data can be read into the program from standard NORESS tapes or from disk file images of the tapes. The program also has the capability of writing and reading data to disk files in its own format for temporary storage. The data storage part of the program is organized as a signal stack, that is, it is a first-in first-out push down stack, where entries on the stack are signals. Signals may be popped off of the top of the stack into the local-format files, or pushed onto the stack from those files.

The top of the stack is the reference point for all commands. The default operand for all unary operations is the top signal on the stack, and for binary operations the default operands are the top two signals. Usually, a command can be extended to apply to any number of operations, such as scaling, absolute value, square root, are provided as well as binary operations like addition, subtraction, multiplication, division of signals. These are pointwise operations. Basic filtering, spectral analysis, and array processing functions, such as stacking and FK calculations, are also incorporated.

Several canned plotting routines are available to plot trace data, array response patterns and FK spectra as contour maps or perspective drawings, power spectra, and maps of array geometry (Fig. VII.5.1 and VII.5.2). To a limited extent, the plots can be titled and labeled. The viewing window for the trace data plotting command is under cursor as well as keyboard control. This provides for convenient zooming on a

particular window and also for cursor selection of the analysis window for analysis functions that operate on some restricted domain of interest.

The code is command driven, rather than menu driven, to enhance the speed of interaction. A help command has been provided to list the available command options and syntax. A primitive macro facility exists as well, permitting groups of commands to be stored in external files and accessed with a single macro call (Fig. VII.5.3). Macro calls can be nested to a maximum depth of four, but may not be recursive.

A facility for storing temporary numerical and character values has been implemented. We have called this facility the "blackboard", although it is far from a blackboard in the expert system sense of the term. Blackboard entries are named, and they may be referred to by name as arguments to all of the commands in the program. Simple arithmetic and string manipulations can be performed on blackboard entries as well.

The purpose of the blackboard is to facilitate automatic processing of large amounts of data. Blackboard entries are useful for passing arguments to macros, effectively turning the macros into subroutines. This approach makes it possible to build up extensive and fairly sophisticated signal processing and measurement capabilities from the primitive operations supplied in the program. Our intent was to provide a flexible "breadboard" for trying new ideas that would also have the capability for production work with a new method, once that method had proved useful.

D.B. Harris, Lawrence
Livermore Ntl. Laboratory
T. Kværna

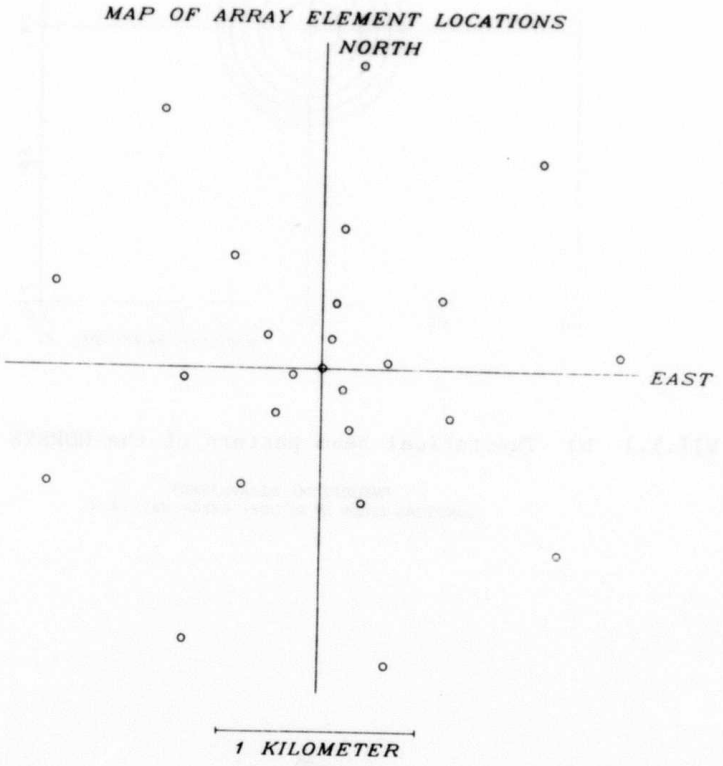

Fig. VII.5.1 a) Locations of the vertical instruments of the NORESS array.

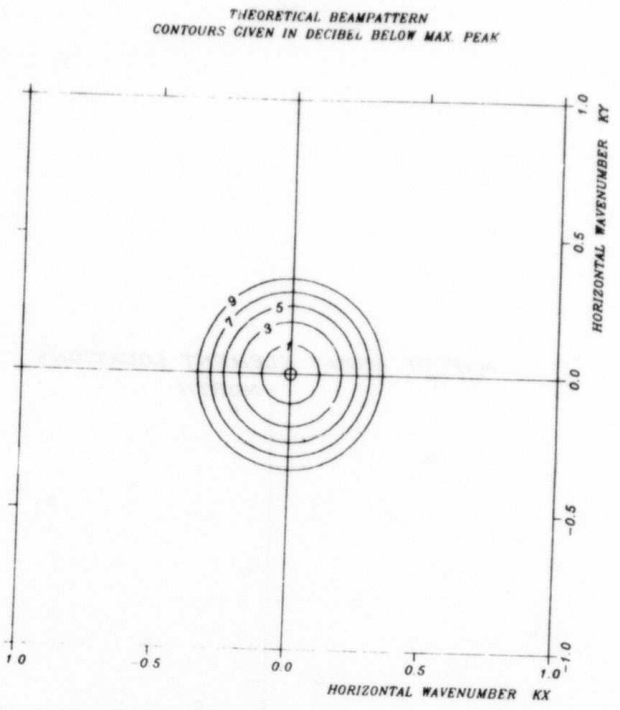

Fig. VII.5.1 b) Theoretical beam pattern of the NORESS array.

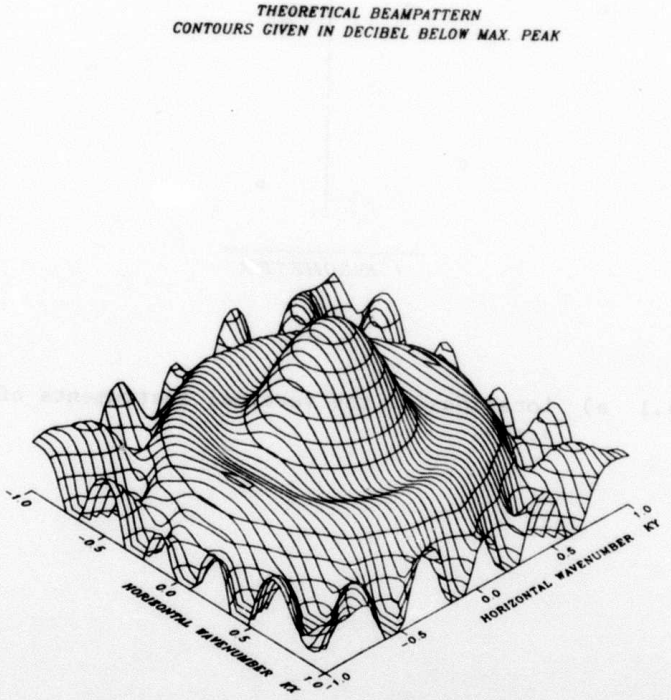

Fig. VII.5.1 c) Perspective view of the theoretical beam pattern of the NORESS array.

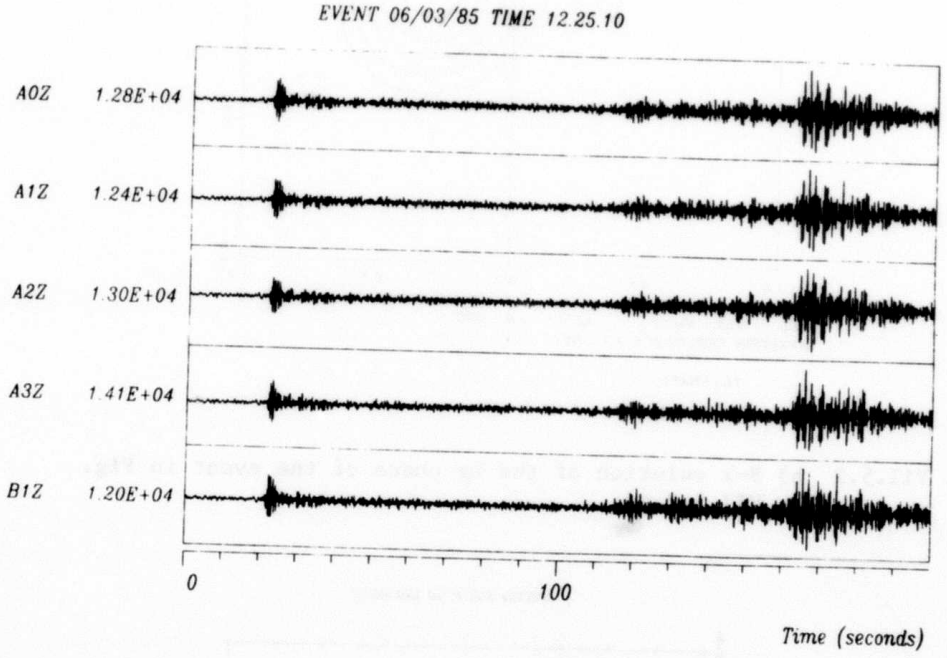

Fig. VII.5.2 a) Example of regional event.

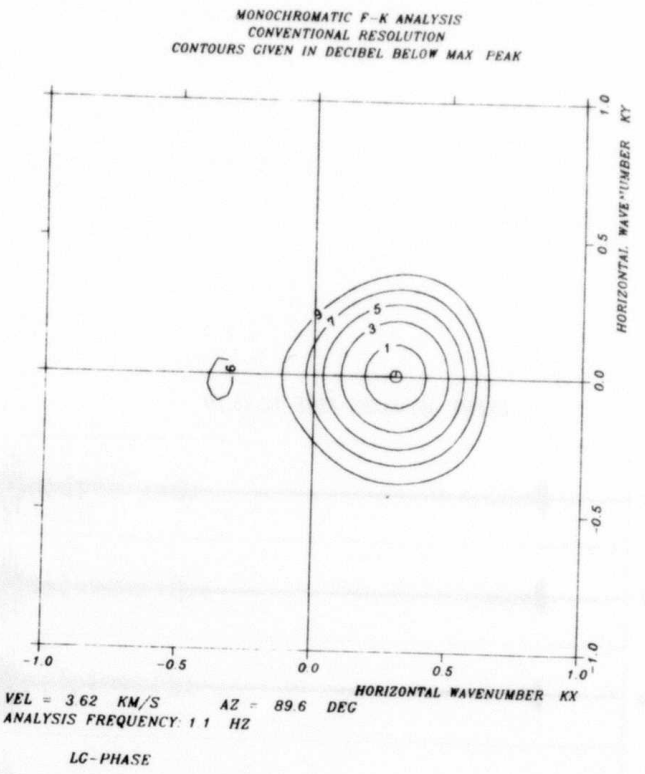

Fig. VII.5.2 b) F-k solution of the Lg phase of the event in Fig. VII.5.2 a).

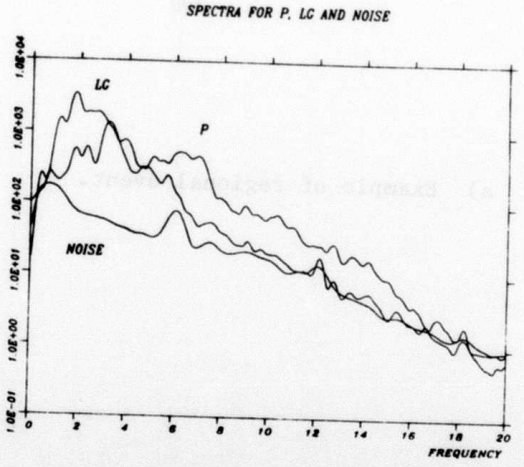

Fig VII.5.2 c) Spectra for noise preceding the P phase, the P phase and the Lg phase of the event shown in Fig. VII.5.2 a).

```
"                    PW-SPECT                                    "

" MACRO TO PREWHITEN TOP STACK SIGNAL AND CALCULATE ITS SPECTRUM WITH "
"   THE EFFECTS OF PREWHITENING COMPENSATED FOR.  EFFECTIVELY        "
"   FLUSHES THE TOP STACK SIGNAL.  SPECTRUM ON TOP OF STACK.         "
 1
 2   PREWHITEN .
 3   SWAP .
 4   SETW ON :SIGNAL-START :SIGNAL-STOP .
 5   CUT .
 6   SETW OFF .
 7   WINDOW COSINE .
 8   PAD TO 1024 .
 9   FFT .
10   SQR 2 .
11   ADD .
12   SWAP .
13   FLUSH .
14   SWAP .
15   FFT .
16   SQR 2 .
17   ADD .
18   SWAP .
19   FLUSH .
20   SWAP .
21   DIVIDE .

22   TERMINAL .
```

LOGIC OF THE PW-SPECT MACRO

```
 1 SIGNAL ON TOP OF THE STACK
   STACK: SIGNAL
```

Fig. VII.5.3 PW spectra (page 1 of 3).

```
 2 PREWHITEN .
   PREWHITEN THE THE TOP SIGNAL AND PUT THE PREWHITENING FILTER ON
   TOP OF THE STACK (1024 POINTS).
   STACK: PREWHITENING FILTER, SIGNAL

 3 SWAP .
   SWAP THE TWO FIRST SIGNALS
   STACK: SIGNAL, PREWHITENING FILTER

 4 SETW ON :SIGNAL-START :SIGNAL-STOP .
   SET ANALYSIS WINDOW ON THE SIGNAL TRACE . THE VALUES OF SIGNAL-START
   AND SIGNAL-STOP ARE CALLED FROM THE BLACKBOARD .
   STACK: SIGNAL, PREWHITENING FILTER

 5 CUT .
   STORE THE PART OF THE SIGNAL WITHIN THE ANALYSIS WINDOW, ERASE THE
   REST .
   STACK: SIGNAL (NOW SHORTER), PREWHITENING FILTER

 6 SETW OFF .
   SET ANALYSIS WINDOW OFF THE SIGNAL TRACE .
   STACK: SIGNAL, PREWHITENING FILTER

 7 WINDOW COSINE .
   WINDOW THE TOP SIGNAL WITH A COSINE WINDOW .
   STACK: SIGNAL, PREWHITENING FILTER

 8 PAD TO 1024 .
   INCREASE THE LENGTH OF THE SIGNAL TO 1024 POINTS BY ADDING ZEROS .
   NECESSARY TO MAKE IT COMPARABLE TO THE PREWHITENING FILTER.
   STACK: SIGNAL, PREWHITENING FILTER

 9 FFT .
   TAKE THE FFT OF THE TOP SIGNAL AND STORE THE REAL AND IMAGINARY
   PART ON TOP OF THE STACK.
   STACK: SPECTRUM (REAL), SPECTRUM (IMAGINARY), SIGNAL, PREWHITENING
          FILTER

10 SQR 2 .
   SQARE THE TWO TOP SPECTRA .
   STACK: SPECTRUM (REAL), SPECTRUM (IMAGINARY), SIGNAL, PREWHITENING
          FILTER

11 ADD .
   ADD THE TWO TOP SPECTRA .
   STACK: ENERGY DENSITY SPECTRUM, SIGNAL, PREWHITENING FILTER
```

Fig. VII.5.3 PW spectra (page 2 of 3).

```
12 SWAP .
   SWAP THE TWO FIRST SIGNALS .
   STACK: SIGNAL, ENERGY DENSITY SPECTRUM , PREWHITENING FILTER

13 FLUSH .
   FLUSH OFF THE TOP SIGNAL .
   STACK: ENERGY DENSITY SPECTRUM , PREWHITENING FILTER

14 SWAP .
   SWAP THE TWO FIRST SIGNALS .
   STACK: PREWHITENING FILTER, ENERGY DENSITY SPECTRUM

15 FFT .
   TAKE THE FFT OF THE TOP SIGNAL AND STORE THE REAL AND IMAGINARY
   PART ON TOP OF THE STACK.
   STACK: SPECTRUM (REAL), SPECTRUM (IMAGINARY), PREWHITENING FILTER,
          ENERGY DENSITY SPECTRUM

16 SQR 2 .
   SQARE THE TWO TOP SPECTRA .
   STACK: SPECTRUM (REAL), SPECTRUM (IMAGINARY), PREWHITENING FILTER,
          ENERGY DENSITY SPECTRUM

17 ADD .
   ADD THE TWO TOP SPECTRA .
   STACK: ENERGY DENSITY SPECTRUM (PREWHITENING FILTER), PREWHITENING
          FILTER, ENERGY DENSITY SPECTRUM

18 SWAP .
   SWAP THE TWO FIRST SIGNALS .
   STACK: PREWHITENING FILTER, ENERGY DENSITY SPECTRUM (PREWHITENING
          FILTER), ENERGY DENSITY SPECTRUM

19 FLUSH .
   FLUSH OFF THE TOP SIGNAL .
   STACK: ENERGY DENSITY SPECTRUM (PREWHITENING FILTER), ENERGY DENSITY
          SPECTRUM

20 SWAP .
   SWAP THE TWO FIRST SIGNALS .
   STACK: ENERGY DENSITY SPECTRUM, ENERGY DENSITY SPECTRUM
          (PREWHITENING FILTER)

21 DIVIDE .
   DIVIDE THE TWO TOP SPECTRA POINT BY POINT TO ACCOUNT FOR THE EFFECT
   OF PREWHITENING.
   STACK: ENERGY DENSITY SPECTRUM

22 TERMINAL .
   RETURN FROM THE MACRO MODE .
```

Fig. VII.5.3 PW spectra (page 3 of 3).

VII.6 Analysis of teleseismic P coda using NORSAR and NORESS

The teleseismic P coda consists of the presumably scattered energy that arrives in the first few minutes following first P from teleseismic events. It has been suggested that it could be used as a yield estimator (see, for example, Ringdal, 1983), and work reported here also suggests that it may also be useful as a discriminant for crustal events. This study examines the problem of the teleseismic P coda from the standpoint of determining the place where the waves in the coda are scattered, with the aim of producing a quantitative model of the coda.

The "starting model" is shown in Fig. VII.6.1. The P coda is considered to be produced by scattering of Lg to P in the crust near the source and by scattering of P to Lg near the receiver. The power spectrum P_c of the coda as a function of time t then has the form, for single scattering,

$$P_c(f,t) = |A|^2 \cdot G \cdot \exp[-2\pi ft/Q] \qquad (1)$$

where f is frequency, A(f) is the Fourier transform of the first P pulse, G is a scattering parameter called the turbidity and Q is the Q. The parameters G and Q will refer only to the receiver site for the case of a deep-focus event and will depend on both the source and receiver sites for the case of explosions and shallow earthquakes.

Fig. VII.6.2 shows a plot of Fourier amplitude against time for a Semipalatinsk explosion for a frequency of 3.6 Hz. At this high frequency the exponential decay model of Eq. (1) seems to fit the data well for the time range 20 sec to 200 sec after first P. For lower frequencies, the influence of PP is important (King et al, 1975). Values for Q of 850 ± 50 (deep-focus events), 1200 ± 150 (Semipalatinsk explosions) and 1200 ± 250 (Semipalatinsk crustal earthquake, March 20, 1976; Pooley et al, 1983) have been obtained. These values suggest Q at both NORSAR and Semipalatinsk is high. Values of G of about 10^{-3} km^{-1} are found for both deep-focus events and Semi-

palatinsk explosions, suggesting that the size of the coda generated near Semipalatinsk is at most of the same order as that generated near NORSAR. On the other hand, the crustal earthquake near the Semipalatinsk test site gives a value for G of around 5×10^{-2} km^{-1}, considerably larger than the explosion value. This can be explained by efficient generation of Lg by a dislocation source followed by scattering of Lg to teleseismic P.

To try and determine the relative contribution of scattering near the source, near the receiver and from any other mechanism, analysis of NORESS data has begun. NORESS is uniquely capable of determining crustal phase velocities (3.5 - 8 km/sec) and azimuths at high frequencies. From Fig. VII.6.1, the model predicts that a component of the coda should have a phase velocity and azimuth appropriate to teleseismic travel from the source, and another component having phase velocities appropriate to Lg (3.5 - 4.5 km/sec) and random azimuth. Fig. VII.6.3 is a contour plot of a wavenumber spectrum of a 5-second window in the coda of a Semipalatinsk explosion, 5 seconds after P onset. There is indeed evidence of both a high phase velocity peak at the appropriate azimuth, and energy at Lg velocities off azimuth.

A. Dainty, Georgia Inst.
of Technology

References

King, D.W., R.A.W. Haddon and E.S. Husebye (1975): Precursors to PP. Phys. Earth Planet. Inter., 10, 103.

Pooley, C.I., A. Douglas and R.G. Pierce (1983): The seismic disturbance of 1976 March 20, East Kazakhstan: earthquake or explosion? Geophys. J., 74, 621.

Ringdal, F. (1983): Magnitude from P-coda and Lg using NORSAR data. Fifth Ann. DARPA Symp. on Seismic Detection, Analysis, Discrimination and Yield Determination, p. 34.

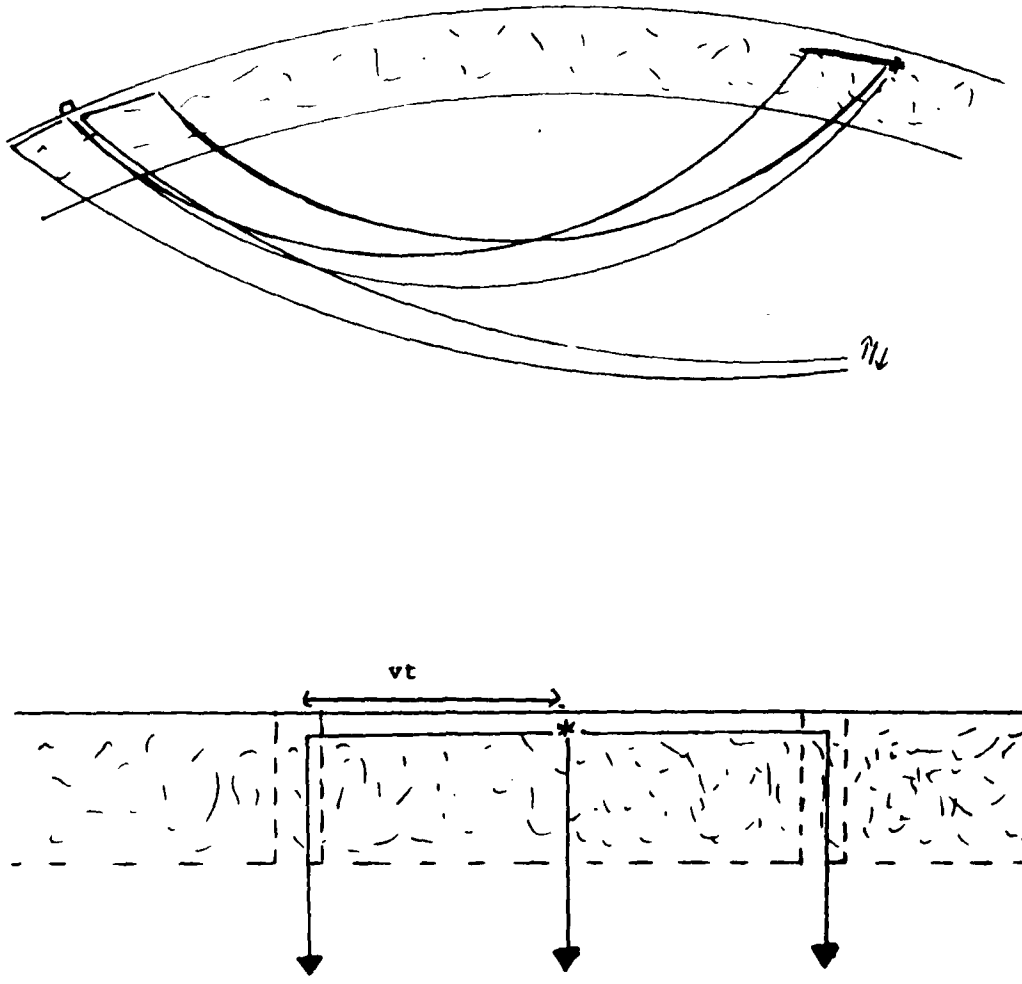

$$P_c(F,T) = A_p^2 . G . \exp(-2\pi FT/Q)$$

$$G = G_{pL} \qquad \text{(DEEP FOCUS)}$$

$$G = (A_L^2/A_{po}^2) . G_{Lp} + G_{pL} \qquad \text{(EXPLOSION)}$$

Fig. VII.6.1 Model of coda (Top). Generation of coda by Lg → P scattering near source, P → Lg scattering near receiver (Middle). Detail of Lg → P scattering near source (Bottom). Formulas for coda power spectrum as a function of time in time range 20 - 200 sec after first P. See text for discussion.

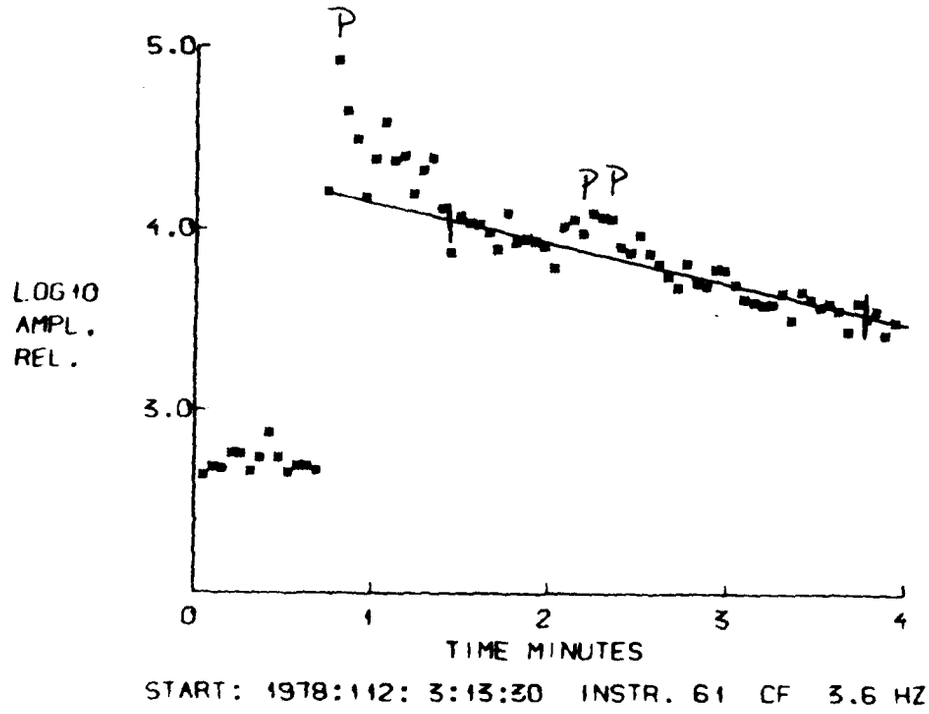

Fig. VII.6.2 Fourier amplitude as a function of time for a Semipalatinsk explosion, April 22, 1978. Line indicating fit of equation (1), ticks indicate range over which fit is taken. Analysis frequency, 3.6 Hz. Note contamination of coda by PP.

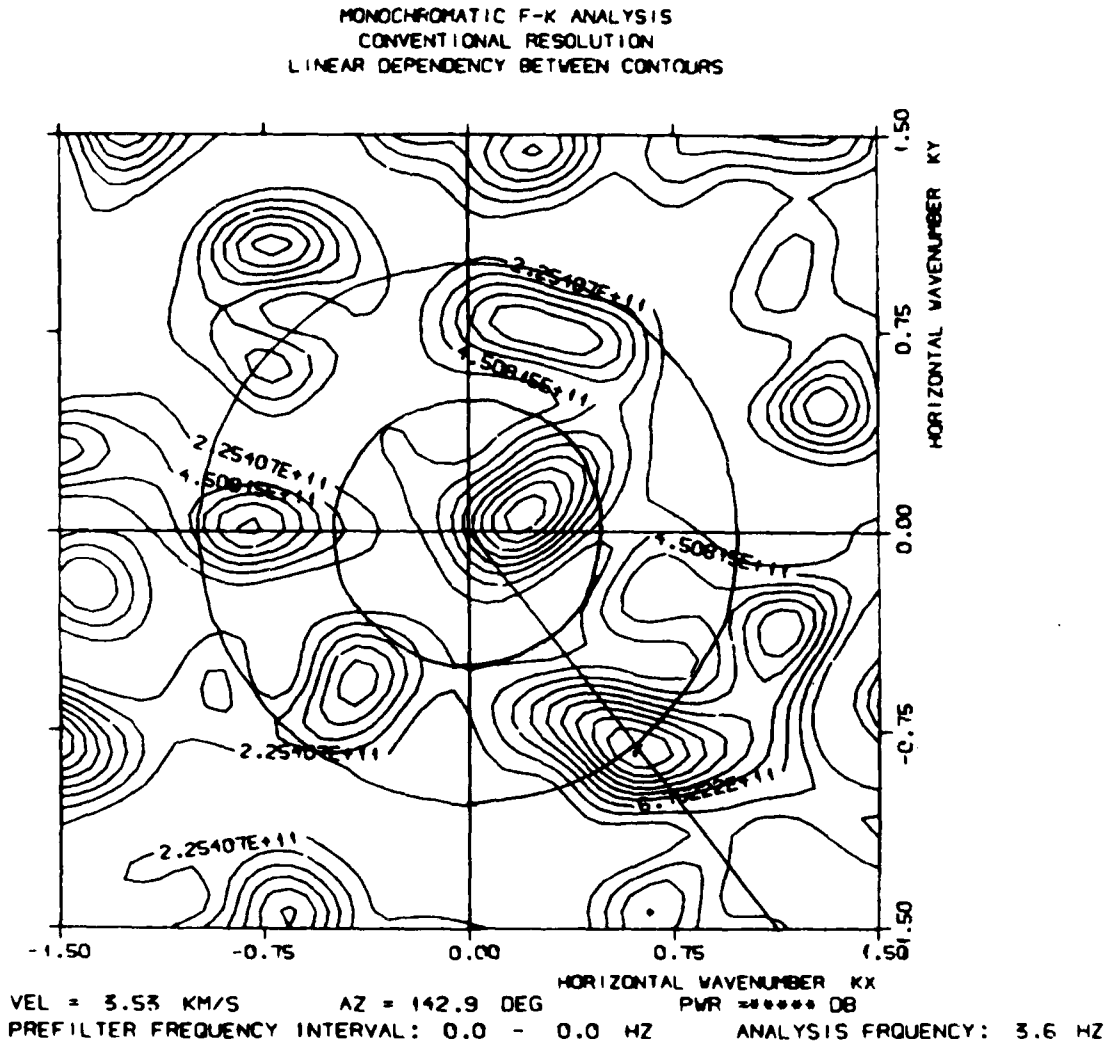

Fig. VII.6.3 Contour plot of wavenumber spectrum, KX linear wavenumber East, KY linear wavenumber North, for a 5-second coda window 60 sec after 1st P. Analysis frequency is 3.6 Hz, linear wavenumber is (1/wavelength). Circles are at phase velocities of 8 km/sec (inner) and 3.6 km/sec (outer).

VII.7 3-component seismogram analysis

A properly equipped seismograph station or array always includes 3-component instrumentation for the very simple reason that the seismic wavefield comprises vertical and horizontal ground motions and combinations thereof. Seismologists have for many years successfully exploited the information potential of 3-component records for wave propagation modelling, retrieval of structural information (tomography) and source parameters, but these efforts have mainly been tied to the low frequency part of the wavefield. Likewise, many efforts have been invested in extracting similar information in the high frequency range, say of 1-10 Hz, but in this case less successfully as judged from current literature. The reason for this appears to be twofold: i) high frequency records are rather complex due to scattering, mode conversions, multipathing and similar wave propagation effects and ii) the analysis techniques used fail to produce extracted wavefield parameters in an easily interpretable format. For example, a common procedure is to produce particle motion plots reflecting the structure in the wavefield, but since such plots generally are messy, the analysis is often left at that.

The problem addressed in this note is that of a new approach to extracting parameter characteristics, the wave field structure on the basis of a priori models for P, S, Love and Rayleigh wave particle motions. Special attention has been given to the problem of presenting results in an easily interpretable manner or extracting signal parameters convenient for a wide variety of research applications. These points will be amply demonstrated in the Results section.

3-component analyzing technique - wavefield modelling

Any approach to extracting signal parameters from a seismogram is based on certain assumptions or models regarding the signals or wavelets constituting the records and the background noise. In our case these are: i) noise is orthogonal between the 3-components (vertical, radial, transverse; or Z, E-W, N-S) and ii) particle motion is as derived from classical wave theory. The analyzing technique, as used in prac-

tice, is tied to the theoretically expected particle motion covariance matrix which is compared to that observed in given time and azimuth windows. Then using a max. likelihood formulation the primary result is simply the likelihood that a wavelet is either P, S, Love or Rayleigh against the null hypothesis of being noise. Concurrent with the likelihood estimation is that of extracting the axis of the particle motion ellipse (linear for body waves) which in turn can be converted into angle of approach of the incoming wavefront, that is, angle of incidence (azimuth is already known). Details on this particular particle motion analyzing technique is presented by Christoffersson et al, 1985. To summarize, wavefield information extraction from our 3-component signal analysis procedure is as follows:

- Likelihood of presence (0.4 triggering level) of P, S, Love and Rayleigh type of wavelets as a function of azimtuh (dAzi ~ 1 to 5 deg), and time (dT ~ 1 sec, updating interval 0.5 sec).

- Angle of incidence for triggered body wave type of wavelets.

As mentioned, special attention was given to results or extracted wavefield parameter presentations which presently are in the following forms:

i) Likelihood contouring as a function of azimuth (ranges typically 60-180 degrees) and time (ranges typically 20-50 sec).

ii) Particle motion filtering on the basis of the estimated likelihood function, that is, simply weighting the original records with the likelihood function and confining to an azimuth window of ± 30 to ± 40 deg relative "true" azimuth.

iii) Angle of incidence estimates converted to apparent phase velocity (so far for P only) via Herrin tables, and then plotted as a function of time and azimuth.

iv) Azimuth and incident angle of the very first P wavelet transformed to estimates of epicenter coordinates.

We remark that presently our work on 3-component seismogram analysis is just in a rather preliminary stage; the use of other types of ML-estimates has not been explored, nor the use of more complex particle motion models. Other types of problems are those of better handling interference phenomena typical of the Lg wavetrain and S-wave splitting, but a requirement here seems to be access to 5-component instrumentation (1 vertical and 4 horizontal). On the application side, we have not explored the possibility of coda decomposing in deterministic and random scattering contributions, and perhaps most challenging that of what we term earth fingerprinting. With this is meant that the large number of signal parameters extracted may exhibit stationary patterns reflecting structural heterogeneities characteristic of specific site and source regions.

It may also be appropriate with a few words on how our technique compares with others tied to analysis of 3-component data. The feature in common is that of estimating the axis of the particle motion ellipse, but to our knowledge nobody has tried to include model fit in probabilistic terms nor to use sliding time/azimuth windows permitting a rather comprehensive decomposition of the whole recorded wavetrain. The preliminary results to be presented stem from analysis of the 3-component recordings from the new NORESS array, and obviously some comparison has to be made between outcome of our decomposition technique and similar results obtained by f-k analysis using all 25 vertical components of the array. Without going into detail here, it suffices to state that 3-component results (single site) compare favorably to the f-k results; in fact quite often they do better in terms of improved time and azimuth resolutions. The reason for this is

that f-k analysis requires longer time windows (a minimum of 2.5 sec is used) to account for move-outs across the array, and in case of interfering signals "averaged" results are produced. Not to forget, the consistency and stationarity of particle ground motion even for short wavelets are at least for us unexpectedly good.

Preliminary results

It has taken considerable time to program our 3-component analyzing technique; the first rough version became operational quite recently, so comprehensive analysis of many event recordings has not been completed yet. However, preliminary results from a few rather typical event recordings mostly from the NORESS 3-component station C2 will be presented in the following, so as to illuminate in our opinion the strength and potential of 3-component analyzing techniques. Results are presented event-wise (in appendices) using unfiltered data as standard recursive Butterworth filtering produces severe phase distortions. It should be added that so far mostly P-modelling has been attempted.

Case 1, Event No. 84301: Caspian Sea/W. Kazakh. Feature: travel time triplication(s).

Case 2, Event No. 84327: Local explosion. Feature: complex local record; energy migration.

Case 3, Event No. 84328: E. Kazakh event. Feature: triplication of wave train ?

Case 4, Event No. 85041: Semipalatinsk event. Feature: apparent velocity analysis of the first 25 sec of the record.

Case 5, Event No. 85060: "Leningrad" event. Feature: this is actually a double event easily separated by 3-component analysis.

Case 6, Event No. 85081: Finland/USSR event. Feature: worst case event with exceptionally poor SNR, but 3-component analysis still seems to work.

Concluding remarks

The preliminary results obtained from our variant of particle motion analysis of high-quality 3-component records from the new NORESS array in Norway are considered very encouraging and thus justify research on a broader scale into this kind of problems. Methodological problems are those of more eficient ML estimators, proper parameter settings including shorter updating rates, and potential for real-time event detection. In the latter case, fast algorithms are clearly needed. In fact, a solution of the latter problems has now been obtained, that is, the probability of P wave presence in the records estimated independently of azimuth. However, the associated calculations are rather demanding and indeed not considered justified. Our recommendation is to use a Walsh detector but using a low threshold (high false alarm rate) and then introducing 3-comp. analysis for testing precursor of P waves in an off-line mode.

Surprisingly, epicenter location capabilities appear to be relatively good, azimuth estimates so far seldom exceeded ± 5 deg (often around ± 2 deg), while distance is more problematic unless secondary phases (triplications) are clearly identified. In the same way as the azimuth angle is measured in the 3-comp. analysis, we can measure similarly for the angle of incidence in the vertical plane and then convert to epicentral distance via standard travel time tables. Experiments with a Semipalatinsk event gave worst-case distance error of 5 deg (see also Sec. VII.8). Another interesting aspect of 3-comp. seismogram analysis is that of identifying pP and thus significantly improving

focal depth estimates which besides are highly diagnostic of source type.

A. Christoffersson, Uppsala Univ.
E.S. Husebye
S.F. Ingate, ERL, MIT

Reference

Christoffersson, A., E.S. Husebye and S.F. Ingate (1985): Phase identification on the basis of particle motion structure in 3-comp. seismograms. Manuscript in preparation.

CASE 1

Event No. 84301:

Caspian Sea/W. Kazakh

PDE azi: ~ 106°, Δ ~ 25°

NORESS azi: = 110°, vel. = 12.4 km/s

Note: Triplication features

Fig. A: Original unfiltered data
Fig. B: Probability of P-wave presence
Fig. C: Probability function of Fig. B used as a filter
Fig. D: King & Calcagnile travel time model; epicenter distance marked

Comments: The particle motion filter "produces" phase arrivals in very good agreement with expected travel time curves. The surplus arrival may be associated with a hypothesized discontinuity at ca 550 km depth. Epicenter locations better than 1 deg are deemed feasible in such cases, as triplications when identified give very precise distance estimates.

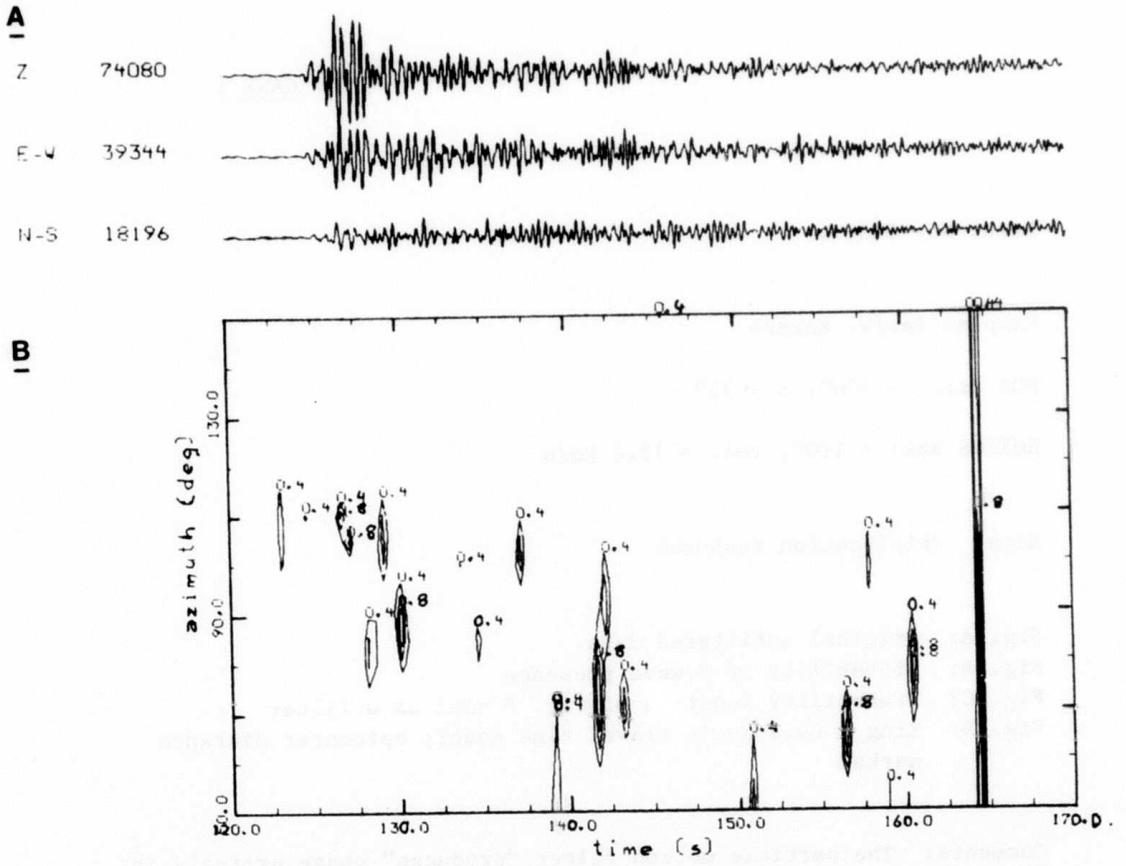
A
Z 74080
E-W 39344
N-S 18196
B
azimuth (deg)
130.0
90.0
50.0
120.0
130.0
140.0
150.0
160.0
170.0
time (s)
C
Z 67976
E-W 34623
N-S 15501

D

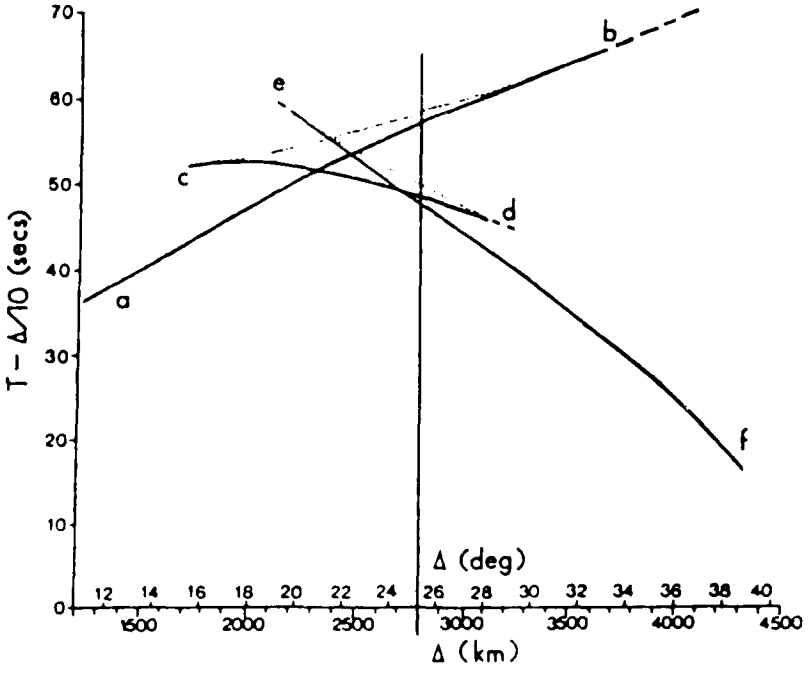

Travel-time distance curves for the KCA P-velocity model of the upper mantle beneath the Baltic Shield.

CASE 2

Event No. 84327:

Local explosion.

NORESS: Azi = "south"

Fig. A: Original data
Fig. B: Probability of P-wave presence; note trend of migrations in pattern
Fig. C: Particle motion filtered output

Comments: At a later stage filters based on S (SV & SH), SV, Love and Rayleigh presence will be introduced. The off-azimuth triggering at about 260-300 deg may reflect sort of side lobe effects. Anyway, 3-component filtering of complex local records seems clearly to be feasible.

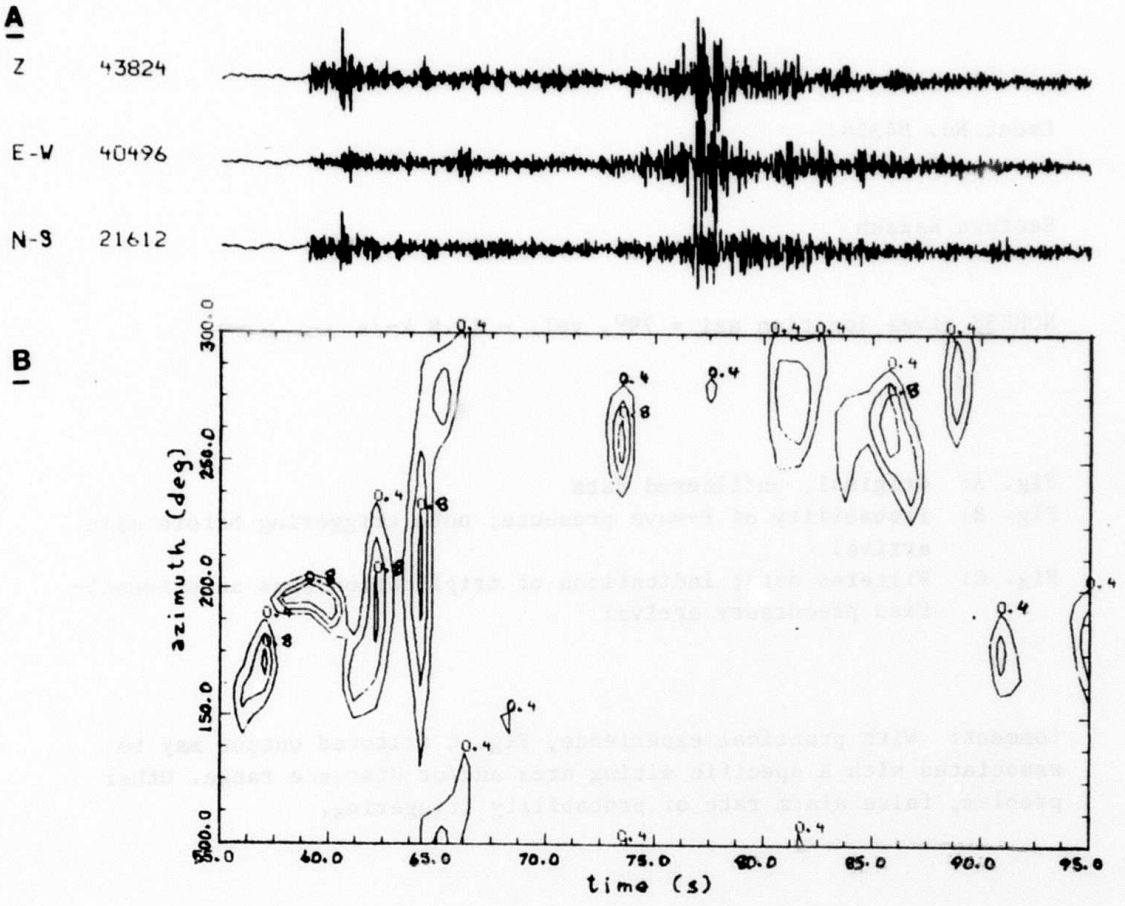
A
Z 43824
E-W 40496
N-S 21612
B
azimuth (deg)
300.0
250.0
200.0
150.0
100.0
55.0
60.0
65.0
70.0
75.0
80.0
85.0
90.0
95.0
time (s)
C
Z 22180
E-W 16511
N-S 16213

CASE 3

Event No. 84328:

Eastern Kazakh

NORESS gives location azi = 79°, vel. = 13.8 km/s

Fig. A: Original, unfiltered data
Fig. B: Probability of P-wave presence; note triggering before main arrival
Fig. C: Filtered data; indications of triplication plus an unidentified precursory arrival

Comment: With practical experience, Fig. C filtered output may be associated with a specific siting area and/or distance range. Other problem, false alarm rate of probability triggering.

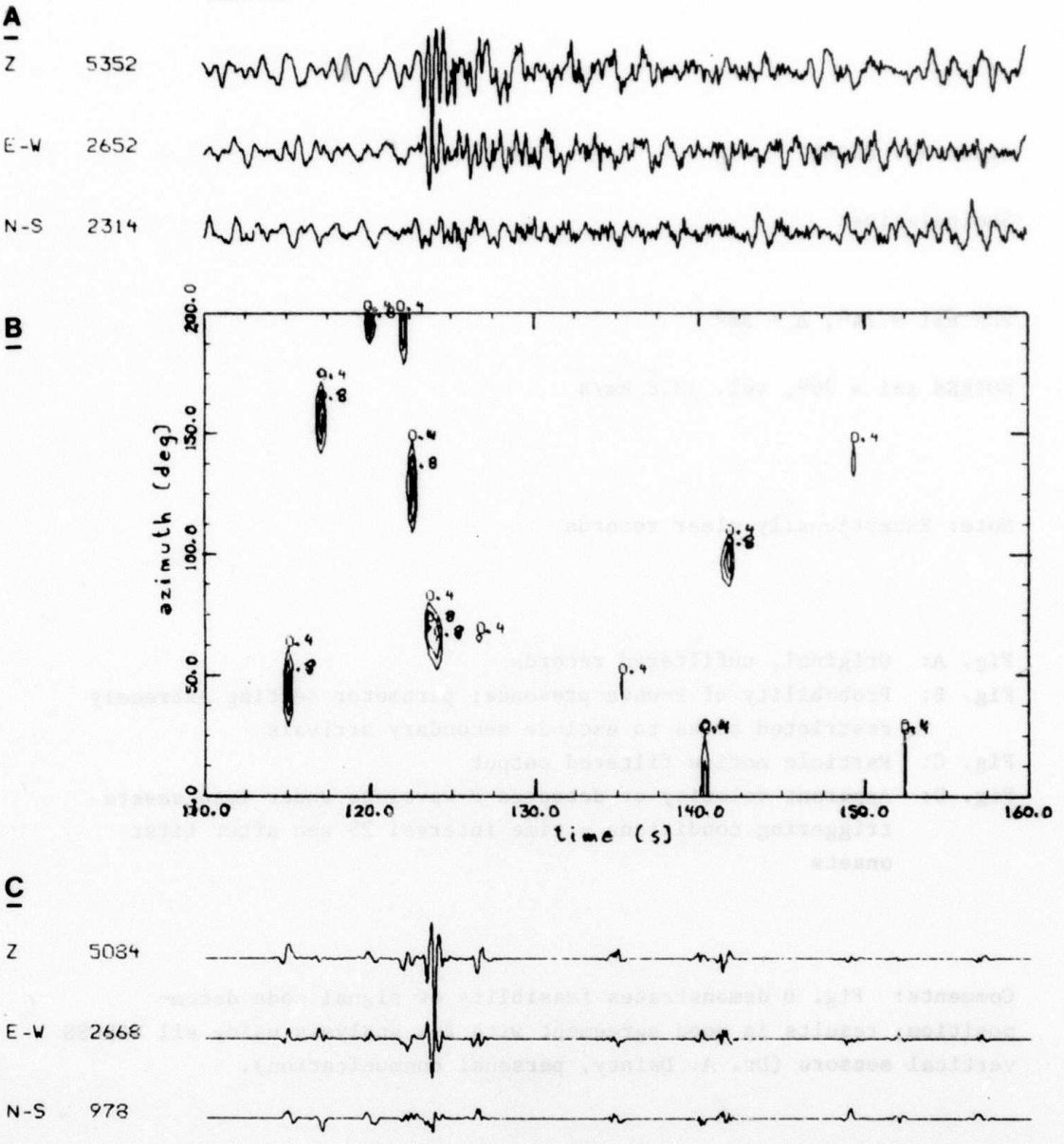
A
Z 5352
E-W 2652
N-S 2314
B
azimuth (deg)
time (s)
C
Z 5084
E-W 2668
N-S 978

CASE 4

Event No. 85041

Semipalatinsk

PDE azi = 74°, $\Delta \sim 38°$

NORESS azi = 79°, vel. 13.8 km/s

Note: Exceptionally clear records

Fig. A: Original, unfiltered records
Fig. B: Probability of P-wave presence; parameter setting extremely restricted so as to exclude secondary arrivals
Fig. C: Particle motion filtered output
Fig. D: Apparent velocity of detected P-wavelets under less severe triggering conditions - time interval 25 sec after first onsets

Comments: Fig. D demonstrates feasiblity of signal coda decomposition; results in good agreement with f-k analysis using all NORESS vertical sensors (Dr. A. Dainty, personal communication).

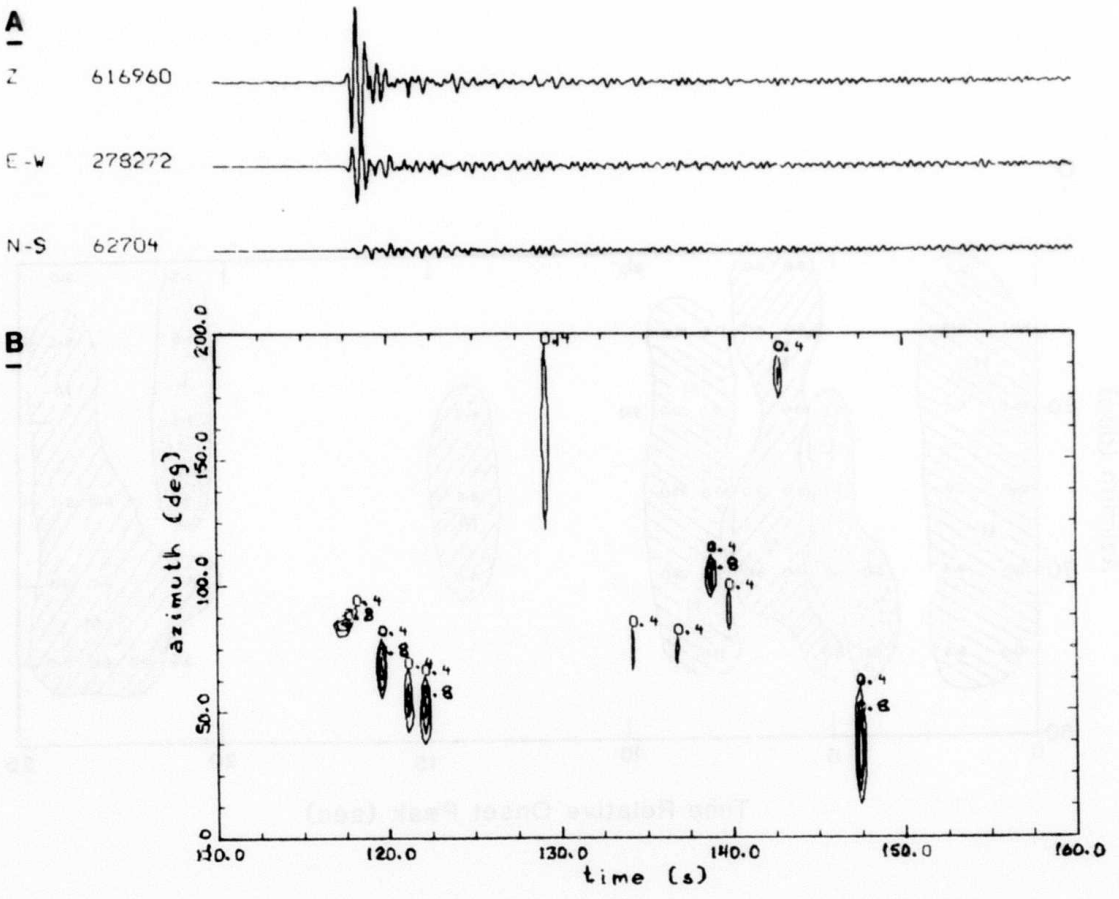
A
Z 616960
E-W 278272
N-S 62704
B
azimuth (deg)
200.0
150.0
100.0
50.0
0
110.0
120.0
130.0
140.0
150.0
160.0
time (s)
0.4
.8
C
Z 185285
E-W 74389
N-S 41090

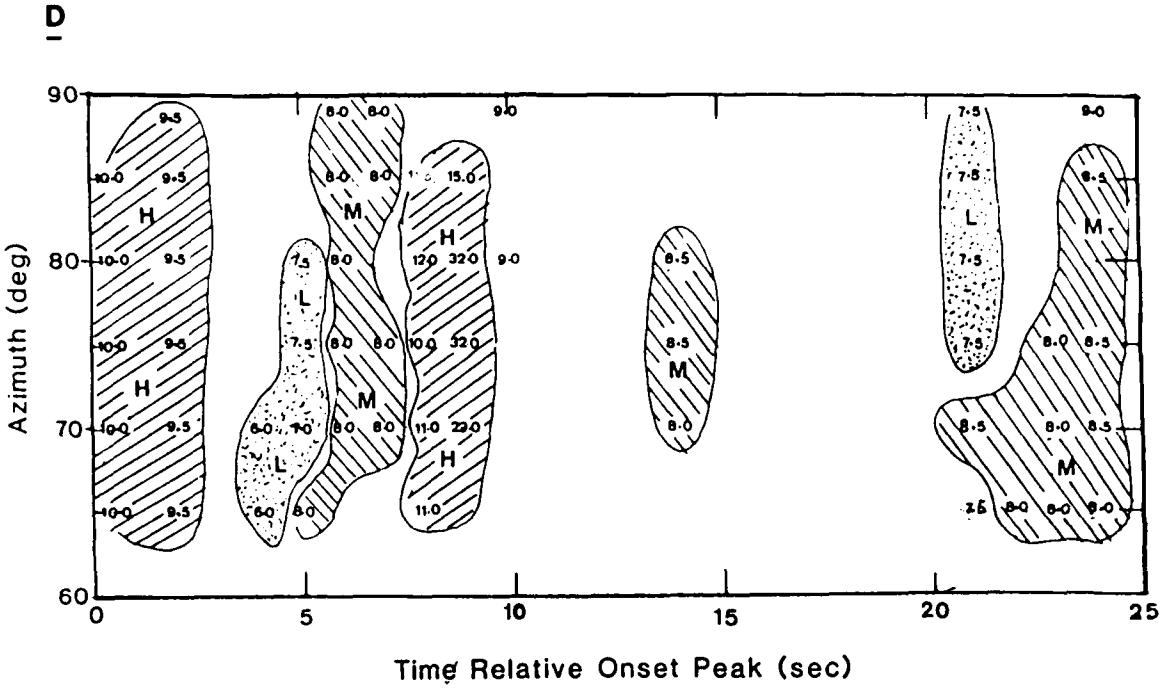

Velocity analysis as a function of time and azimuth after first P-wave onset of the data for case 4.

CASE 5

Event No. 85060

Leningrad event; azi. ~ 87°, Δ ~ 8.8°

NORESS: azi. ~ 87°, vel. = 12.1 km/s

Note: This is actually a double event, the first arriving at approx. 120 sec, azi. ~ 200°, and "Leningrad" at 127 sec, azi. ~ 90°. Both seen in the 3-component analyzing results.

Fig. A: Original, unfiltered traces; the two arrival marked 1 and 2, respectively
Fig. B: Probability of P-wave presence
Fig. C: Particle motion filtered output

Comments: Our 3-component analyzing technique appears to have some potential for real-time event detection.

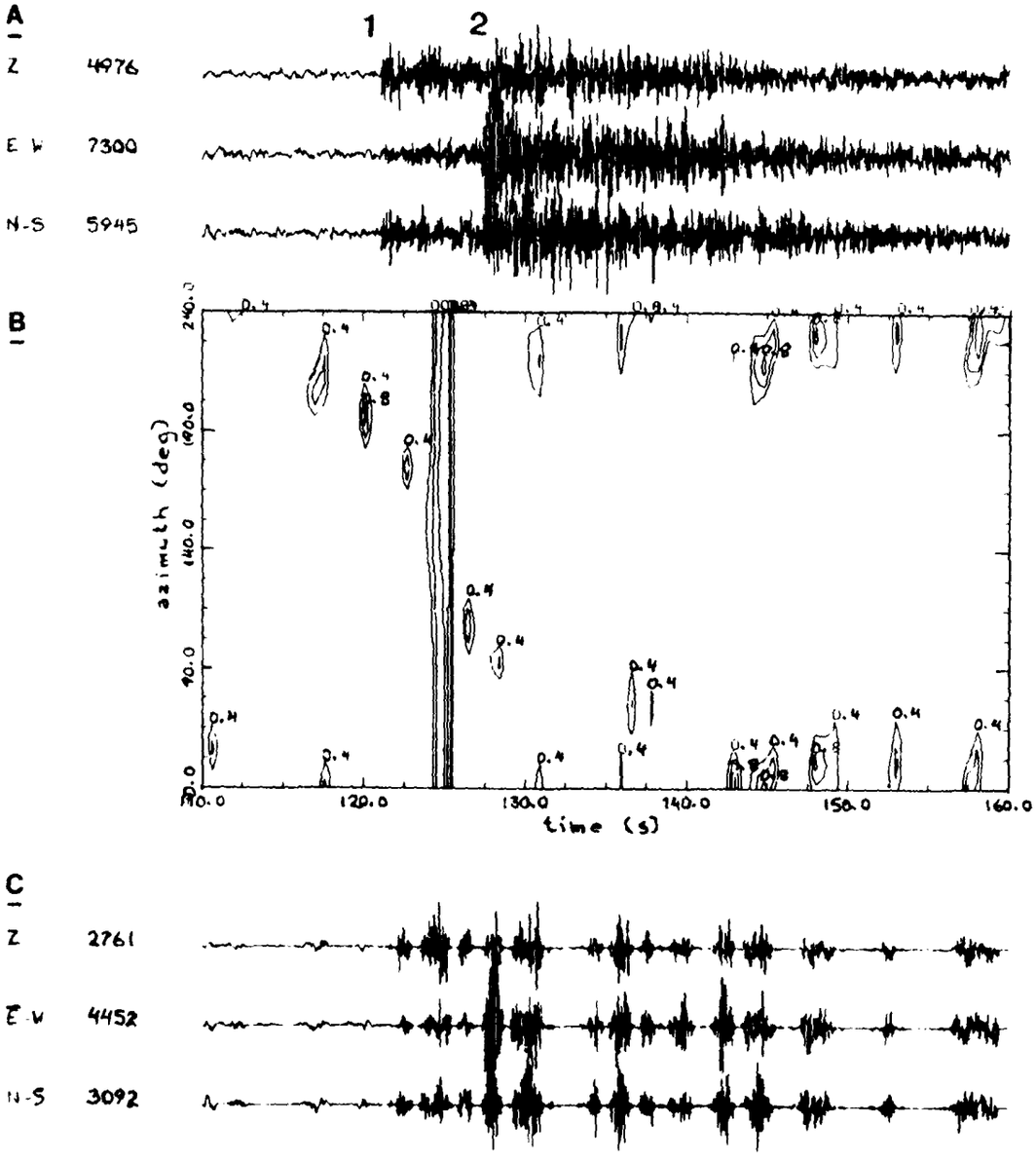
A
1
2
Z 4976
E-W 7300
N-S 5945
B
azimuth (deg)
240.0
190.0
140.0
90.0
0.0
110.0
120.0
130.0
140.0
150.0
160.0
time (s)
C
Z 2761
E-W 4452
N-S 3092

CASE 6

Event No. 85081

Finnish epicenter location at Finland/USSR Border gives azi. ~ 71°, $\Delta \sim 9.8^{\circ}$

NORESS: azi. ~ 90°, vel. = 16.7 km/s

Note: The unfiltered data used in our analysis have exceptionally poor SNR; phase arrival(s) relatively clearly visible in full NORESS record display.

Fig. A: Original, unfiltered data
Fig. B: Probability of P-wave presence
Fig. C: Particle motion filtered record

Comments: P-wave particle motion structure appears to be preserved to some extent even for poor SNRs.

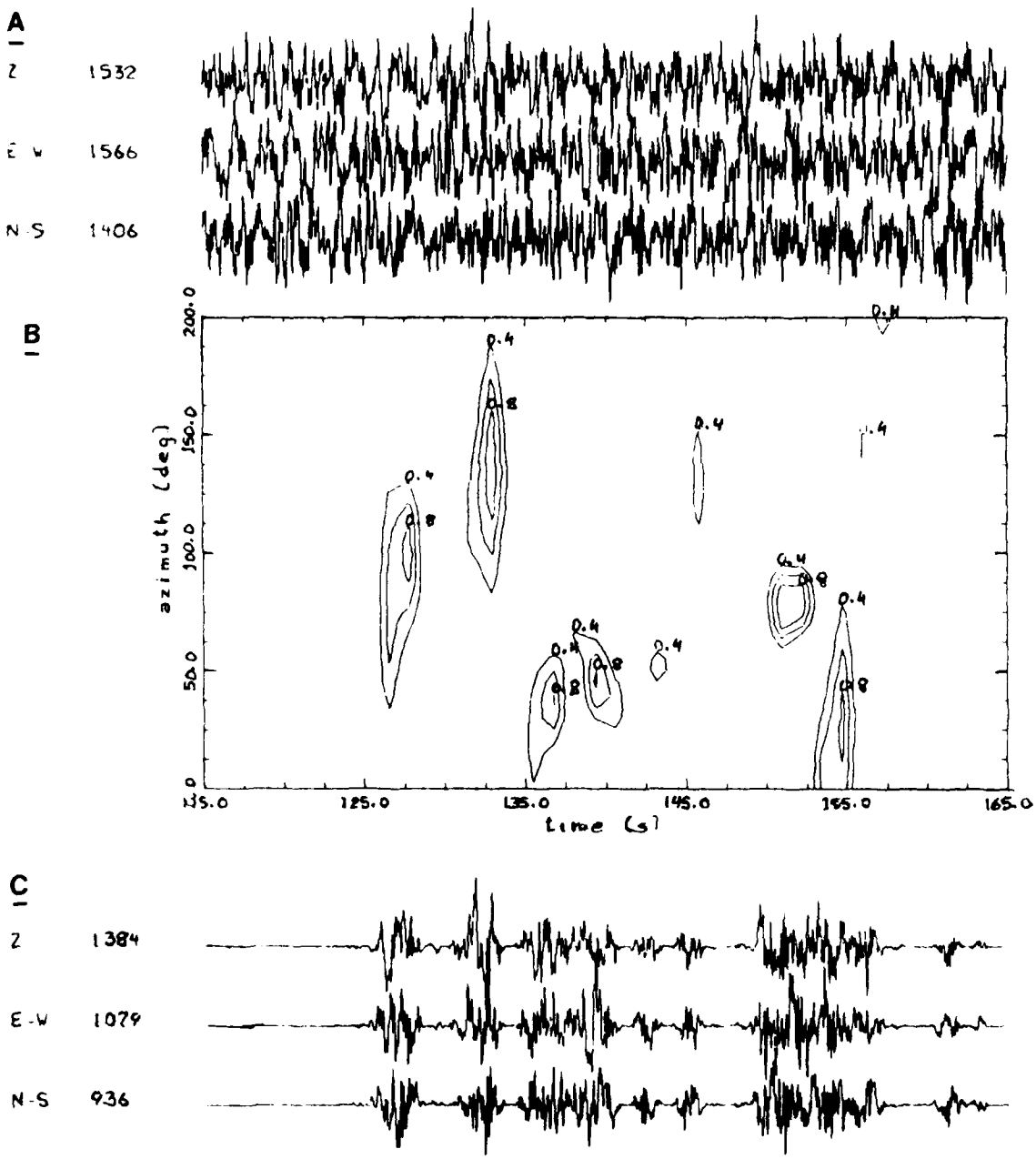
A
Z 1532
E-W 1566
N-S 1406
B
azimuth (deg)
200.0
150.0
100.0
50.0
0
125.0
135.0
145.0
155.0
165.0
time (s)
0.4
0.8
C
Z 1384
E-W 1079
N-S 936

VII.8 Epicenter location scenarios

Traditionally, P-wave arrival time observations from 4 stations are required for the estimation of the four focal parameters epicenter location (σ, λ), focal depth and event origin time. The computational techniques in use are well documented in the scientific literature, although an occasional severe practical problem is that of proper phase association. The latter difficulty stems from inadequate grouping of event P reportings when several events "overlap" in a given time window. Such ambiguities are easily resolved when array/3-comp. station estimates are available. In this section three scenarios for event location will be discussed, namely: i) single station (3-comp.) array event location; ii) two station/array event location; and iii) precise event location using a regional network of high quality stations.

i) Single station/array event location

The problem is illustrated in Fig. VII.8.1a and VII.8.2, and obviously the accuracy in the epicenter location estimate reflects precision in azimuth and distance estimates. As demonstrated in Section VII.7, a single 3-comp. station can provide azimuth estimates within 5 degrees or even within 2 degrees in good cases. Distance estimates are more problematic unless secondary phases confidently can be identified. This is indeed feasible at local (Pn, Sn, Lg, etc.) and regional (400 km and 650 km travel time triplication curves) distances, while slowness estimates are not too accurate at teleseismic distances. Using 3-comp. recordings, the measured angle of incidence can provide distance estimates which appear to be more precise than those stemming from slowness measurements say via F-k analysis of dat afrom small aperture arrays. Another advantage with 3-comp. data analysis is that phase identification becomes more objective, and may even provide a means for focal depth estimation via "detection" of the pP-phase.

ii) Two station/array event location

The problem is illustrated in Fig. VII.8.1b and VII.8.3, and the most important parameters needed are azimuths and relative P arrival times as a substitute epicentral distance estimates. With reasonable geometries, epicenter location should be within a few hundred kilometers or even less.

Comments. Gjøystdal et al (1973) have extensively dealt with one- and two-array event location capabilities and their techniques naturally apply to azimuth and distance estimates extracted from the 3-comp. station data. Naturally, the accuracy in the epicenter locations made depends on geometry (see Fig. VII.8.1), as wavefront angles scale differently with distances. An interesting problem here, now under investigation, is whether the pattern of secondary arriving phases as derived via our new 3-comp. data analysis can be used for refining epicenter distance estimates.

iii) Use of regional networks for event locations

In the context of a potential comprehensive test ban treaty, precise event locations are a necessity, and this can only be achieved by having access to recordings from a network of regional stations (for small events). A number of computer schemes, such as HYPO 75, exist for solving this kind of problems, but a general drawback here is that the crustal model used is considered a bit crude. For example, what is the velocity distribution in the crust? Is it constant, depth dependent only; is lateral variation significant or do we have to take potential anisotropy into account? A related problem is which phases are actually observable in the seismogram and what are their respective ray paths. Do we actually see waves refracted from the Conrad discontinuity; the Pn phase may be a head wave or perhaps better modelled as a diving wave? Likewise, reflections from Conrad and/or Moho if observable would constrain focal depth estimates. Clearly, precise event locations using regional recordings are much dependent on the velocity distribution in the crust and lithosphere and our ability to model it properly, and equally important, extract relevant

phase information from the seismogram. Extensive use of S-phases is clearly an advantage here in view of their short wave lengths.

A long-term research project is now under way at NORSAR for solving these kinds of problems; the principal goals are those of inverting available travel time information for a multitude of phases in order to produce a tomographic image of the crust and lithosphere structures and, important, jointly extract relevant focal parameters. The research strategy here is outlined in some more detail by Gubbins (1985), while Christoffersson et al (1985) have presented a novel approach to both quantitative and qualitative extraction of significantly more phase information from 3-comp. seismogram recordings (e.g., see Section VII.7).

A. Christoffersson,
Uppsala Univ.
D. Gubbins, Cambridge
Univ.
E.S. Husebye

References

Christoffersson, A., E.S. Husebye and S.F. Ingate (1985): Phase identification on the basis of particle motion structure in 3-comp. seismograms, Manuscript in preparation.

Gjøystdal, H., E.S. Husebye and D. Rieber-Mohn (1973): One-array and two-array location capabilities, Bull. Seism. Soc. Amer., 63, 549-569.

Gubbins, D. (1985): Use of arrays to determine crustal and upper mantle structure, and locating events using travel times. Unpublished note.

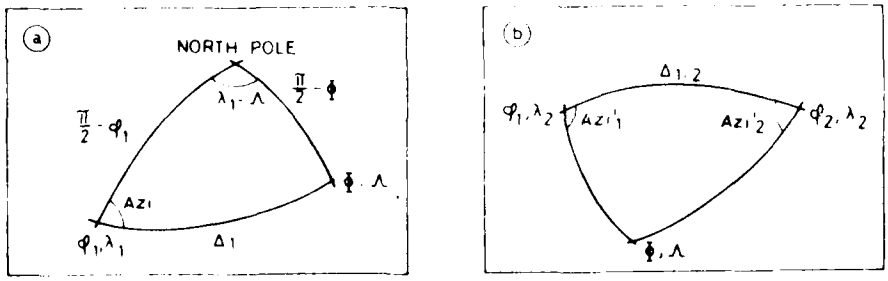

Fig. VII.8.1 Principles for epicenter locations using one and two arrays, or one and two three-component stations. In each case, at least two sides and angles, etc., are known in the given spherical triangles. Array (station) and epicenter coordinates are denoted by (σ, λ) and (Φ, Λ), respectively. The indices 1 and 2 denote different arrays (stations).

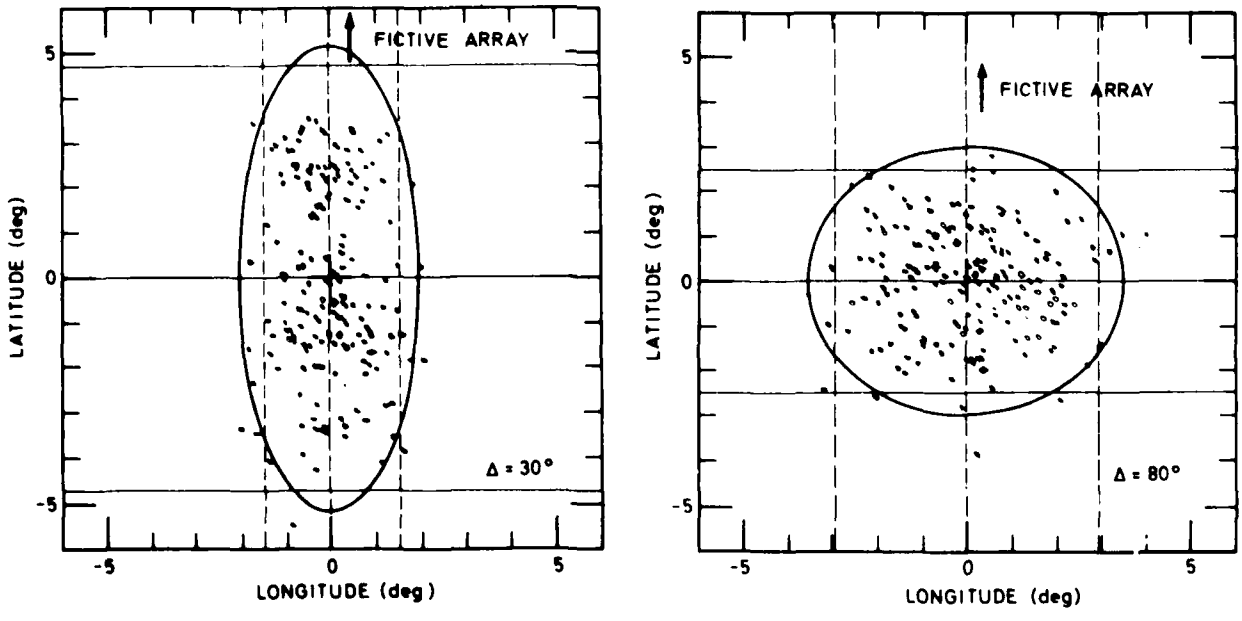

Fig. VII.8.2 The 95 per cent confidence ellipses of simulated one-array (or one 3-comp. station) location capabilities for epicentral distances of 30° and 80°. Standard deviations of azimuth and slowness are 1.5° and 0.10 sec/deg, respectively, and the number of trials is 200. Note how the axis of the error ellipse changes with distance (figure after Gjøystdal et al, 1973).

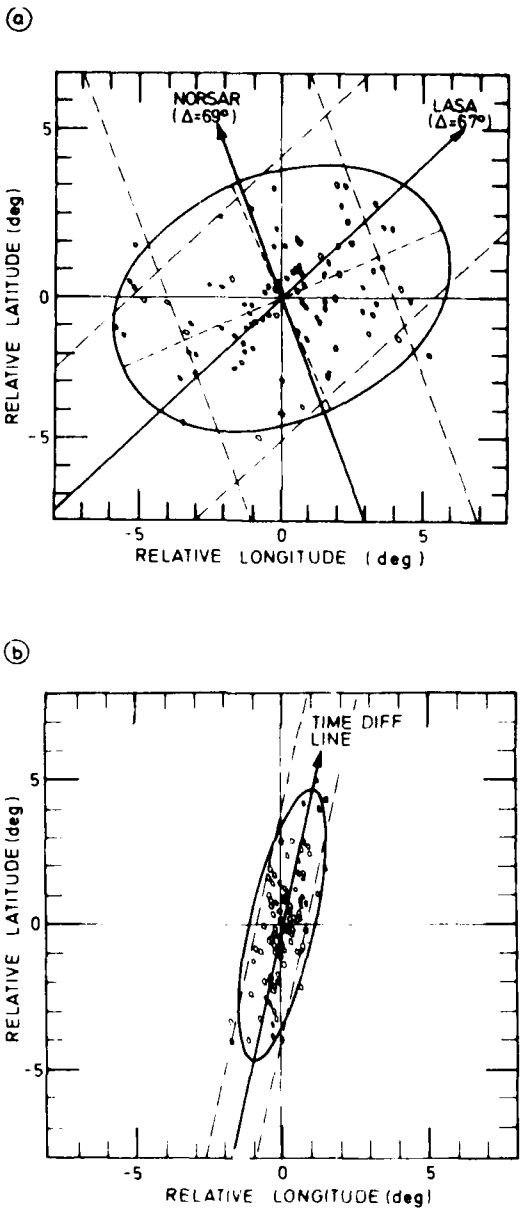

Fig. VII.8.3 Simulated 2-array (or two 3-comp. stations) event locations at 45.3°N, 149.3°E for NORSAR and LASA. In case a) only azimuth observations are used (σ = 2 deg), while in case b) further constraints are added by using P arrival time differences (σ = 2.0 sec).

VII.9 The RST/RSTE research project - current status

The RST/RSTE (Remote Seismic Terminal Enhanced) project is aimed at developing an intelligent seismic field terminal with capabilities of detecting and analyzing events in an automated mode. The operational capabilities would be roughly equivalent to those of the dedicated data center for a large-aperture array, although the number of channels to be handled would be far less. This entails a multitude of tasks like real-time event processing, off-line processing of detected events, and external transfer to an RST of raw and processed signal data. The viability and realizability of the RST/RSTE concept was demonstrated in Geneva in 1982 (e.g., Husebye and Thoresen, 1984); for a schematic view, see Fig. VII.9.1.

The mentioned operational task, say for 8 short period seismometers, can be "accomodated" with a hardware framework of mini -or personal computers like the IBM PC AT. The corresponding software implementation requires a highly efficient multitasking operating system, as well as a high level programming language. Our choice was polyFORTH II, which is an integrated operating system/high level language (FORTH). The detection process is a voting one tied to STA/LTA thresholding on individual channels - a Walsh detector replacement is under consideration. In the event processor detected signals would be subjected to f-k analysis, and a suitable phase picker for signal onset times. Important, in view of the very recent 3-comp. seismogram analysis results reported in Section VII.7, a viable alternative here would be to replace the mini-array with 3-comp. high-quality instrumentation. It should be added that recent progress in fault mechanism studies entail that reasonable moment tesnor solutions are feasible in many cases, even when single 3-comp. station records are used (prof. A. Dziewonski, personal communication).

Seismological motivations for RST/RSTE

Theoretical advances in seismology cannot be sustained unless researchers have easy access to an abundance of high-quality seismic data in digital form. The NORSAR array and the SRO and ASRO seismic observatories are typical examples of realizations of these data collection goals. On the other hand, most seismometers in operation are tied to analog recording systems (photographic paper to be changed daily). In other cases the seismometer outputs are transmitted continuously say via dedicated telephone lines to a data center, although only a few per cent of the data flow contains significant event information. Also, the use of small arrays/3-comp. stations will very much facilitate signal analysis, that is, Level 1 data extraction, both qualitatively and quantitatively. The obvious thing to do here is naturally to decide at the seismometer site which part of the recordings are useful, and in this way greatly reduce excessive transmission costs. Likewise, extraction of Level 1 data in the field would permit much faster and more advanced event analysis with a minimum of analyst interaction and delays. It should be noted that if mass data storage in the field is found desirable by any user, this can be achieved by installing minitape recorders. For example, makes currently available can store about 70 Mbytes of data (cost ~ $3000), while most recent models can store ca 130 Mbytes (at the same price) which is equivalent to the standard 9T 6250 BPI computer tape.

We feel confident that our hardware/software designs of the RST and RSTE to be detailed in the next chapters will accomplish these goals. Finally, let us add that in the case of broad-band seismograph stations the data recording is primarily of interest for research and in such cases the RST/RSTE would serve as a data logger system.

RSTE and RST software developments

Basically, our intention is to make the RSTE a smart peripheral device interfaceable to a variety of host computers or RSTs. Its main task is time series analysis in the field and data transfer on the basis of

intelligent handling of outputs from a variety of geophysical instrumentation, like small arrays of short period seismometers, hydrophone arrays and 3-component broadband seismometers. Naturally, we do not intend to incorporate all possible functions and tasks in one RSTE, instead aim at designing a flexible software framework from which special purpose RSTEs can be realized relatively easily. For example, seismic data recording and subsequent analysis are real-time multitasking processes which motivated the choice of polyFORTH (Whitney and Conrad, 1983) as programming language. This is an integrated operating system/high level language with minimal overhead for multitasking. Likewise, the choice of the KERMIT protocol for two-way RST-RSTE communication was motivated by its extensive use in universities and research institutions (e.g., see DaCruz and Catchings, 1984a,b).

The RSTE functional structure as realized in the software is shown in Fig. VII.9.2. All boxes in the figure represent independent and concurrent processes, each having a well-defined function and interface. These concurrent processes are executed and synchronized by the Round Robin multitasker of polyFORTH on a single processor. The arrows visualize the communication between processes, with the vertical line in the middle representing a "software bus". All processes connected to this software bus may "talk" to one another. The actual implementation of inter-process communication is done using "mailboxes". Each process has an associated mailbox where other processes may put messages. Details on the RSTE software processes shown in Fig. VII.9.3, most of them now completed, are given below.

KERMIT

This process implements the communications channel to the outside world, using a modified/extended version of the KERMIT protocol. The extensions include having KERMIT running permanently in server-mode, login procedure, long packets (up to 255 bytes) and transfer of 8-bit data without quoting. File transfers are handled in cooperation with the File System. Commands received through KERMIT are handed over to the "Command Interpreter" for parsing. The KERMIT protocol is imple-

mented as a "finite state machine", and an example of state description of the protocol is illustrated in Fig. VII.9.4. It is a pleasure to note that a seismic data logger under development at Harvard University will feature a KERMIT protocol very similar to ours (J. Steim, personal communication).

MODEM

This is the interface between KERMIT and the hardware used for communications. MODEM accepts commands (DIAL, DISCONNECT, INITIALIZE, ...) and data-packets from KERMIT, while sending messages (incoming call, carrier lost, etc.) and data-packets back to KERMIT.

KA

KA is short for "KERMIT Allocator", and is needed because the communications channel cannot be shared. Every process wishing to use KERMIT must first allocate it for exclusive use, and this is done through requests to KA.

COMMAND INTERPRETER

This process is responsible for parsing and execution of commands received through KERMIT.

FILE SYSTEM

The function of this process is obvious: it offers all other processes necessary file-handling functions. Multiple open files are allowed. The file system can be implemented using one or both of RAM (memory) and disk storage. The actual implementation is transparent to the rest of the system. Standard DOS naming conventions are used with up to 8 characters name and 3 characters extension.

CONFIG

Activated by a command from the COMMAND INTERPRETER, this process enables remote configuration of the entire RSTE-system. This includes setting filter parameters, sampling frequency, detection sensitivity,

type of post-processing to be used and so on. The required configuration is specified in a file that has been prepared transparently and transferred in advance by the controlling RST.

OPSYS

OPSYS is nothing more than a collection of utilities and system functions needed by other processes.

EVENT FILE DISPATCHER

This process handles dispatching (and possible queuing) of event files that have been declared "interesting" by the EVENT post-processor. The EVENT FILE DISPATCHER has available a phone directory, which is used to dial an RST and transfer the file.

WATCHDOG

The WATCHDOG is responsible for monitoring the state of the system, reporting and logging minor errors. If this process after crash does not restart and external timer, that timer will automatically restart the system.

EVENT POSTPROC

The EVENT post-processor, one of the major RSTE modules, consists of various analysis programs that are run in background on data stored by the DATAFLOW PROCESS. These are data blocks which are part of the output from the real-time event detection operation. The principal task here is to provide a listing of detected events in terms of extracted Level 1 parameters and rough epicenter locations.

TIME

TIME is just an interfae to the available real-time hardware, offering precise absolute and relative time to all processes.

TEST & CALIBRATION

This process, together with some external hardware (oscillator), provides the ability to calibrate seismometers.

DATAFLOW PROCESS

This is the critical module in the RSTE handling system. The seismometer data stream is subdivided into many small concurrent processes, each implementing a part of the data-flow like the multiplexed digitizer, data windowing and filtering, etc.

Comments. The RSTE software system is now nearing completion with the EVENT POSTPROC being a major exception here. The reason for this is that we are currently somewhat ambivalent about whether the "best" solution would be a miniarray or a high-quality 3-comp. installation. The latter alternative is rather attractive not only as regards decomposition of complex recordings but also for simpler field logistics (avoiding stretching of cables, etc.).

RST functional structure

The RST functional structure, shown in Fig. 9, is grossly similar to that of the RSTE. Of course, the RST has no DATAFLOW process and no EVENTFILE DISPATCHER, while the KERMIT/MODEM/KA and FILE SYSTEM perform the same functions as in the RSTE.

There is little concurrency in the RST. Only two tasks are sharing the processor: KERMIT/FILE SYSTEM and the COMMAND INTERPRETER. Boxes to the right of the "software bus" denote subprograms (modules), to be outlined below, that are activated one at a time under control of the COMMAND INTERPRETER, which is responsible for the user interface.

Signal analysis and displays

This module enables the user to do different kinds of analysis on data received from RSTEs. This includes:

- Display of traces with zoom/pan on both color graphics screen and printer/plotter. Use of joy stick/mouse would enable an analyst to re-estimate onset time, signal amplitude and period, etc.

- Spectral, f-k plots and/or 3-comp. wave train decomposition

- Joint display of traces from more than one RSTE.

RSTE configuration utilities
This module is not required to receive/analyze event files, but instead is aimed at easy preparation of configuration files, for use in the remote RSTE.

Device-drivers
Modules named "PRINTER", "PEN PLOTTER" and "GRAPHICS DISPLAY" are simply device-drivers used by the various display functions of ANALYSIS.

Concluding remarks

Our RST/RSTE concepts have evolved from what we may term Personal Seismometry Now, as demonstrated in Geneva in 1982 (Husebye and Thoresen, 1984) to "Seismic Arrays for Everyone" as sketched by Husebye et al (1985). The motivation for undertaking this project is simply the obvious need for the seismological community at large to have easy access to high-quality short period seismic data and without literally being ruined in the process. Similar concerns are shared as regards broadband seismometry which has motivated the establishment of regional and global broadband station networks.

The RST/RSTE system is modular and flexible, and this can be modified/extended to meet special user modifications. An important step in this direction is the planned replacement of the present RSTE microcomputer OMNIBYTE with an IBM PC AT. In the extreme this would

entail RST/RSTE to serve either as a data logger or at the other end as a seismological analyst work station.

E.S. Husebye
E. Thoresen, Consultant
J.A. Mathiesen
I.C. Myrvold

References

Allen, R. (1982): Automatic phase pickers: their present use and future prospects, BSSA, 71, 225-242.

Anderson, K.R. (1978): Automatic processing of local earthquake data; Ph.D. thesis, MIT, Cambridge, Mass 02139, USA.

DaCruz, F. and B. Catchings (1984a): KERMIT: A file transfer protocol for universities. Part 1: Considerations and specifications, Byte, June 84.

DaCruz, F. and B. Catchings (1984b): KERMIT: A file transfer protocol for universities. Part 2: States and transitions, heuristic rules, and examples, Byte, July 84, 143.

Goforth, T. and E. Herrin (1981): An automatic seismic signal detection algorithm based on the Walsh transform, BSSA, 71, 1351-1360.

Husebye, E.S. and E. Thoresen (1984): Personal seismometry now!, EOS, 65, 441-442.

Husebye, E.S. and S.F. Ingate (1985): Seismic arrays - a new renaissance, submitted for publication.

Husebye, E.S., E. Thoresen and S.F. Ingate (1985): Seismic arrays for everyone, Terra Cognita, in press.

Ingate, S.F., E.S. Husebye and A. Christoffersson (1985): Regional arrays and optimum data processing schemes, BSSA, in press.

Murdock, J.N. and C.R. Hutt (1983): An algorithm that detects and analyzes earthquake signals - a fast signal detector analyzer, Albuquerque Seismological Lab., U.S. Geol. Survey technical note.

Romanowizc, B. (1984): Project GEOSCOPE, Technical Rep., Inst. de Phys. du Globe, Paris, France.

Smart, E. and E. Flinn (1971): Fast frequency-wavenumber analysis and Fisher signal detection in real-time infrasonic array data processing, Geophy. J. R. Astron. Soc., 26, 279-284.

Whitney, A. and M.C. Conrad (1983): Call FORTH for realtime control programming, Computer Design, April 1983, 81-84.

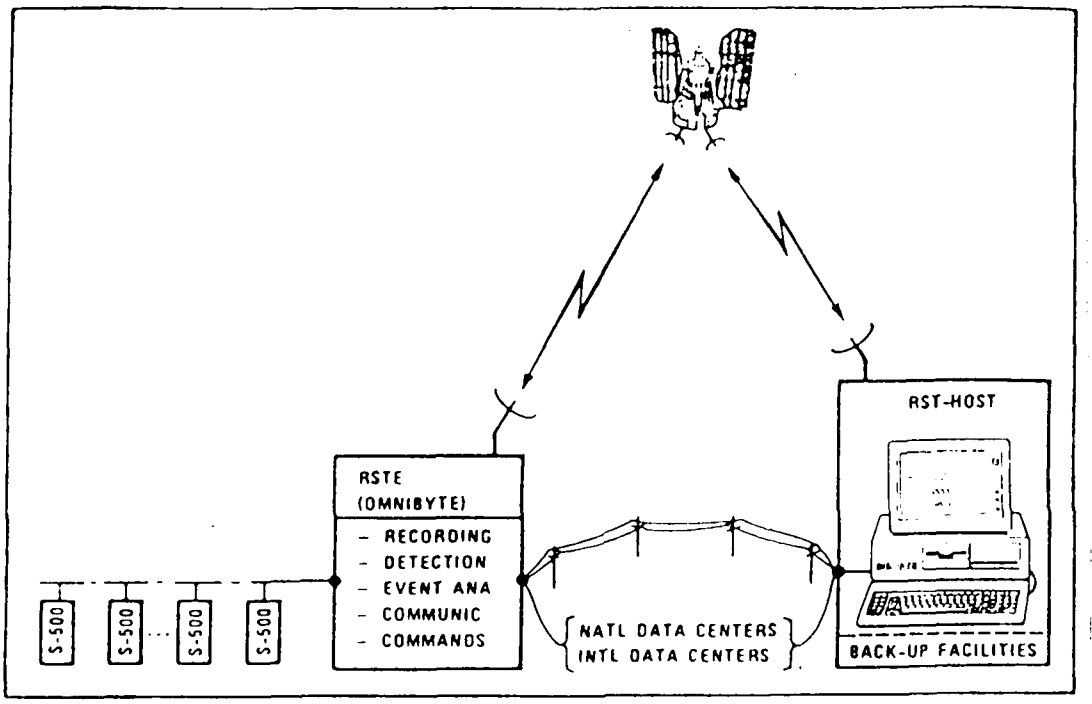

Fig. VII.9.1 Schematic view of the RST/RSTE concept.

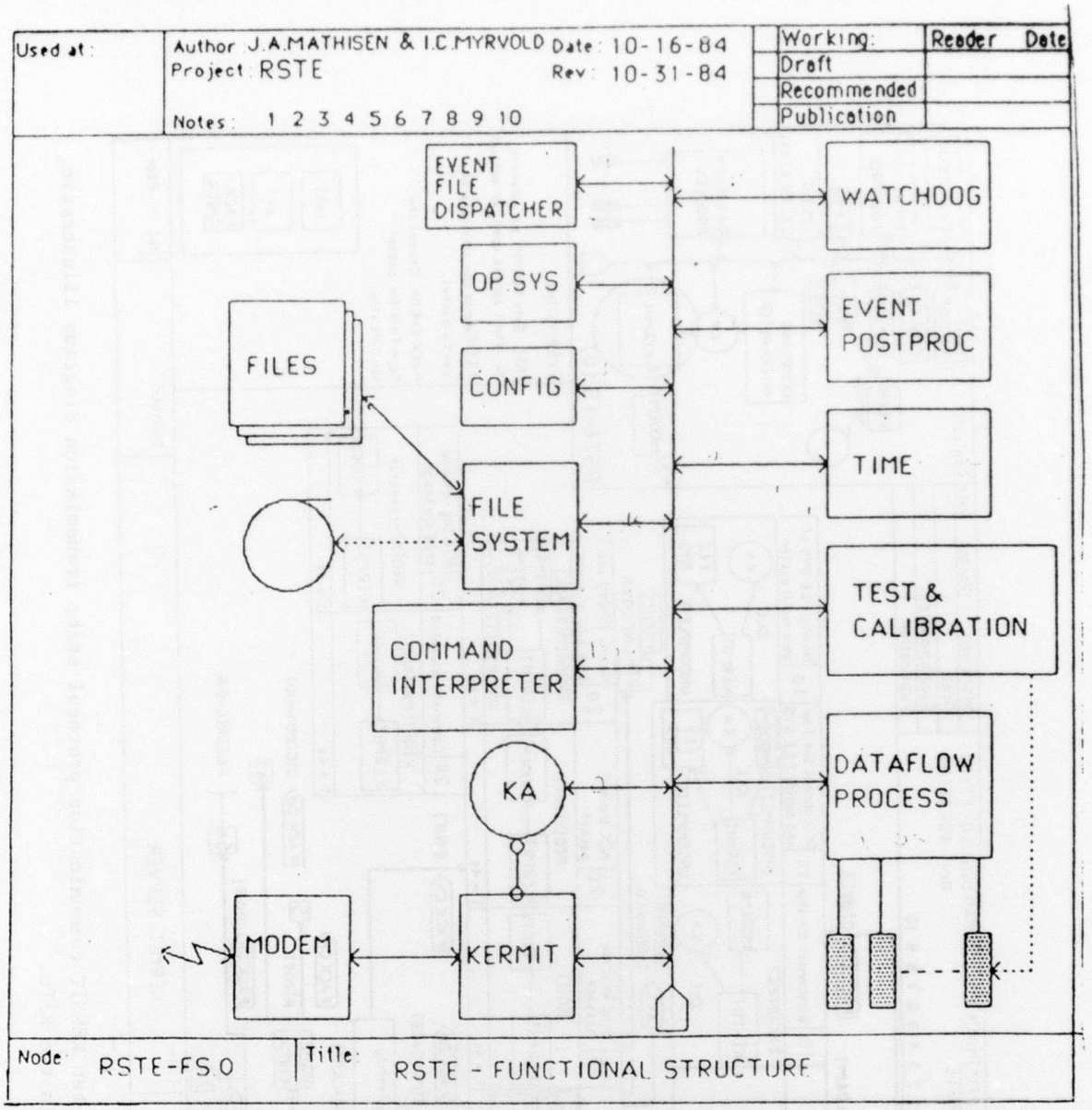

Fig. VII.9.2 The RSTE functional structure. Details on functional tasks are given in the text.

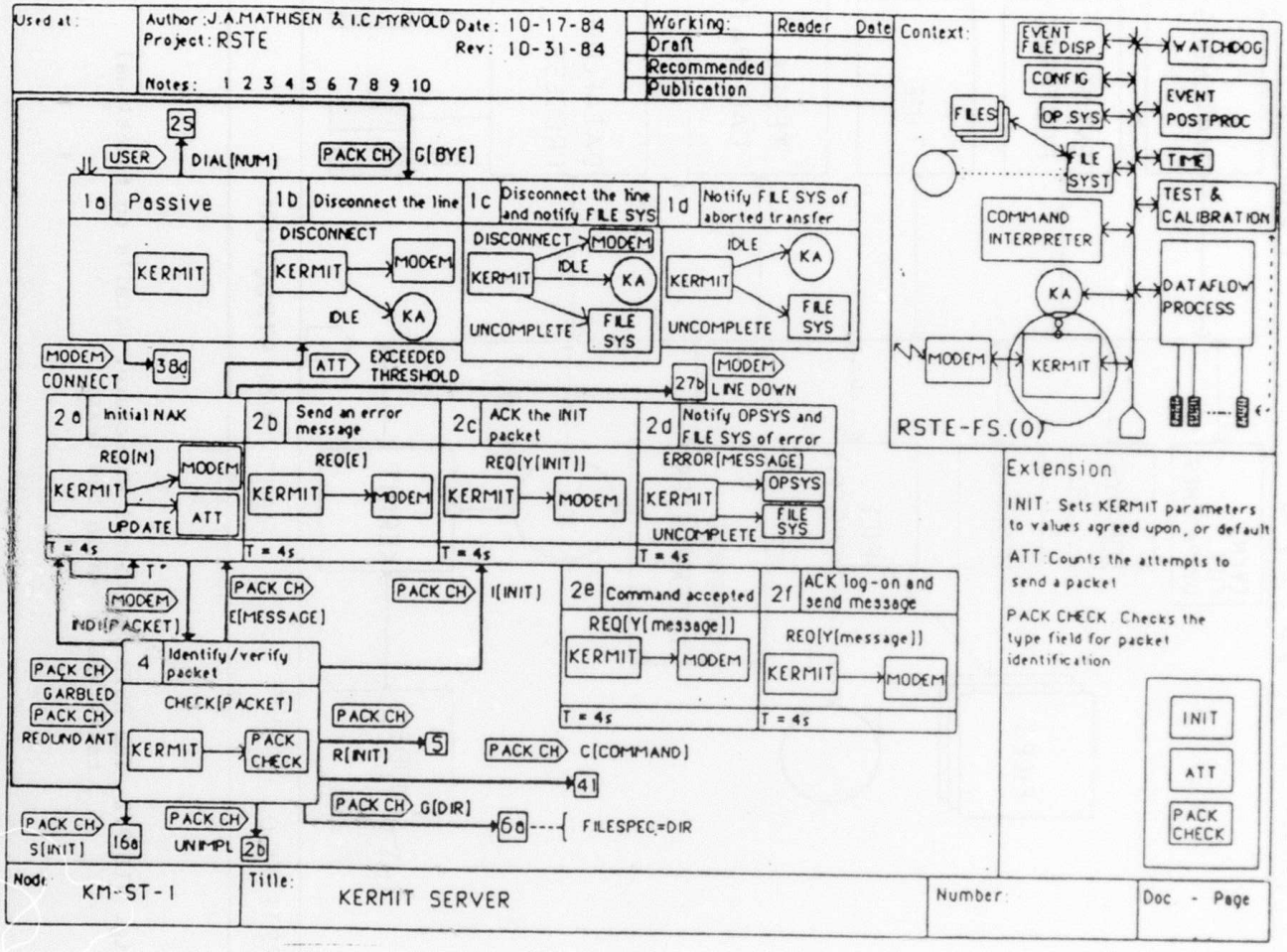

Fig. VII.9.3 One out of ten KERMIT communication protocol state transmission diagrams illustrating its usage in the RSTE.

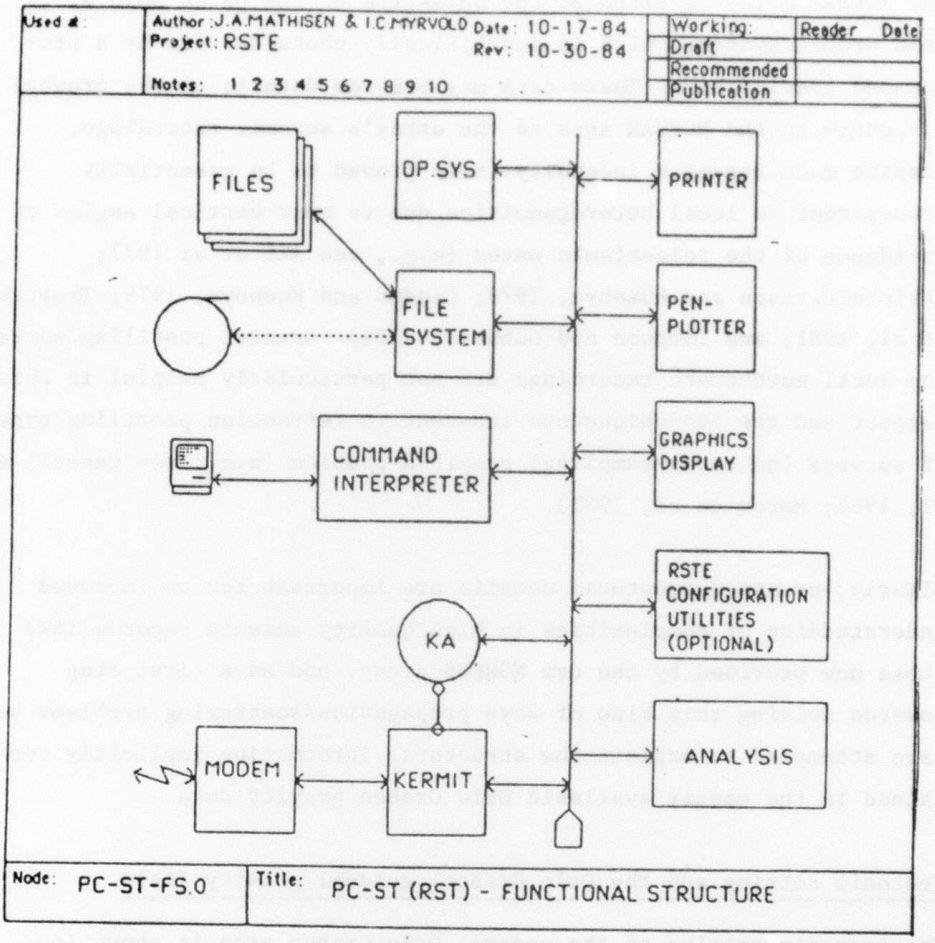

Fig. VII.9.4 The RST functional structure. Details on tasks are given in the text.

VII.10.1 Crustal structure in the NORSAR array siting area derived from gravity observations

The NORSAR array is sited at the outskirts of the paleo Oslo Rift/ Oslo Graben system, which is geophysically characterized by a pronounced gravity high. These data may provide details on the crustal structure in the NORSAR area as the array's seismic recordings, despite much research ingenuity, have proved to be essentially transparent to local heterogeneities due to near-vertical angles of incidence of the teleseismic waves (e.g., see Aki et al 1977; Christoffersson and Husebye, 1979; Haddon and Husebye, 1979; Troitskiy et al, 1981; and Tompson and Gubbins, 1981). Crustal profiling surveys and local earthquake recordings are not particularly helpful in this respect and the non-uniqueness inherent in refraction profiling types of surveys (no cross-sampling) remain a problem (e.g., see Cassell et al, 1983; Mereu et al, 1983).

Clearly, crustal structural details are important for an improved understanding of complexities in high quality seismic records like those now provided by the new NORESS array, and as a first step towards solving this kind of wave propagation/scattering problems we have attempted to exploit the structural information implicitly contained in the easily available Oslo Graben gravity data.

Tectonic setting and the Oslo Graben residual gravity field

The tectonic setting of the general Oslo Graben area is shown in Fig. VII.10.1 and clearly implies that its evolution has been rather complex. However, on the other hand the geophysical imprints of past orogens, etc., are not preserved indefinitely, and today the Oslo Graben gravity high appears to be the outstanding feature reflecting past taphrogenesis. The gravity data coverage of the general graben area is relatively dense, altogether more than 5300 measurements have been carried out (e.g., see Ramberg, 1976). His residual gravity field is

shown in Fig. VII.10.2, and this map formed the basis for our reinterpretation (inversion) of the gravity data pertaining to the Oslo Graben area.

For the sake of completeness it should be mentioned that Ramberg attributed the observed anomalies to intrusion of relatively dense material at the base of the crust (Moho upwarp) while Husebye et al (1978) using Parker's (1975) Ideal-Body Concept gave a mid-crust location of the intrusive body. Parker's technique is very different from standard approaches as in order to reduce the non-uniqueness inherent in gravity interpretations, information extraction is optimized with respect to either density contrast or distance to causative body.

Linear density inversion

The gravity field, being a potential field, invites ambiguity in interpretations which was duly recognized at a relatively early stage of exploration. However, techniques differ in their ability to reduce the number of plausible solutions without invoking a priori information about the heterogeneous body such as density contrasts and geological structural boundaries (outcrops). Thus, inverse methods are favored because they require a minimum number of subjective judgements on the part of the interpreter.

The physical model used (see Fig. VII.10.3) is of the $2\frac{1}{2}$-D kind and consists of N block-formed prisms of 200 km extent matching the approximate length of the Oslo Graben. For the i-th prism the gravitational attraction g_{ij} at the j-th observation point is a linear function of density ρ_i, that is:

$$g_{ij}(\rho_i) = \gamma\rho_i \int_V \vec{z} \cdot r_o \frac{1}{|r-r_o|} dV = a_{ij}\rho_i \qquad (1)$$

where γ = universal gravitational constant, and the volume integral equals the geometrical weighting funtion a_{ij} relating volume of the prism and its distance from the observation point.

The theoretical gravity G_j^t at N observation points is:

$$G_j^t = F_j(\vec{\rho}) = \sum_{i=1}^{M} g_{ij}(\rho_i) \qquad j = 1,N \tag{2}$$

To estimate a density distribution, we note that by substituting the "true" density values, ρ_T, into eq. (2), we get

$$G_j^t = F_j(\vec{\rho_T}) = G_j^o \qquad j = 1,N \tag{3}$$

where G_j^o is the observed gravity at point j. Since F_j is linear in density and noting that our initial density model ρ_o is related to ρ_T by

$$\vec{\rho_T} = \vec{\rho_o} + \vec{\Delta\rho} \tag{4}$$

we achieve

$$F_j(\vec{\rho_o}+\vec{\Delta\rho}) = F_j(\vec{\rho_o}) + F_j(\vec{\Delta\rho}) = G_j^o \qquad j = 1,N \tag{5}$$

Eq. (1), (2) and (5) combine to yield

$$G_j^o \cdot F_j(\vec{\rho}_o) = F_j(\vec{\Delta\rho}) = \sum_{i=1}^{M} a_{ij}\Delta\rho_i \qquad j = 1,M \tag{6}$$

Using matrix notation,

$$\vec{\Delta G} = \vec{G^o} - \vec{G^T} = A\vec{\Delta\rho} \tag{7}$$

A least squares solution to eq. (7) for $\Delta\rho$ is obtained by solving the normalized system:

$$A^TA\ \Delta\rho = A^T\ \Delta G \tag{8}$$

where T denotes transpose. Now, A can be decomposed as:

$$A = U\ \Lambda\ V^T \tag{9}$$

Inserting this in eq. (8) and taking the generalized inverse of A^TA, the estimate of the correction vector becomes:

$$\Delta\rho = V\ \Lambda^{-1}U^T\ \Delta G = H\ \Delta G \tag{10}$$

The $\Delta\rho$ estimation procedure is strictly linear since the A-matrix remains invariant.

Important by-products of the inversion procedure are the resolution and the information density matrices, defined respectively as:

$$R = HA = V\ V^T$$

$$S = AH = U\ U^T$$

For details on techniques used for solving the eq. (7) type of linear equations, reference is made to Backus and Gilbert (1968). We want to remark that the presence of small eigenvalues may cause the solution to oscillate markedly, so a lower cutoff value has to be selected. In practice, this was achieved by retaining the variance of the parameter estimate relatively small without sacrificing too much of the resolution which amounts to eliminating the influence of short wavelength noise in the data. Added flexibility in using the above inversion scheme is often desired as the initial systems of prisms (or blocks) may at a later stage in the analysis prove to be somewhat awkward. For example, it may be desirable to reduce the number of unknowns by merging prisms, or to build in a priori geological information about the likely shape of the anomalous body. Christoffersson and Husebye (1979) have demonstrated a simple scheme for incorporating such modifications without completely restructuring the A-matrix. To do so we introduce a vector θ of "free" parameters which are related to the original parameter vector via a matrix *T*, *that is*:

$$\Delta\rho = T\,\theta \qquad (11)$$

For the general case, eq. (7) and eq. (11) are to be combined:

$$\Delta G = A\,T\,\Delta\theta$$

Details on estimating resolution, standard errors, etc., for the original variables using the eq. (11) transformation can be found in Husebye and Hovland (1982).

Gravity inversion results

All the 8 residual gravity anomaly profiles (III to X) shown in Fig. VII.10.2 have been analyzed using the inversion scheme outlined in the previous section. For illustrative purposes we only display results for 3 of the profiles (Figs. VII.10.3-5), namely, III, VI and IX, as these profiles are representative of the northern, central and southern segments of the Oslo Graben. As regards practical details of

the inversion analysis like initial and final numbers of prisms used, number of eigenvalues ignored in thesolution, etc., this information is included in the respective figure captions. Furthermore, similar results and details for the other profiles can be found in Wessel (1984).

The two striking features characteristic of all profiles are: i) the small density contrast resolved and ii) the depth to the causative body. No higher value than 0.06 cm g^{-3} for the anomalous body wave were encountered during the analysis, while the corresponding excess masses are concentrated in the depth interval 15 to 20 km. The only exception here is profile III where significant excess masses are found down to 25 km. The size of the anomalous body gradually increases southward implying a widening of the graben in that direction as indicated by the surface geology as well. Furthermore, the very small discrepancies between observed and calculated gravity are reflected in low relative RMS-values of the order of 0.05 mgal.

Very recently Kibsgaard (1985) has studied fault mechanisms of small earthquakes in the northern part of the Oslo Graben (close to profile III). The very interesting feature here is that foci positions appear to be located on the flanks of the anomalous body derived from the gravity study (see Fig. VII.10.6). A tenative, physical explanation here is as follows; the primary lithosphere stress field in Fennoscandia is caused by ridge push forces originating in the Norwegian Sea (e.g., see Husebye et al, 1978) whose orientation in the graben area coincide with the compression axis reported by Kibsgaard in his study. The interaction of this field with loading stresses caused by the "heavy" intrusive body in the graben give rise to stress amplifications being largest on the lower periphery of the body and ultimately becoming causative of the majority of local earthquakes observed.

Extensive details on the gravity inversion investigation reported here, including hypotheses on Oslo Graben taphrogenesis, can be found in Wessel (1984) and Wessel and Husebye (1985).

Concluding remarks

The crustal structure model presented here and derived primarily on the basis of gravity observations is to our knowledge the most detailed ever presented for the NORSAR array siting area. Important, work is already under way to compute the "seismic responses" of these structures on crustal travelling waves. Part of the motivations for undertaking such work is that preliminary 3-comp. seismogram analysis results clearly demonstrate a consistent migration off azimuth of later arriving phases.

There is also another aspect of the Oslo Graben results, namely, the underlying dynamic mechanisms causing the formation of the relatively dense body in the central crust. To improve our ability to handle this kind of problems, a cooperative research venture with Professor H.-J. Neugebauer, Clausthal, FRG, is in the planning stages. Tangible results here so far are a simplified modelling experiment with magma intrusion in the crust as demonstrated in Fig. VII.10.7 and conducted by Dr. Neugebauer.

E.S. Husebye
P. Wessel, now at LDGO,
Columbia University

References

Aki, K., A. Christoffersson, and E.S. Husebye, Determination of the three dimensional structure of the lithosphere, J. Geophys. Res., 82, 277-296, 1977.

Backus, G., and F. Gilbert, The resolving power of gross earth data, Geophys. J. Roy. Astron. Soc., 16, 169-205, 1968.

Cassell, B.R., S. Mykkeltveit, R. Kanestrøm, and E.S. Husebye, A North Sea - southern Norway seismic crustal profile, Geophys. J. Roy. Astron. Soc., 72, 733-753, 1983.

Christoffersson, A., and E.S. Husebye, On 3-dimensional inversion of P-wave time residuals - Option for geological modeling, J. Geophys. Res., 84, 6168-6176, 1979.

Haddon, R.A.W., and E.S. Husebye, Joint interpretation of P-wave time and amplitude anomalies in terms of lithospheric heterogeneities, Geophys. J. Roy. Astron. Soc., 55, 19-44, 1978.

Hovland, J., E.S. Husebye, C.E. Lund, K. Åstrøm, and A. Christoffersson, A tomographic image of the S. Scandia lithosphere and asthenosphere, M/s in preparation, 1985.

Husebye, E.S., H. Bungum, J. Fyen and H. Gjøystdal, Earthquake activity in Fennoscandia between 1497 and 1975 and intraplate tectonics, Nor. Geol. Tidsskr., 58, 51-68, 1978.

Husebye, E.S., and J. Hovland, On upper mantle seismic heterogeneities beneath Fennoscandia, in: E.S. Husebye (Ed.), The structure of the lithosphere-asthenosphere in Europe and the North Atlantic, Tectonophysics, 90, 1-17, 1982.

Husebye, E.S., and I.B. Ramberg, Geophysical investigations, in: The Olso Paleorift, Nor. Geol. Unders., No. 337, Universitetsforlaget, Oslo, Norway, 1978.

Husebye, E.S., I.B. Ramberg, and P.C. England, The ideal-body concept in interpretation of Oslo Rift gravity data and their correlation with seismic observations, in: Ramberg, I.B., and E.-R. Neumann, (Eds.), Tectonics and Geophysics of Continental Rifts, NATO Advanced Study Institute Series C, 37, 313-327, 1978.

Ingate, S.F., E.S. Husebye, and A. Christoffersson, Regional arrays and optimum processing schemes, Bull. Seism. Soc. Am., 75, Aug 1985.

Kibsgaard, A., Fault mechanism studies using the SV/P ratio tecnique; practical application for earthquakes in Stiegler's Gorge, Tanzania, and in the Oslo Graben, Norway, Cand. scient. thesis, Inst. for Geophysics, Univ. of Oslo, Norway.

Parker, R.L., The theory of ideal bodies for gravity interpretation, Geophys. J. Roy. Soc. Lond., 149, 747-763, 1975.

Ramberg, I.B., Gravity interpretation of the Oslo graben and associated igneous rocks, Nor. Geol. Unders., 325, 193 pp, 1976.

Ramberg, I.B., and S.B. Smithson, Gravity interpretation of the southern Oslo Graben and adjacent Precambrian rocks, Norway, Tectonophysics, 11, 419-431, 1971.

Thomson, C.J., and D. Gubbins, Three-dimensional lithospheric modelling at NORSAR: linearity of the method and amplitude variations from the anomalies, Geophys. J. Roy. Astron. Soc., 71, 1-36, 1982.

Troitskiy, P., E.S. Husebye, and A. Nikolaev, Lithospheric studies based on holographic principles, Nature, 294, 618-623, 1981.

Wessel, P., Gravity inversion and Oslo Graben taphrogenesis, Cand. scient. thesis, Dept. of Geology, Univ. of Oslo, Oslo, Norway.

Wessel, P., and E.S. Husebye (1985): The Oslo Graben gravity high and taphrogenesis, manuscript submitted for publication.

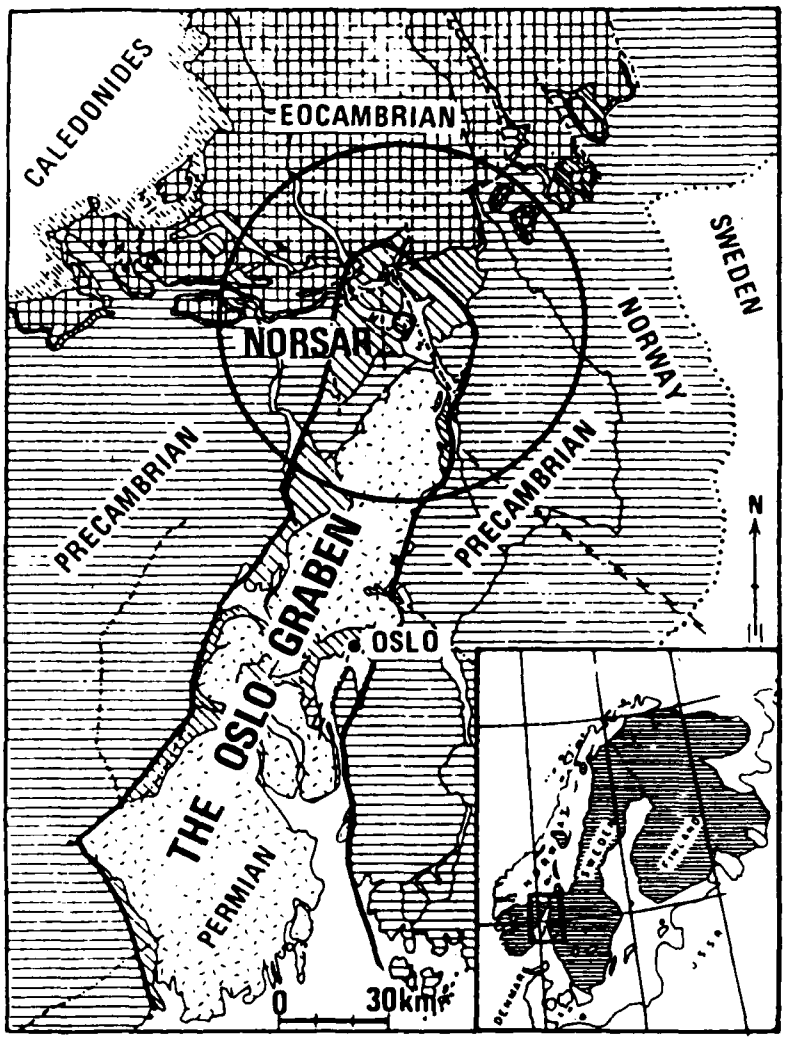

Fig. VII.10.1 The geology of the Oslo Graben and adjacent areas.

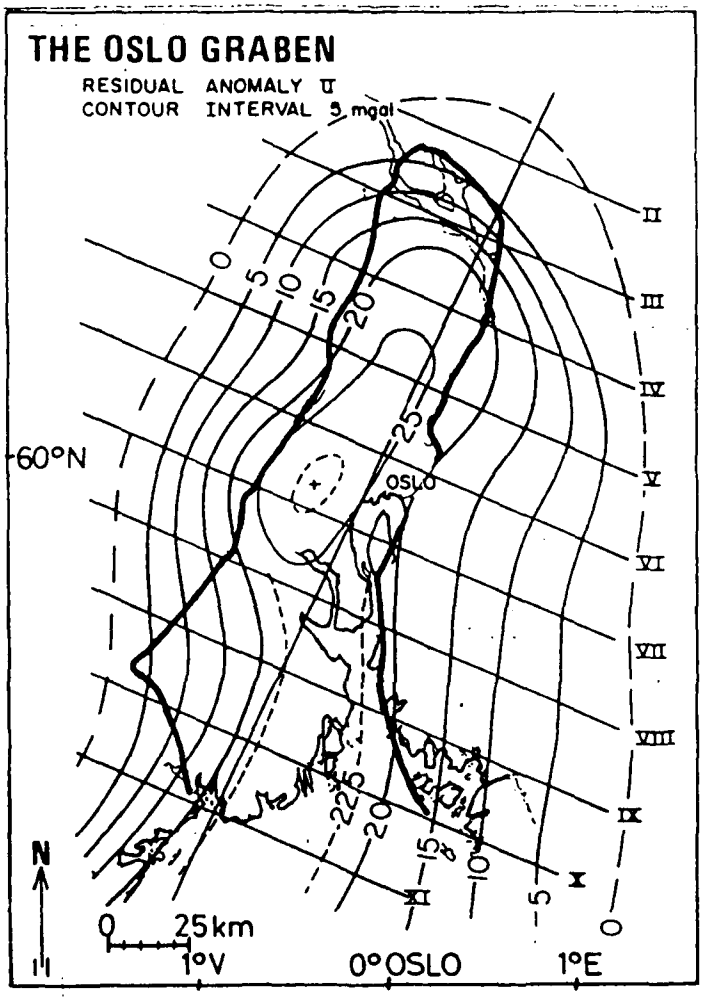

Fig. VII.10.2 The Oslo Graben residual gravity anomaly redrawn from Husebye and Ramberg (1978). The cross-sections (profiles) subjected to our block inversion analysis are indicated.

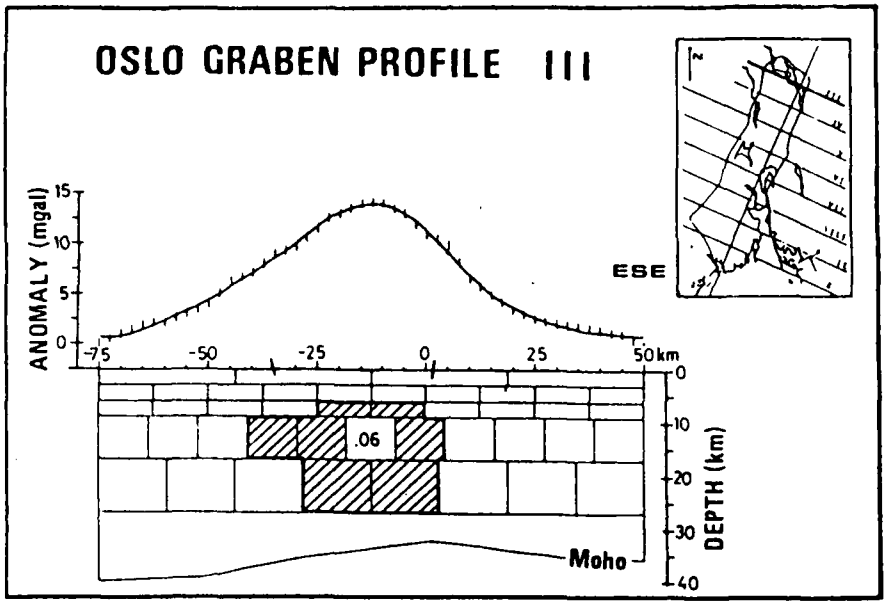

Fig. VII.10.3 Inversion results in terms of $2\frac{1}{2}$-D density contrast distribution obtained for profile III. The initial model consisted of 44 prisms, finally reduced to 35 by combining those having equal density contrast. Density contrasts for the non-hatched prisms amounted at most to $\pm$ 0.01 gcm^{-3} and this was not considered significant. Observed (vertical bars) and calculated (solid lines) gravity (RMS = 0.045) together with the Moho contours are also shown.

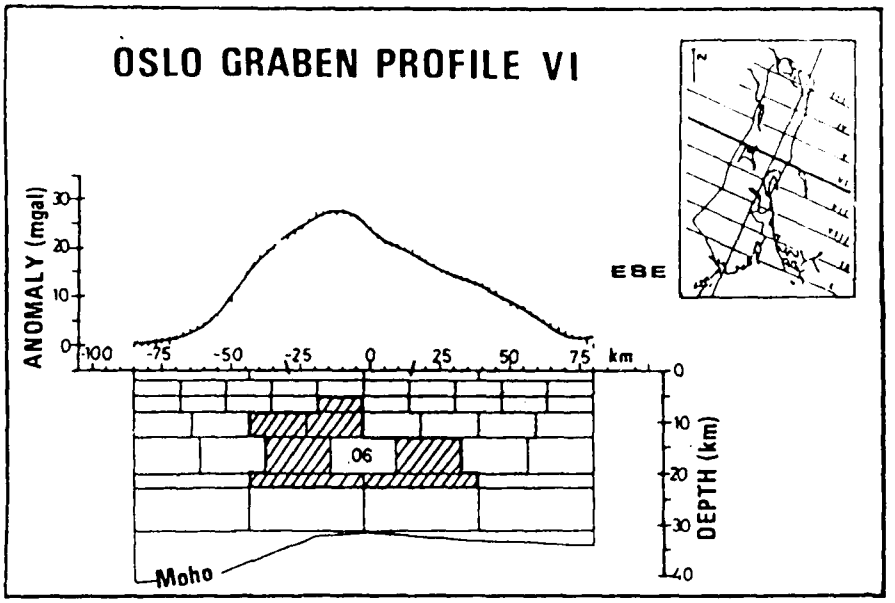

Fig. VII.10.4 Same as Fig. VII.10.3, but with initial model consisting of 48 prisms, reduced to 35. RM value = 0.050.

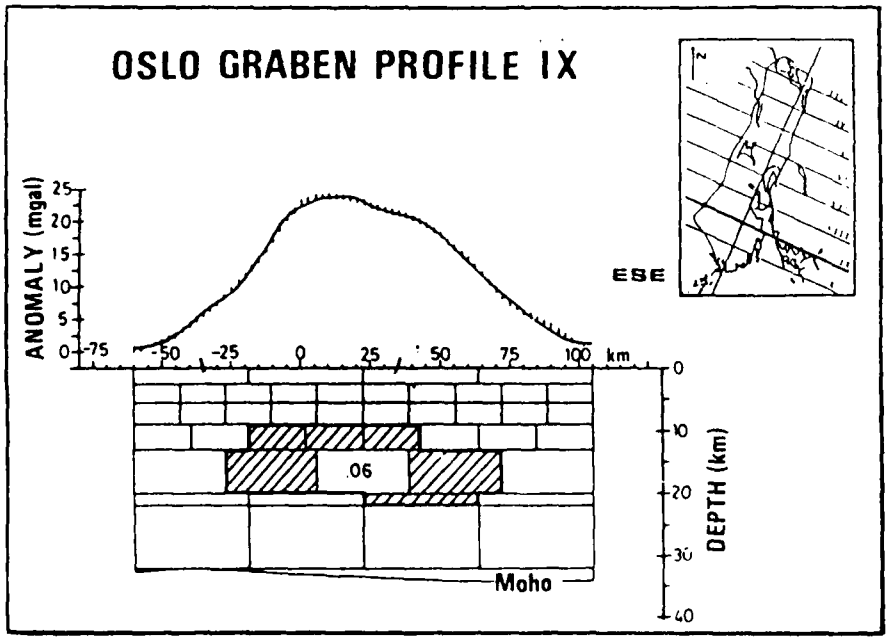

Fig. VII.10.5 Same as Fig. VII.10.4, but with initial model consisting of 46 prisms, reduced to 33. RMS value = 0.049.

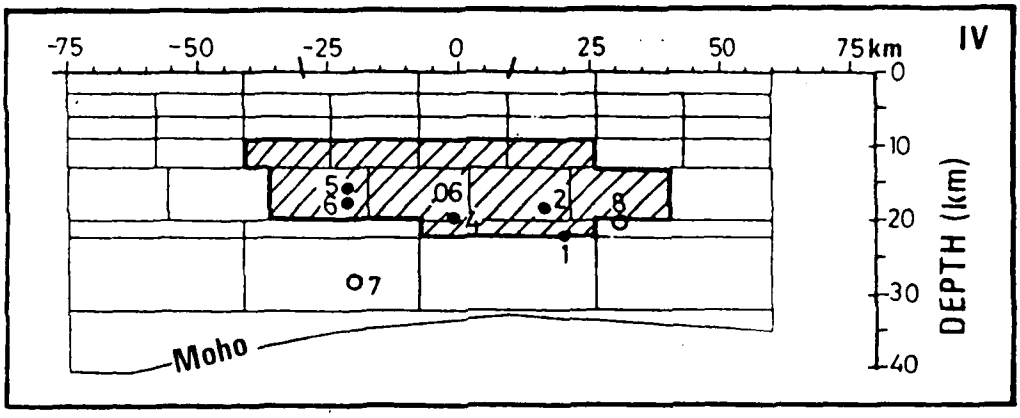

Fig. VII.10.6 Projection of hypocenters into the profile IV cross-section. It is rather remarkable that all events are located at (wrapped around) the lower part of the gravity derived anomalous body. The poorest fit is seen for event 7 whose projection into profile III gives a much better fit vs the location of that anomalous body.

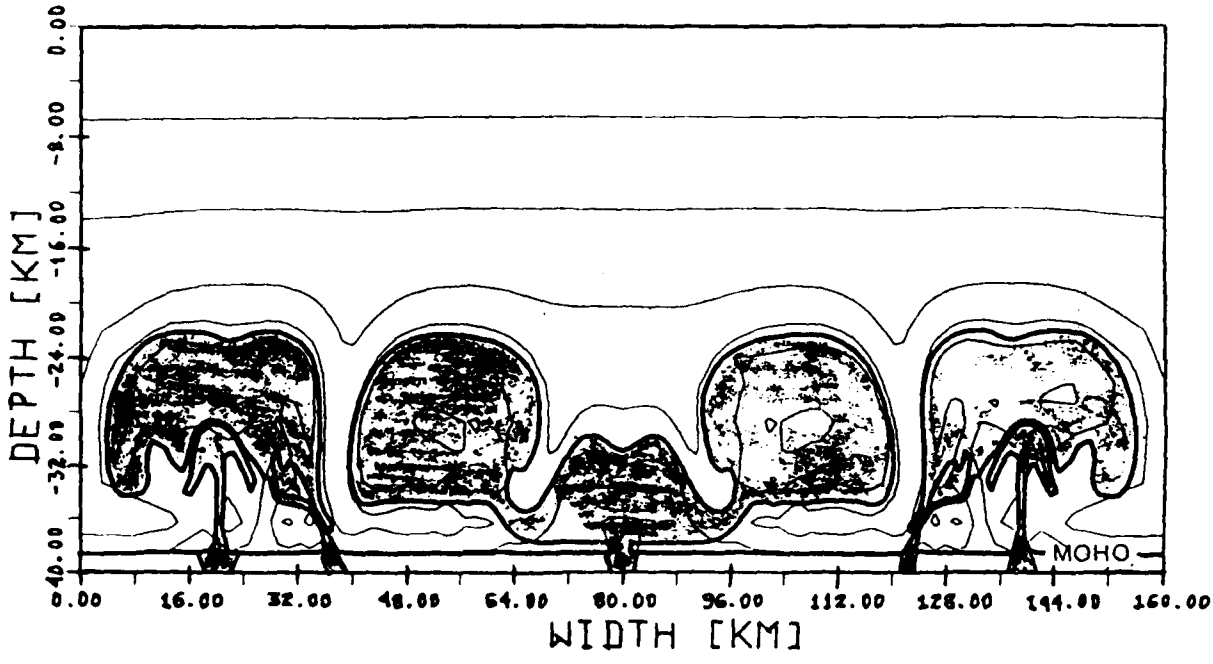

Fig. VII.10.7 Synthetic modelling of crustal intrusions for providing a deeper insight on the mechanism by which the relatively dense body in the Oslo Graben was formed. Thick lines: boundaries of intrusions; thin lines: temperature intervals of 200° (zero at surface and 1200° at bottom or Moho). Originally the model had one homogeneous intrusion, vertical viscosity contrast being 5 orders of magnitude. In the beginning the intrusion would represent a density inversion. When cooling and constracting the density contrast would be positive, but located in the lower crust, contrasting our gravity results for the Oslo Graben. All calculations here have been made by Professor H.-J. Neugebauer, Clausthal, FRG.